Implementation of Accelerometer-Based Adaptive Noise Cancellation in a Wireless Wearable Pulse Oximeter Platform for Remote Physiological Monitoring and Triage

A Thesis

Submitted to the Faculty of

WORCESTER POLYTECHNIC INSTITUTE

in partial fulfillment of the requirements for the

Degree of Master of Science

By

Gary W. Comtois

August 31, 2007

Professor Yitzhak Mendelson, Major Advisor
Department of Biomedical Engineering

Professor Glenn R. Gaudette, Committee Member
Department of Biomedical Engineering

Professor R. James Duckworth, Committee Member
Department of Electrical and Computer Engineering

ABSTRACT

A wireless wearable battery-operated pulse oximeter has been developed in our laboratory for field triage applications. The wearable pulse oximeter, which uses a forehead-mounted sensor to provide arterial oxygen saturation (SpO_2) and heart rate (HR) information, would enable field medics to monitor vital physiological information following critical injuries, thereby helping to prioritize life saving medical interventions. This study was undertaken to investigate if accelerometry (ACC)-based adaptive noise cancellation (ANC) is effective in minimizing SpO_2 and HR errors induced during jogging to simulate certain motion artifacts expected to occur in the field. Preliminary tests confirmed that processing the motion corrupted photoplethysmographic (PPG) signals by simple Least-Mean-Square (LMS) and Recursive Least-Squares (RLS) ANC algorithms can help to improve the signal-to-noise ratio of motion-corrupted PPG signals, thereby reducing SpO_2 and HR errors during jogging. The study showed also that the degree of improvement depends on filter order. In addition, we found that it would be more feasible to implement an LMS adaptive filter within an embedded microcontroller environment since the LMS algorithm requires significantly less operations.

ACKNOWLEDGEMENTS

I would like to express my gratitude to the following individuals:

My advisor, Dr. Yitzhak Mendelson, for his expertise, guidance and patience over the past two years.

My thesis committee, Dr. Glenn R. Gaudette and Dr. R. James Duckworth, for reviewing my work and making thoughtful contributions to my thesis.

The students in the Department of Biomedical Engineering at WPI for their friendship and to all those who participated in my jogging experiments, especially Stuart Howes and Piyush Ramuka.

Will Johnston for helping me transition into the pulse oximeter project.

My friends and family for always being there for me, especially my Mom and Dad for their continuous love and encouragement, and my brother, Nicholas, for being my favorite brother.

My wife Diana for her love and inspiration.

This work is supported by the U.S. Army Medical Research and Material Command under Contract No. DAMD17-03-2-0006. The views, opinions and/or findings are those of the author and should not be construed as an official Department of the Army position, policy or decision unless so designated by other documentation.

TABLE OF CONTENT

LIST OF FIGURES

LIST OF TABLES

GLOSSARY OF ABBREVIATIONS

Abbreviation	*Meaning*
λ	Recursive Least-Squares Forgetting Factor
μ	Least-Mean-Square Step-Size
μC	Microcontroller
ACC	Accelerometer
ANC	Adaptive Noise Cancellation
ANOVA	Analysis of Variance
BP	Band-Pass
CI_{95}	95% Confidence Interval
COTS	Commercial-off-the-shelf
ECG	Electrocardiograph
FFT	Fast Fourier Transform
FIR	Finite Impulse Response
Hb	Deoxygenated Hemoglobin
HbO_2	Oxygenated Hemoglobin
HR	Heart Rate
HRV	Heart Rate Variability
IC	Integrated Circuit
ICA	Independent Component Analysis
IR	Infrared
IRB	Institutional Review Board
IHR	Instantaneous Heart Rate
LED	Light Emitting Diode
LMS	Least-Mean-Square
LP	Low-Pass
M	Filter Order
MEMS	Micro-Electromechanical System
PCA	Principal Component Analysis
PD	Photodiode
PDA	Personal Digital Assistant
PPG	Photoplethysmographic
R	Red
R	Ratio-of-ratios
RLS	Recursive Least-Squares
RM	Receiver Module
RMSE	Root Mean Squared Error
RR	Respiration Rate
SEE	Standard Error of the Estimate
SET	Signal Extraction Technology®
SD	Standard Deviation
SM	Sensor Module
SNR	Signal-to-Noise Ratio
SaO_2	Arterial Oxygen Saturation

SpO_2	Estimate of Arterial Oxygen Saturation
TI-MSP430	Texas Instruments-Mixed Signal Processor
w_i	Tap-weight

1. INTRODUCTION

Obtaining vital signs in real time from wearable physiological monitoring devices would enable medical personnel and first responders to assess quickly and effectively the health status of soldiers, hazmat workers, firefighters, and mountain climbers and manage patient triage from a remote location. During battlefield missions, specifically the Vietnam conflict, Zajtchuk and Sullivan described that although 67% of casualties occurred within 10 minutes from the onset of injury, the remaining 33% could have benefited from advanced diagnostic devices [1]. The implementation of wearable sensors could provide a medic with vital physiological information from several combatants.

To address the need for remote monitoring technology, considerable work has been described in the field in recent years regarding monitoring devices that could be utilized to indicate the health status of individuals [2-11]. Much of the effort to develop wearable diagnostics for remote physiological assessment has involved pulse oximeters since these devices have the potential to provide real-time arterial oxygen saturation (SpO_2), heart rate (HR), heart rate variability (HRV) and respiration rate (RR) readings [12]. Pulse oximeters being developed for use in the field must be resistant to the effects of motion artifacts which are known to degrade considerably the accuracy of SpO_2 and HR readings since signal components affected by motion can appear as normal arterial pulsations [13]. Implementation of software algorithms has been suggested in the literature as a means of reducing the effects of motion on wearable pulse oximeters. For example, Wendelken et al have suggested software routines for incorporation into a wearable system based on a forehead-mounted pulse oximeter sensor [6, 7]. Likewise, Asada et al have suggested implementing algorithms within a wearable device based on a custom ring-worn sensor

[8, 9].

McGrath and coworkers developed a system known as ARTEMIS (Automated Remote Triage and Emergency Management Information System) which was designed to provide a means of indicating the status of military combatants during battlefield missions (*Fig. 1.1*) [14]. This system incorporates a commercial forehead-worn pulse oximeter sensor (Nonin®) with a custom "fuzzy logic" based decision-making algorithm that is utilized to interpret data from the wearable sensor.

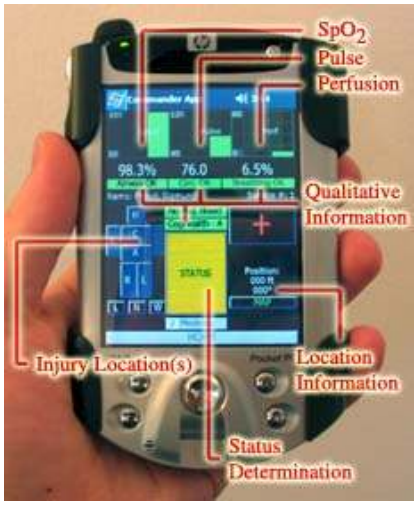

Figure 1.1. *ARTEMIS graphical user interface [14].*

Wendelken et al have suggested that the ARTEMIS system could be utilized to provide medics with an indication of the level of severity of an injury. An algorithm could be implemented in software to interpret data acquired by a PPG sensor and help medics to evaluate physiological parameters such as blood circulation and breathing rate. The unique feature of the ARTEMIS algorithm is the incorporation of a medical model in order to determine the health status of monitored individuals [15]. By incorporating physiological readings acquired from a wearable pulse oximeter, input from the monitored individual and input from a medic, the model utilized in ARTEMIS could potentially classify the severity of injuries in the field. This could increase the speed of

treatment and triage of injured combatants.

Despite the potential utility of ARTEMIS, experiments have been limited to laboratory simulations while field implementation of the device has not been reported. Additionally, since only simulations were performed, the software associated with ARTEMIS may not be effective during periods of motion which is a crucial design constraint for real-time monitoring of mobile individuals. Without the utilization of robust software algorithms to reduce the effects of motion artifacts, the readings extracted from PPG signals remain unreliable. Therefore, motion tolerant algorithms are a crucial component to a system used for remote physiological assessment and triage of mobile individuals.

Asada et al developed a wearable ring-type sensor for continuous monitoring applications [8]. This device (*Fig. 1.2*) was designed to be low power, unobtrusive and resistant to the effects of motion artifacts [8, 9]. It was suggested that an outer ring could be utilized to protect an inner ring from physical disturbances. This could reduce motion-induced noise in the PPG signal since the sensing component of the pulse oximeter was embedded within the inner ring [8]. By reducing the effect of physical disturbances, this design could help to reduce the effects of motion artifacts. In addition to this novel dual-ring design, it was also suggested that accelerometer (ACC)-based adaptive noise cancellation (ANC) software could be incorporated into the ring-sensor to obtain potentially more accurate measurements during jogging [16]. Briefly, this software acquires signals from an ACC attached to the ring sensor and uses these signals as a motion reference for the ANC algorithm. Asada et al have suggested that the ACC signals could be used to reduce the effects of motion artifacts in photoplethysmographic

(PPG) signals acquired during jogging [16]. Although these features suggest that the device could become a promising platform for continuous monitoring applications, the ability of the ring sensor to provide reliable readings is limited since the fingers are known to be especially prone to motion artifacts [12]. In addition, it was described by Nagre et al [17] that the forehead is a more stable location from which to acquire PPG data. Therefore, measurements obtained from the forehead would be preferred.

It should be noted that although jogging is not the primary activity of military combatants in the field, studies that consist of jogging exercises are worth pursuing since this can help to address the types of motion artifacts that occur in the field. For example, it is known that PPG signals can become corrupted by motion artifacts even in a clinical setting, where body movements are generally less intense. Therefore, to determine the feasibility of reducing the effects of motion in a field setting, more intense motions, such as jogging, should be investigated.

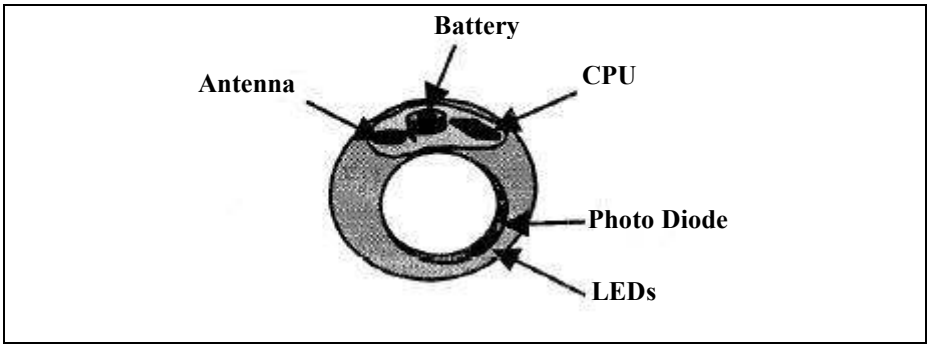

Figure 1.2. *The wearable ring-sensor developed by Asada et al [18].*

Inadequacies of previously designed pulse oximeter-based systems suggest that a novel wearable system with resistance to the effects of motion artifacts would provide a more suitable platform for telemedicine applications, which are base on the use of communication technologies for more rapid and efficient transfer of medical information [19]. Potential arenas in which a wireless wearable pulse oximeter could be utilized

include military settings, firefighters, mountain climbers as well as home-based care. Features of a wearable system for remote physiological monitoring would include small-size, light-weight, power efficiency, and capability of providing reliable readings even during periods of movement. Thus, the focus of this thesis is to address the feasibility of reducing the effects of motion artifacts in wearable pulse oximetry.

The next section describes the significance of wearable pulse oximetry for telemetry applications. Since commercially available pulse oximeters are not designed for use in the field, a more robust pulse oximeter must be devised in order to obtain reliable readings from moving individuals. A more motion-tolerant pulse oximeter would enable medics to obtain more accurate measurements in the field even during patient motion.

2. SIGNIFICANCE

A wearable remote physiological monitoring device could help to save lives by providing continuous readings to medical personnel. Individuals that would benefit from this technology include persons operating in high-risk environments, such as military combatants, firefighters, and other first responders, as well as individuals in need of continuous at-home monitoring.

In a battlefield setting, this would enable medics to assess the health status of combatants more quickly, which would help to expedite the delivery of medical treatment and triage of injured individuals. Faster treatment and triage in the field could help medics save the lives of injured individuals as well as reduce the amount time that the life of the medic is in danger. Additionally, simultaneous observation of several individuals could enable more efficient utilization of medical professionals so that treatment is delivered where it is most urgently needed.

Commercial-off-the-shelf (COTS) technology is not adequate for use during field applications since these devices are typically designed for use in a clinical setting. Intense movements in the field would reduce the accuracy of measurements obtained from a commercial pulse oximeter and, therefore, limit its effectiveness for remote monitoring and triage applications.

Advances in remote monitoring could provide medical personnel with a more direct link to injured persons [1]. Obtaining more accurate and reliable physiological readings remotely would enable medics to diagnose multiple injured individuals with a high degree of confidence. This would significantly expedite the delivery of treatment which could greatly reduce the amount of casualties that occur in military combat.

Pulse oximetry represents a promising platform for remote physiological monitoring since SpO_2, HR, HRV, and RR readings can be extracted in real-time from the PPG signal, which can be obtained by a wearable pulse oximeter sensor. These measurements would enable a medic to make more accurate diagnoses for medical treatment and triage of injured combatants. These physiological parameters would also be useful for at-home and clinical monitoring applications.

Although pulse oximeters can provide several physiological measurements, the accuracy and reliability of existing pulse oximeters is inadequate for field applications since PPG signals degrade as a result of patient motion. Improving the reliability of readings obtained by pulse oximeters during motion would significantly expand the utility of wearable monitoring for telemedicine applications.

3. PULSE OXIMETRY BACKGROUND

3.1. LIGHT ABSORPTION

Oximetry is a noninvasive, optically-based technique that utilizes light absorption properties of blood constituents to measure the concentration of oxygen in arterial blood [13]. The amount of light absorbed in a given substance is defined by the Lambert-Beer Law which associates the degree of light absorption with the wavelength of the incident light, the optical path length and the absorption coefficient of the substance [20]. By illuminating a tissue bed with light emitting diodes (LED) and measuring the amount of light absorbed by the tissue using a light-sensitive photodiode (PD), it is possible to estimate the concentration of oxygen in the arterial blood.

A pulse oximeter utilizes LEDs that emit red (R) (e.g. 660nm) and infrared (IR) light (e.g. 940nm) since these wavelengths are absorbed by oxygenated (HbO_2) and reduced hemoglobin (Hb) to different degrees. Fig. 3.1 shows that Hb absorbs R light to a greater extent than IR light, although HbO_2 more readily absorbs IR light. Therefore, by measuring the relative amounts of R and IR light absorptions, which indicate the proportion of HbO_2 and Hb components, the concentration of oxygenated arterial blood can be measured [20].

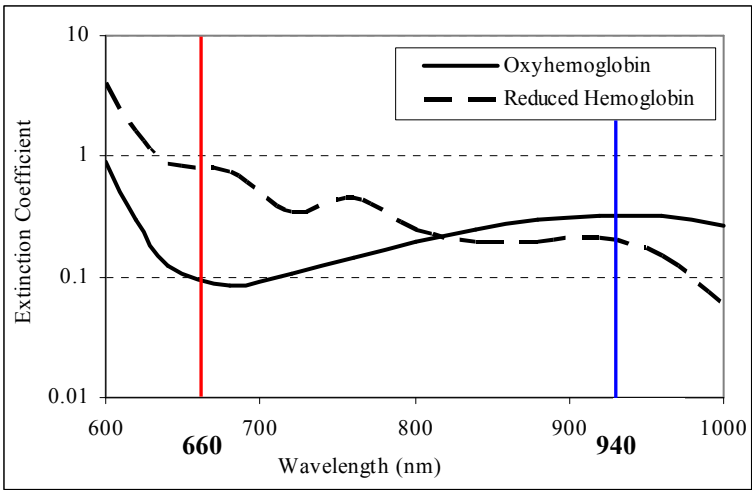

Figure 3.1. *Optical absorption spectra of HbO_2 and Hb [13].*

Light illuminated a region of tissue is absorbed by skin, blood, tissue and bone, as illustrated in Fig. 3.2. The remaining light that is not absorbed is incident upon a light-sensitive PD. The AC portion of the PPG signal is due to pulsatile arterial blood which causes variations in light intensity; the DC portion is due to non-pulsatile arterial blood, venous blood, skin, tissue and bone.

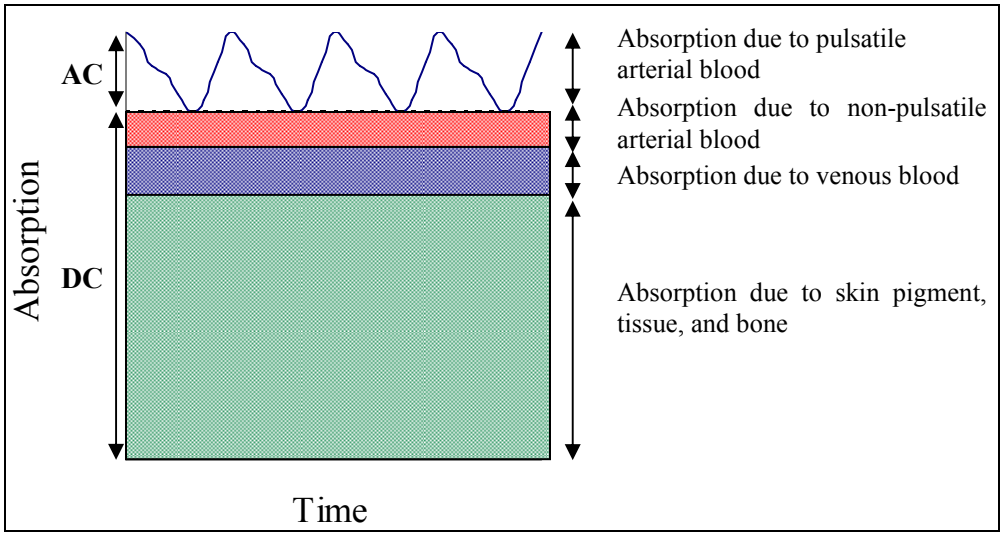

Figure 3.2. *Optical absorption as a function of blood, skin pigment, tissue and bone [13].*

The pulsatile portion of the PPG signal is caused by changes in the arterial blood volume during the cardiac cycle, associated with the contraction (systole) and relaxation

(diastole) phases. The contraction of the heart drives oxygenated arterial blood throughout the systemic arteries, which partially attenuate the illuminating R and IR light incident upon the PD. As blood returns to the heart via the venous system during diastole, the arterial blood volume decreases which allows more light to illuminate the PD. Consequently the cardiac cycle produces the sinusoidal-shaped PPG signal shown in Fig. 3.3.

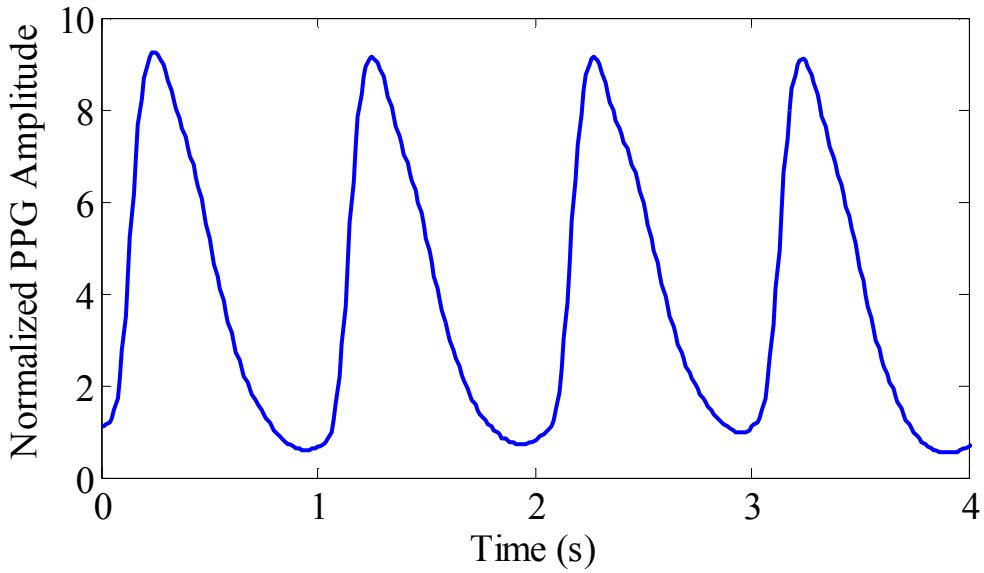

Figure 3.3. *Typical resting PPG signal.*

3.2. Operating Modes

PPG signals can be obtained utilizing either transmittance or reflectance mode optical transducers. Transmittance mode sensors, which are commonly worn on the fingers, measure light that passes through tissue by a PD located on the opposite side of a tissue bed, as depicted in Fig. 3.4. The reflectance operating mode, also illustrated in Fig. 3.4, measures the reflected, or back-scattered, light by a PD positioned adjacent to the R and IR LEDs. A pulse oximeter that employs a reflectance mode sensor is typically forehead-mounted but other body sites can be used to derive similar information.

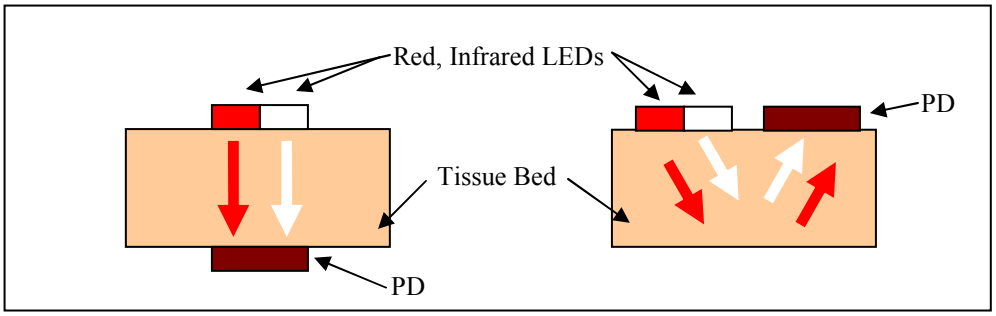

Figure 3.4. *Transmittance (left) and reflectance (right) operating modes in pulse oximetry.*

3.3. Measurement Sites

In a clinical environment, PPG signals are typically obtained from the fingers, although PPG signals obtained by forehead-worn sensors have been shown to provide accurate and reliable measurements.

For field applications, such as physiological monitoring of military combatants and firefighters, it would be more practical to implement a forehead-worn sensor than a finger-worn sensor since utilizing the forehead as a measurement site does not limit hand movement. Furthermore, PPG signals obtained from the forehead are generally less sensitive to motion artifacts than PPG signals measured from the fingers [17, 21], and SpO_2 readings obtained from the forehead respond faster to physiological changes due to the proximity of the head to the heart.

Vital physiological information is contained within the amplitude and spectral content of PPG signals which can be processed to extract SpO_2, HR, HRV and RR [12]. This thesis focuses on software algorithms to extract more accurate and reliable SpO_2 and HR measurements during activity.

3.4. SpO_2 MEASUREMENT THEORY

The noninvasive measurement of arterial oxygen saturation (SaO_2) by pulse oximetry (SpO_2) is a crucial reading for physiological monitoring since a lack of oxygen to the brain for a prolonged period of time can be fatal. For a healthy individual breathing atmospheric air, readings typically range from 96% to 98%. Commercial pulse oximeters typically report a measurement accuracy of ± 2% during rest [13]. Additionally, it was reported that the Masimo SET™ provides ± 3 digits during light motion artifacts associated with the clinical setting [22].

SpO_2 is derived from the relative concentrations of HbO_2 and Hb in arterial blood. It can be determined from the ratio of R to IR light absorbed in a tissue bed. The ratio of normalized R light (AC_R/DC_R) to normalized IR light (AC_{IR}/AC_{IR}) known as the ratio-of-ratios, or $\boldsymbol{R}$ value (3.1), is utilized in (3.2) to calculate SpO_2, where A and B are constants derived during empirical calibration of a pulse oximeter. A typical calibration curve is shown in Fig. 3.5.

$$\boldsymbol{R} = \frac{AC_R / DC_R}{AC_{IR} / DC_{IR}} \tag{3.1}$$

$$SpO_2 = A - B \cdot \boldsymbol{R} \tag{3.2}$$

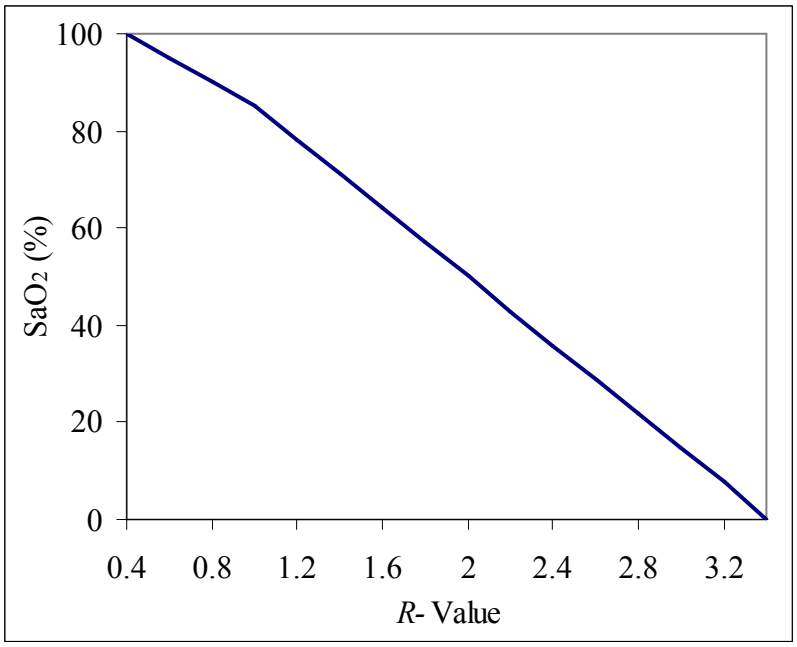

Figure 3.5. *Typical SaO_2 calibration curve* [13].

Time and frequency domain algorithms can be used to obtain noninvasive SpO_2 readings from PPG signals. Scharf et al have suggested that an algorithm based on spectral analysis can be implemented by making use of the Fast Fourier Transform (FFT) for the measurement of SpO_2 with clinically acceptable accuracy [23-25]. In a study that involved the design of a number of SpO_2 extraction algorithms for resting conditions, it was demonstrated that a time-domain algorithm based on differential changes in PPG signals provided accurate SpO_2 measurements, although spectral analysis produced similar results [12].

3.5. HR MEASUREMENT THEORY

Pulse oximeters provide HR readings since this measurement can help to determine physiological status. HR readings fluctuate with the physiological and psychological states and can indicate changes in the sympathetic nervous system [14]. Additionally,

heart rate variability (HRV) readings can be derived from HR measurements to help to assess the overall level of health [26].

The pulsatile (AC) component of the PPG is a function of the contraction (systolic) and relaxation (diastolic) phases of the cardiac cycle [13]. The upstroke of a PPG waveform tends to have a noticeably sharp rising slope which facilitates peak detection. The time between consecutive peaks is used to extract an average HR reading [13]. Another method to determine HR consists of applying spectral analysis and measuring the frequency corresponding to the most prominent spectral peak [23, 24], although a slope-detection routine, as demonstrated by Johnston, has been shown to provide the most accurate HR readings during resting conditions [12].

3.6. CUSTOM PULSE OXIMETER PLATFORM

A wireless wearable pulse oximeter platform was developed in our laboratory for remote physiological assessment and triage applications [26]. This thesis investigates the feasibility of increasing measurement reliability of the custom pulse oximeter. The custom platform fulfills essential design criteria for continuous real-time monitoring in field applications, including small-size, light-weight, unobtrusiveness, and low-power consumption.

The prototype wearable system is comprised of three units: A battery-operated optical Sensor Module (SM) mounted on the forehead, a belt-mounted Receiver Module (RM) mounted on the subject's waist, and a Personal Digital Assistant (PDA) carried by a remote observer. R and IR PPG signals acquired by the small (ϕ = 22mm) and lightweight (13g) SM are transmitted wirelessly via an RF link to the RM. The data

processed by the RM can be transmitted wirelessly over a short range to the PDA or a PC, giving the observer the capability to monitor multiple subjects simultaneously. The system, illustrated in Fig. 3.6, can be programmed to alert on alarm conditions, such as sudden trauma, or when physiological values are out of their normal range. Dedicated software is used to filter the reflected PPG signals and compute SpO_2 and HR based on the relative amplitude and frequency content of the signals. A triaxial MEMS ACC is incorporated to detect changes in body activity. In addition, the information obtained through the tilt sensing property of the ACC is used to determine body posture. Posture and acceleration measurements, combined with physiological information, can be useful to assess the status of (injured) persons/individuals in the field.

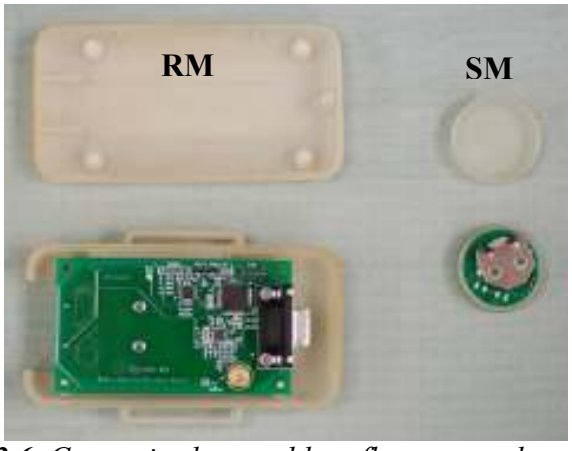

Figure 3.6. *Customized wearable reflectance pulse oximeter.*

3.7. LIMITATIONS TO PULSE OXIMETRY

A significant step in implementing a pulse oximeter for remote physiological monitoring is minimizing signal corruption due to movement induced artifacts, which cause a significant reduction in the SNR of the PPG signals. Motion artifacts can arise from perturbing motions during tidal breathing and shivering to more pronounced disturbances such as running [28-31]. Additionally, it has been suggested in the literature

that motion artifacts may arise from changes in arterial blood volume rather than decoupling between the PPG sensor and vascular tissues [32]. Similarly, some investigators suggested that the effects of motion artifacts arise from changes in venous blood volume [33].

Preliminary studies showed that the frequency of the PPG signal acquired from a forehead-worn reflectance transducer during indoor jogging consists of significant energy corresponding to the spectrum of the stepping frequency. For example, the frequency spectra of a PPG signal acquired while resting and running were derived using the FFT and are illustrated in Fig. 3.7A and 3.7B, respectively. These spectra suggest that the frequency of the PPG signal obtained during jogging is composed of the motion-induced noise, which decreases the SNR of the PPG and in turn the accuracy of SpO_2 and HR readings. The body acceleration data, depicted in Fig. 3.7C, was acquired during jogging trials in order to verify that the frequency of motion corresponds with the noise frequency present in the FFT of the PPG signal.

The frequency spectra of the body acceleration and PPG signals depicted in Fig. 3.7 provide evidence that during jogging, the underlying cardiac frequency spectrum is contained in the PPG signal although the motion frequency spectrum is more prominent. This demonstrates that the effects of motion artifacts significantly affect the SNR of the PPG signal.

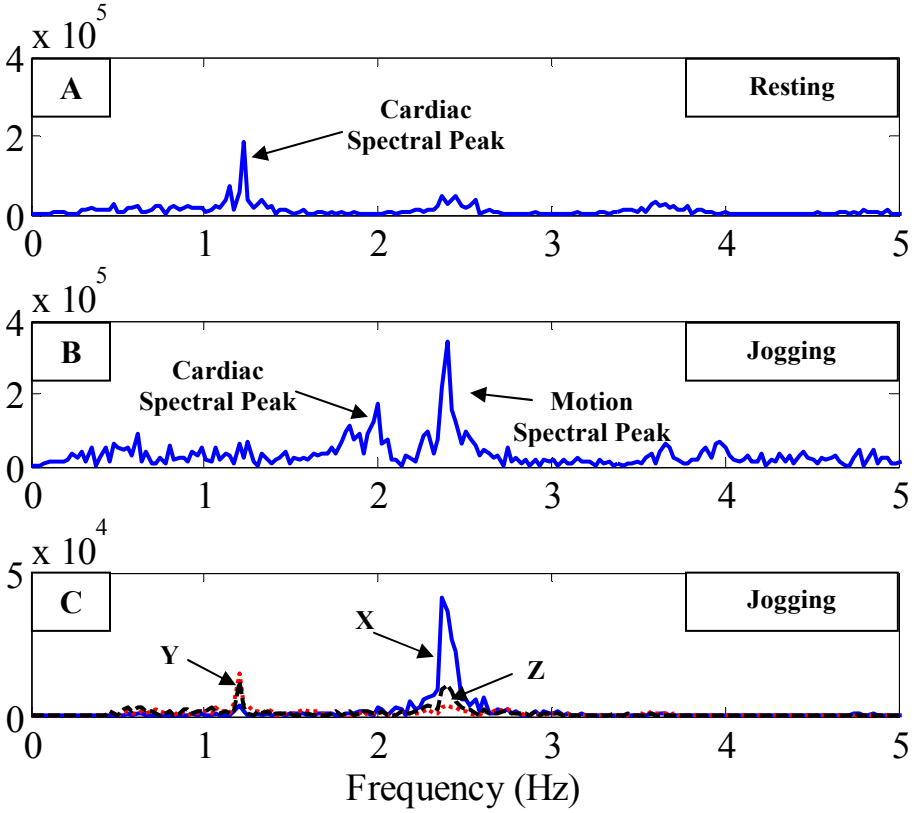

Figure 3.7. *(A) Frequency spectra of resting PPG signal, (B) PPG signal during indoor jogging, (C) and tri-axial ACC signals during indoor jogging.*

4. THE EFFECTS OF MOTION ARTIFACTS

Preliminary experiments were conducted to determine the effects of motion artifacts on SpO_2 and HR measurements during jogging. To extract measurements from PPG signals acquired during jogging the data were processed by algorithms developed by Johnston offline in Matlab™ [12]. Additional preliminary experiments were conducted to determine the effects of changes in physiology on measurement accuracy. To collect readings during exercises without significant head movements, experiments were performed using a stationary bicycle.

4.1. ACCURACY OF SpO_2 MEASUREMENTS DURING JOGGING

As described in the Background Section, SpO_2 measurements were obtained by estimating the relative concentration of HbO_2 to total arterial hemoglobin. The *SpO_2 Differential* algorithm developed by Johnston utilized signal derivatives to measure relative amplitudes of AC_R and AC_{IR} signals [12]. It was shown that accurate readings were measured by using this algorithm to process PPGs acquired during rest as well as during hypoxic events [20, 34].

The *SpO_2 Differential* algorithm calculated SpO_2 by using AC_R and AC_{IR} derivatives and raw DC_R, and DC_{IR} signal values. AC and DC signals were obtained by filters in software. AC derivatives that were equal to 0 were removed from the calculation of SpO_2 since these represented signal values are associated with motion artifacts [12]. To smooth the data, measurements were averaged by a moving average window.

Although the *SpO_2 Differential* algorithm could be used to record accurate measurements during rest, we found that the measurement accuracy diminished

significantly during activity due to reduced SNR of the PPG signals [35, 36]. Signal conditioning included low-pass (LP) and band-pass (BP) filtering to isolate the cardiac spectral band although advanced processing was limited. Generally, the SpO_2 extraction software was designed for resting conditions, so the algorithm did not incorporate sophisticated features to process motion-corrupted PPG signals.

Fig. 4.1 shows typical SpO_2 readings obtained by the algorithm devised by Johnston [12] and the Masimo pulse oximeter during periods of rest and jogging. It is clear that for resting conditions, there is less than a 2% mean difference between the SpO_2 readings obtained from the custom device and the Masimo reference measurements. During jogging, the readings obtained from the *SpO_2 Differential* algorithm developed by Johnston [12] deviated from the Masimo reference by over 7%, which suggests that an improved algorithm is required to obtain potentially more accurate SpO_2 measurements during activity. Fig. 4.1 shows that using the algorithm designed by Johnston [12], SpO_2 readings approached 85% for cases where the PPG signal was dominated by the effects of motion artifacts, which has also been described in [13]. This occurs since during intense movements, the effects of motion artifacts dominate the AC_R and AC_{IR} signals which cause the amplitudes to be equivalent. The resulting R values equal 1, so SpO_2 readings of 85% are calculated [13].

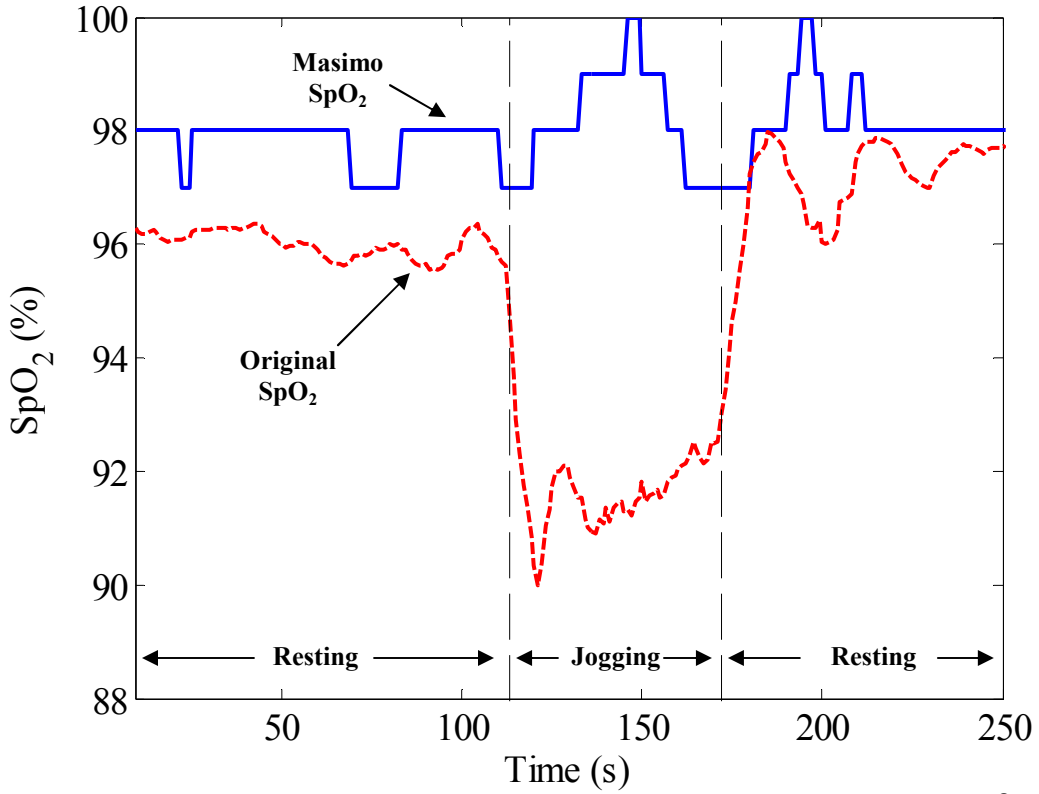

Figure 4.1. *Typical resting and jogging SpO_2 readings measured by Masimo® SET (solid) and the SpO_2 algorithm devised by Johnston (dashed) [12].*

4.2. ACCURACY OF HR MEASUREMENTS DURING JOGGING

The *Signal Derivative* algorithm developed by Johnston was used to extract HR readings from PPG signals. The *Signal Derivative* algorithm calculated HR readings obtaining differentials of PPG signals and peak identification [12]. The algorithm also incorporated a *Peak-Count Based* averaging routine in order to derive a HR reading from several instantaneous heart rate (IHR) measurements.

Despite promising results obtained during rest [12], this algorithm was not suitable for accurate HR measurement during jogging due to decreased SNR in PPG signals. Fig. 4.2 shows typical HR readings obtained from a forehead-worn PPG sensor during indoor jogging, demonstrating that the *Signal Derivative* algorithm provided unreliable readings during this type of activity. Inaccurate readings were obtained using this algorithm since

it incorporated all IHR values into an average HR reading. Therefore, values due to erroneous and missed peaks were not removed from the calculation of HR. Also, other, more advanced signal processing techniques were not implemented to reduce the effects of motion artifacts in corrupted PPG signals. From the example depicted in Fig. 4.2, it is evident that the HR measurements extracted by the software developed by Johnston [12] were relatively inaccurate. These measurements were due to missed true peaks (false negatives) as well as the detection of erroneous peaks (false positives). HR extracted using the *Signal Derivative* algorithm deviated from the Polar™ reference measurements by more than 15% during movement, although during rest, ± 4bpm was considered a clinically acceptable accuracy [13].

Due to an increased degree of breathing, PPG signals acquired activity jogging showed noticeable amplitude modulation [14]. Preliminary experimentation indicated that fluctuation in signal amplitude during jogging caused signal slopes to change significantly which lead to missed signal peaks when the *Signal Derivative* algorithm was employed. A representative PPG signal acquired during jogging is shown in Fig. 4.3. Due to changes in morphology and slope the signal peaks were missed by the peak detection algorithm. This caused erroneous IHR measurements to be incorporated into the average HR measurement.

Commercially available pulse oximeters, such as Masimo Signal Extraction Technology (SET®), typically employ intelligent software algorithms designed to cancel the effects of motion artifacts in real-time [22]. Despite the success of the Masimo SET®, our preliminary investigation during jogging suggests that measurements remain inconsistent as shown in Fig. 4.3. The acquisition of inconsistent HR measurements from

the Masimo SET® pulse oximeter, which is considered to be a widely popular pulse oximeter, suggests that the Masimo could be inappropriate for use in field applications.

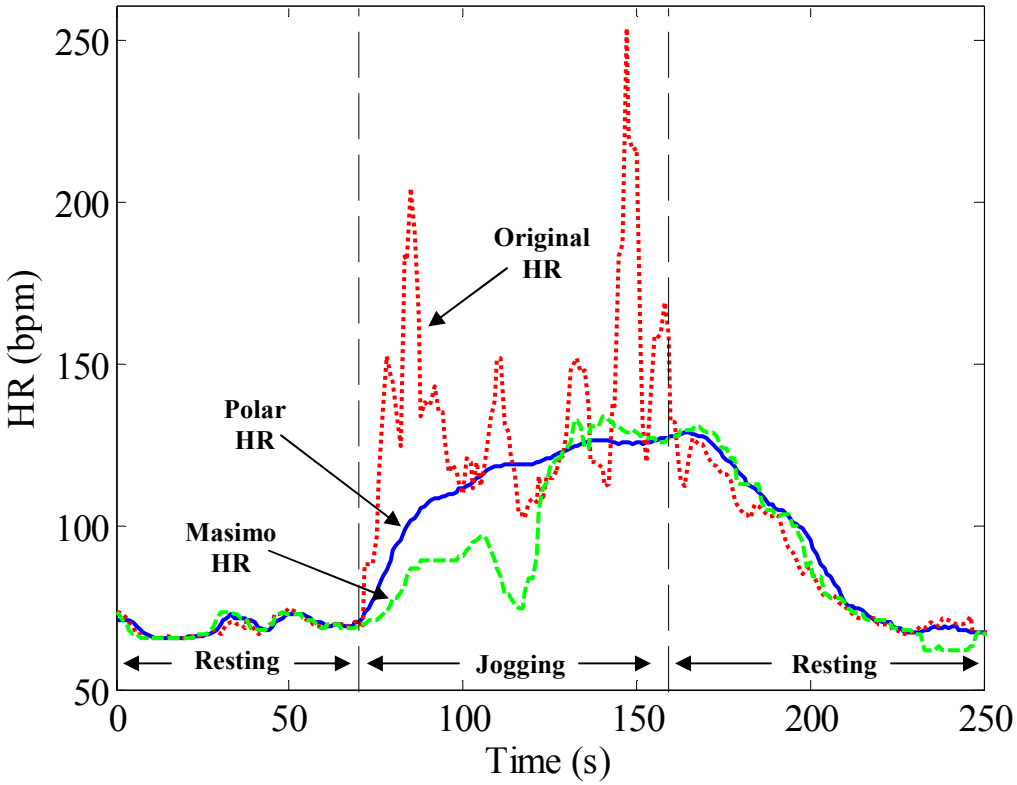

Figure 4.2. *Typical Polar™ ECG reference (solid), Masimo HR (dashed) and HR readings measured by the custom pulse oximeter (dotted) during indoor jogging.*

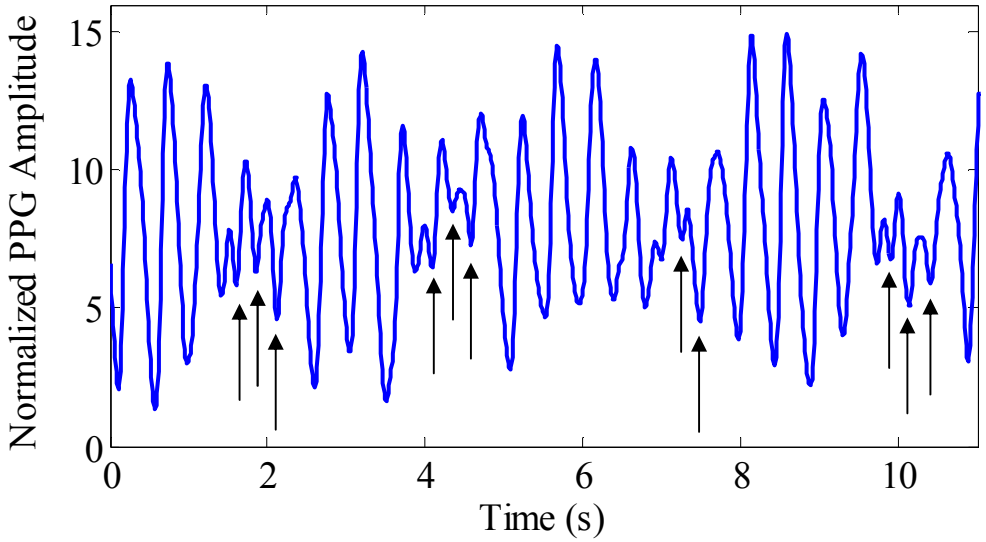

Figure 4.3. *Typical PPG signal acquired during jogging. Arrows designate missed peaks.*

5. Reducing the Effects of Motion Artifacts

Reducing the effects of motion artifact is a challenging problem since the frequency of movement is not known *a priori* and it can be within the range of the cardiac spectrum. Since the body acceleration and cardiac frequency spectra share a frequency band, ordinary LP or BP filters with constant cutoff frequencies cannot be utilized to remove the frequency component that results from body movements (*shown in Fig. 3.7*). Several advanced signal processing techniques suggested in the literature to overcome the effects of motion artifacts were reviewed. The following three sections review several potential methods for the reduction of motion artifacts in PPG signals.

5.1. Independent Component Analysis

A statistical analysis tool known as independent component analysis (ICA) has been studied by Kim et al [37] and Stetson et al [38] to reduce movement artifacts in PPG signals. ICA is a specific form of principal component analysis (PCA) which is a method of transforming a signal, or a dataset, into simpler parts, known as principal components, which can be used to simplify feature extraction in the data. ICA differs from PCA in that the separate components are statistically independent [39, 40].

The ICA model assumes independence between the motion artifact and PPG signal sources [37, 38]. However, some authors have suggested that movement and PPG signals are dependent [41, 42] which contradict the assumption of ICA for motion artifact and PPG signals. Generally, since motion artifacts are considered to arise from sensor movement in relation to the skin, motion and signal components should not be considered independent.

The literature suggests that an ICA-based method could be used to exploit certain statistical characteristics of PPG signals in order to separate and remove interference components from corrupted PPG signals [37, 38]. In simulated conditions, it was shown that an ICA-based approach provided an improvement in the SNR of PPG signals [38]. However, the results were limited to PPG signal quality and improvement in SNR but improvements in measurement accuracy were not reported. Also, since the types of motion artifacts induced included moderate hand motions rather than larger motions that would be observed in the field, the potential advantages of ICA in a practical setting are not clear.

Furthermore, the complexity of the software associated with this method could limit the feasibility of its implementation in an embedded μC [43]. For instance, the implementation of an ICA-based algorithm has not been demonstrated for use in a real-time and wearable device. Therefore, due to limited results as well as the significant degree of complexity regarding implementation of this algorithm, an ICA-based software algorithm was not considered for further study.

Two other approaches that could potentially help to reduce the effects of motion artifacts in PPG signals incorporate additional signals to reduce the effects of motion. These methods include three-wavelength oximetry and accelerometer-based adaptive noise cancellation as described below.

5.2. THREE-WAVELENGTH OXIMETRY

To reduce the effects of motion artifacts, Hayes and coworkers have suggested the use of an LED that emits light at a certain wavelength not common to the conventional R

and IR wavelengths utilized in pulse oximeters [41, 44, 45]. These authors have implied that signals obtained from an LED of a certain wavelength could be used as an indication of the noise present in motion-corrupted PPG signals. This method would require the absorption properties of such a wavelength to be independent of changes in arterial blood volume.

Additionally, despite the claims put forward by Hayes and Smith [41], little evidence has been presented in the literature regarding the implementation of an LED that illuminates at a suitable wavelength for this method. Although, some authors have suggested that this approach could be feasible for improving measurements obtained by a pulse oximeter [46], results have been limited.

For instance, employing this methodology, Hayes and Smith showed improvements in PPG signal quality during moderate hand movements [41, 44, 45]. The method has shown an improvement in SNR of the PPG signal during finger movements, such as tapping and waving, which could be found in a clinical setting [45]. Despite this success, it is disappointing to note that improvements in SpO_2 and HR measurement accuracy have not been reported. Further, a practical disadvantage of this approach is that supplying current to an additional LED could reduce battery life of a wearable pulse oximeter by about 33% which is undesirable for a battery powered device. Additionally, since the methodology assumes that only small changes in path length occur [45], this suggests that the technique would not be feasible for field applications during which larger movements are imposed on the sensor.

Despite the relatively small size of an LED, the integration of an additional LED into a wearable pulse oximeter has several disadvantages. It should be noted that

incorporating a third LED within a conventional pulse oximeter would complicate the sensor as well as the electronics associated with sampling the additional light absorption signal. The increase in power consumption and sensor complexity are significant shortcomings to this method. Also, since light absorption is related to blood constituents, there is limited potential to implement an LED whose absorption properties in tissue are independent of changes in arterial blood volume. Therefore, due to the disadvantages associated with the increasing the complexity of the pulse oximeter, increased power consumption, and since a limited amount of results regarding this approach have been presented, it was eliminated from further investigation.

5.3. ADAPTIVE NOISE CANCELLATION

The most promising approach to reduce the effects of motion artifacts is based on adaptive noise cancellation (ANC). The method utilizes body acceleration signals as a reference to the motion artifact components present in the corrupted PPG signals. ANC implements a notch filter with a rejection band centered at the frequency of body acceleration signal.

Acceleration signals can be obtained from micro-electromechanical system (MEMS) accelerometers (ACC) which are fabricated within small-size and low-power integrated circuits (IC). Employing a MEMS ACC as a noise reference for adaptive noise cancellation of motion artifacts in pulse oximetry has been suggested by several researchers [42, 47-51]. This approach was found to be promising since initial studies have included minor hand motions [47-49] as well as jogging activity [42, 50] which is of particular interest since our goal is to develop a method of remote physiological

monitoring from mobile individuals.

It should be noted that body acceleration signals provided by an ACC can be processed to determine the level of activity and body orientation of an individual [52]. This information would be particularly useful during remote monitoring and triage applications since it would enable medics to determine better the overall physiological state of an individual. Therefore, implementing ACC-based ANC would not increase the power consumed by the pulse oximeter since an ACC would be utilized for body acceleration and orientation information despite the method employed for the reduction of the effects of motion artifacts.

Further, it has been shown in the literature that an accelerometry-based ANC algorithm can provide improvements in HR measurements derived from a sensor attached to the fingers [48, 49, 51]. However, despite promising results, it was not reported whether more accurate SpO_2 measurements could be extracted from the recovered PPG signals and studies did not investigate the potential utility of transducers worn on the forehead which is a more practical measurement location compared to the fingers.

The ANC approach has been particularly promising since initial experimentation conducted for this thesis has demonstrated the efficacy of the ANC approach for the reduction of the effects of motion artifacts by a forehead-mounted PPG sensor during a study which included treadmill jogging [35, 36]. Although methods employing other signal processing techniques have been suggested by other researchers [37, 41], studies have been limited to moderate hand motions rather than running and improvements in SpO_2 and HR measurement accuracy were not reported. Work presented in the literature as well as our preliminary investigations suggest that the ACC-based ANC would be

effective in reducing the effects of motion artifact during jogging which is of particular interest for telemedicine applications.

6. ADAPTIVE NOISE CANCELLATION THEORY

An adaptive filter is a type of filter implemented in software that provides adjustable cutoff frequency based on filter input and output. This type of filter is required for certain applications in which the noise frequency to be removed is not known *a priori*. Adjustment of filter coefficients is performed by software algorithms designed to adapt continually to system input.

An ANC system can be modeled as a notch filter with a variable notch frequency that cancels the frequency of body acceleration which is used as a noise reference input [53]. The principle of noise removal is effective for noise comprised of two frequencies given that these frequencies are provided by the noise reference input [54].

The coefficients of the adaptive filter adjust to possess a band-pass filter (BPF) frequency response with a pass band centered around the frequency of the reference noise signal. Thus, the frequency of the noise present in the reference signal passes through the filter and is subtracted from the desired signal to remove the noise components. Widrow et al have demonstrated an example of adaptive noise cancellation theory applied to biomedical signals by the utilization of a maternal electrocardiograph (ECG) signal as a noise reference to recover the fetal ECG signal which is generally confounded by the frequency of the maternal ECG [54].

The adaptive filtering process consists of three separate stages: (1) filtering the noise reference input signal x[n], (2) subtracting the filtered noise reference input y[n] from the desired signal d[n], and (3) adjusting the filtering coefficients, or tap-weights $w_i[n]$, based on the difference between d[n] and y[n], known as the error signal e[n]. An adaptive filter block diagram is illustrated in Fig. 6.1. An assumption of the ANC system is that the

input noise reference and desired signals are not statistically correlated and that the noise contained in the reference input signal x[n] is added to d[n] as $x_1[n]$, which is the true noise present in the desired signal. The filter tap-weight vector $w_i[n]$ is calculated iteratively based on an updating algorithm such as the Least-Mean-Square (LMS) and the Recursive Least-Squares (RLS) algorithms due to their simplicity and popularity. Fig. 6.2 shows the block diagram of the Adaptive Filter portion of the ANC system. Similar to ordinary LP or HP filters, the adaptive filter component consists of scaling and summing *M* filter inputs. ANC systems are unique since the scaling vector changes continually during use of the adaptive filter.

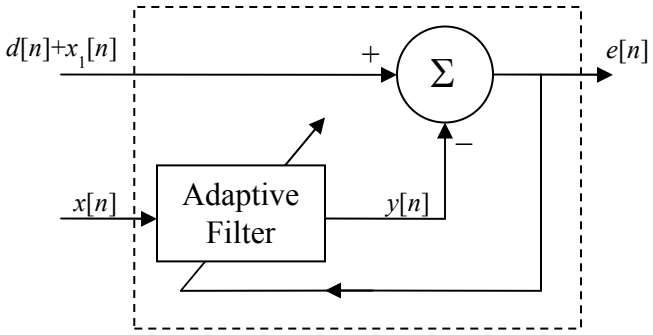

Figure 6.1. *Adaptive noise cancellation block diagram.*

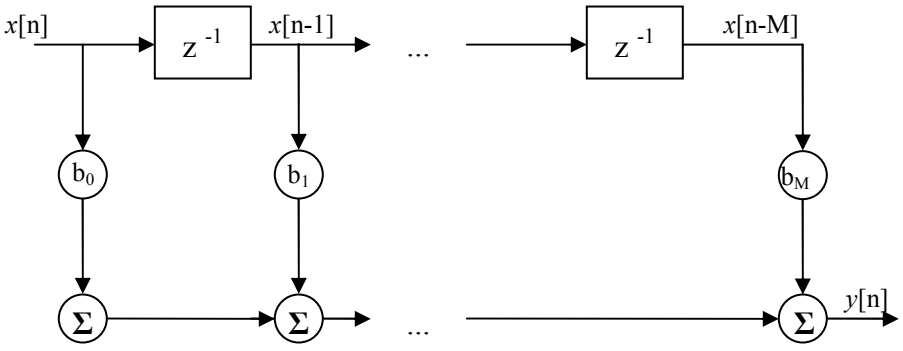

Figure 6.2. *Diagram of adaptive filter component of the ANC system. The noise reference input (x[n]) is passed through a delay line (represented by z blocks); the tap-weights (b_i) multiply the delayed x[n-i] which are summed to form y[n] [53].*

6.1. LMS AND RLS ALGORITHMS

The LMS and RLS are two mean square error reduction algorithms which can be used to update the tap-weights of an adaptive filter.

LMS Algorithm

The LMS algorithm approximates the method of steepest descent optimization function and the instructions used to implement the algorithm can be executed by a small number of discrete-time operations. The number of computations required to implement the LMS algorithm is relative to the filter order, *M*, which is the number of filter coefficients within the adaptive filter tap-weight vector; this degree of complexity is comparable to the complexity of a finite impulse response (FIR) filter with a weight vector composed of fixed values [55].

In additional to the filter order parameter, μ, the LMS algorithm consists of the scalar μ, known as the step-size, which is a design parameter that affects the learning rate, stability, and band-width of the adaptive filter. Step-size is generally chosen empirically based on the statistical properties of the input signal.

Equation (6.1) represents the adaptive filter portion of the LMS filter. y[n] is the adaptive filter output, M is the filter order, $w_i[n]$ is the tap-weight vector, and x[n] is the noise reference input signal.

$$y[n] = \sum_{i=0}^{M-1} w_i[n] \bullet x[n-i] \tag{6.1}$$

The output of the ANC, *e[n]*, is formed by subtracting the filtered input signal, *y[n]*, from the desired signal, *d[n]*, as shown by equation (6.2).

$$e[n] = d[n] - y[n] \tag{6.2}$$

The following equation illustrates the simplicity of the LMS algorithm. The filter tap-weights change dynamically as shown by equation (6.3).

$$w_i[n+1] = w_i[n] + \mu \bullet x[n-i] \bullet e[n] \tag{6.3}$$

where $w_i[n]$ is the present filter coefficient, μ is the step-size, $e[n]$ is the present error signal, $x[n-1]$ is the present input signal, and the index of the filter weights, i, varies from 0 to M-1, where M is the filter order. The LMS adaptive algorithm consists of $2M + 1$ multiplications per iteration [56].

A primary advantage of the LMS algorithm is that a low number of computations are required relative to the RLS-based adaptive algorithm. In general, the amount of resources (i.e. memory, execution time, processor power) needed to implement the LMS algorithm is less than the RLS algorithm.

The μ parameter associated with the LMS adaptive filter affects directly the updating process of the adaptive filter coefficients. For example, the literature shows that high-valued μ (i.e. $\mu = 0.075$) provide a relatively higher rate of convergence compared to small-valued μ (i.e. $\mu = 0.0075$) [53]. However, μ affects the ensemble-average-square error obtained by the adaptive filter. For instance, although there was a longer convergence time associated with $\mu = 0.0075$, the literature showed that this value provided a lower error compared to $\mu = 0.075$ [53]. Similarly, the λ parameter affects the "memory" of the RLS adaptive filter. Although $\lambda = 1$ during theoretical analysis of the RLS algorithm, several authors suggest that $0.9999 \leq \lambda \leq 1$ in practice [53, 57, 58].

RLS Algorithm

The RLS algorithm operates on the same basis as the LMS algorithm although the scaling

factor, known as the step-size parameter of the LMS algorithm, is known as the Kalman gain of the RLS algorithm. Additional signal processing requirement associated with the RLS algorithm provides a faster learning rate and can obtain a smaller error signal at the cost of longer execution time and processor power consumption. Specifically, the RLS algorithm performs $1.5M^2 + 4.5M$ multiplications per iteration.

The filter coefficients change dynamically based on the RLS algorithm which incorporates the following tap-weight update function, shown in equation (6.4).

$$\hat{w}_i[n+1] = \hat{w}_i[n] + k[n] \bullet \xi^*[n] \tag{6.4}$$

where,

$$k[n] = \frac{\pi[n]}{\lambda + u^H[n] \bullet \pi[n]}$$

$$\pi[n] = P[n-1] \bullet u[n]$$

$$\xi[n] = d[n] - \hat{w}^H[n-1] \bullet u[n]$$

and

$$P[n+1] = \lambda^{-1} \bullet P[n] - \lambda^{-1} k[n] \bullet u^H[n] \bullet P[n]$$

Comparison of LMS and RLS Algorithms

Although the LMS and RLS adaptive algorithms provide similar adaptive noise cancellation, the algorithms differ significantly by their learning rate and computational complexity. The learning rates of the LMS and RLS algorithms are quantified as *20M* and *2M*, respectively. This implies that a low order RLS adaptive filter can learn quickly and potentially remove noise from a desired signal to a degree similar to a higher order LMS filter. Filter order has significant implications since a low order filter implies less computational cost, which is desirable in real-time applications. Additionally, the RLS

algorithm requires on the order of M^2 computations per iteration, which is significantly larger than the LMS algorithm which requires only M computations per iteration. The specific processing requirements of the RLS and LMS algorithms include the computation of $1.5M^2 + 4.5M$ and $2M + 1$ multiplications per iteration, respectively. Note that the computational complexity and SpO_2 and HR measurement accuracy are the primary considerations in the implementation of the LMS and RLS algorithms for real-time applications.

6.2. ACCELEROMETER-BASED ANC

It has been suggested that acceleration signals provided by an ACC can be used to model the general motion which corrupts the PPG signal [42]. Preliminary experimentation has confirmed that the frequency of body acceleration is present in PPG signals acquired during jogging and that an ACC integrated within a forehead-worn PPG sensor can be used to measure the frequency of body acceleration. Foo et al [49] have shown promising results by utilizing a triaxial ACC while Asada et al [59] have suggested that using a single-axis ACC could provide significant reduction of the effects of motion artifacts.

7. RESEARCH OBJECTIVES

An accelerometry-based ANC approach was investigated to determine the ability to improve the SNR of PPG signals and to increase the accuracy of SpO_2 and HR measurements extracted from motion corrupted PPG signals. The following is a list of the specific objectives.

Objective 1
To design and test the accuracy of improved software routines developed by Johnston [12] to reject erroneous readings typical during jogging activity and extract SpO_2 and HR from R and IR PPG signals during jogging.

Objective 2
To design and test the accuracy of ACC-based ANC software to adaptively filter corrupted R and IR PPG signals during jogging.

Objective 3
To determine the effects of spectral overlap between ACC and PPG signals.

Objective 4
To determine the feasibility of implementing the proposed ANC software routine within an embedded TI-MSP430 μC environment.

8. METHODOLOGY

8.1. PRELIMINARY EXPERIMENTS

A preliminary study was performed to determine the effects that changes in physiology had on measurements without corruption by motion artifacts. In order to conduct this study, body acceleration, PPG and measurement data were acquired from an individual during 1-minute stationary cycling trials framed by 2-minute sitting periods. Fig. 8.1 shows the commercial stationary bicycle used for preliminary experimentation. The experimental setup also consisted of the custom pulse oximeter (*SM and RM components*) and the Masimo SET™ pulse oximeter employing a forehead-worn sensor, which was used since the hands were needed for body stabilization during cycling.

Figure 8.1. *Commercial stationary bike used for preliminary experimentation.*

8.2. EXPERIMENTS

To address the objectives of this thesis, a series of outdoor and indoor experiments were conducted to determine the feasibility of ACC-based ANC to increase the accuracy of SpO_2 and HR measurements when subjects are active.

8.2.1. EXPERIMENTAL SETUP AND PROCEDURE

Fig. 8.2 shows the experimental setup for data collection during treadmill jogging.

Participants were instructed to grasp the backpack strap to keep the finger-worn sensor in a stationary position during free indoor and outdoor jogging.

As previously described, the forehead-worn reflectance SM consists of an optical transducer, a stack of round PCBs, and a coin-cell battery. It should be noted that the current draw associated with the LEDs located on the SM were configured to the default setting of 5mA. The belt-worn RM is comprised of an embedded μC for processing information acquired wirelessly from the SM via a RF link, an RF transceiver, and two 1.5VDC batteries [27]. For data storage, data were transmitted from the RM via a Universal Asynchronous Receive Transmit (UART) to a laptop PC carried by the PI during the studies.

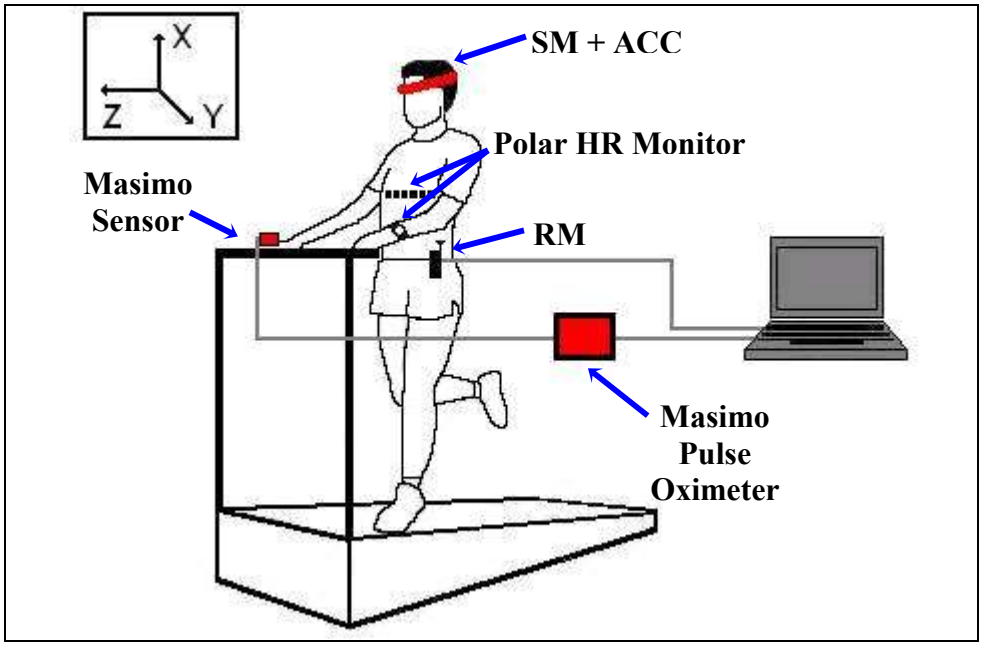

Figure 8.2. *Experimental setup.*

LabVIEW software was utilized for collection of body acceleration, PPG data, and Masimo SET® SpO_2 and HR reference measurements. Jogging experiments were performed on a treadmill (*N = 16*), indoors on free terrain (*N = 12*) and outdoors on free terrain (*N = 4*). Treadmill jogging was incorporated into this study since it ensured that

motion was maintained at a constant rate. Indoor and outdoor jogging allowed volunteers to jog at a free pace and move more naturally.

Participants performed 1-minute jogging trials (*treadmill rates: 3.5 – 6.5mph*) framed by 2-minute resting periods. To test SpO_2 and HR accuracy over a wide range, a brief hypoxic event was incorporated into three trials. SpO_2 and HR reference measurements were acquired from the Masimo SET® pulse oximeter employing a finger-worn transmission sensor which was immobilized during the experiments. In addition, HR reference measurements were obtained from a chest-worn Polar™ ECG monitor. Seven healthy, non-smoking volunteers (*6 males, 1 female)*, ages ranging from 22 to 27 years, participated for this study. Institutional Review Board (IRB) approval was obtained prior to experimentation. For safety reasons, restrictions of the experimental protocol by the IRB required that SpO_2 readings do not drop below 94% for longer than 1 minute and HR values should not exceed 130bpm for more than 2 minutes in a given trial.

8.2.2. DATA ACQUISITION SYSTEMS

The body acceleration and PPG data were acquired by a laptop PC via a DAQCard-6063e data acquisition card, BNC-2120 breakout box and RS-232 serial connection. A custom LabVIEW program was utilized to store body acceleration and PPG data for offline Matlab processing. The custom LabVIEW software also acquired SpO_2 and HR readings from the Masimo pulse oximeter via RS-232 serial connection. HR data acquired by the Polar™ ECG were stored within the Polar™ wrist watch module and extracted after the study was completed.

Raw PPG data were filtered offline in Matlab in order to separate the signal into AC and DC components. A 2^{nd} order Butterworth LPF (F_C = 0.05Hz) and a 6^{th} order

Butterworth BPF (F_{C1} = 0.5Hz, F_{C2} = 3.0Hz) were utilized to obtain DC and AC components, respectively. Similar filters were used by Johnston in order to separate the frequency of interest from the raw PPG signals [12].

The tri-axial ACC provided body acceleration signals, which were sampled by the LabVIEW hardware, although the analog-to-digital converter (ADC) contained within the TI-MSP430 microcontroller (μC) could be utilized to sample the analog output signals from the ACC. The ACC signals were filtered offline in Matlab in order to separate the AC and DC components of body acceleration. AC signals were obtained by using a 6^{th} order Butterworth BPF (F_{C1} = 0.5Hz, F_{C2} = 3.0Hz). The AC signals were utilized in the ACC-based ANC algorithm.

8.2.3. AVERAGING SpO_2 AND HR MEASUREMENTS

Measurement averaging times for the Masimo pulse oximeter were selected as 10s as a compromise between the fast (2s) and slow (16s) averaging settings available in the commercial pulse oximeter; the SpO_2 and HR measurements extracted from the PPG signals acquired unobtrusively from the forehead-worn SM were averaged by 10s averaging windows (*8s was also used for 6 of 32 trials*). To be consistent, the R-wave interval times (RR intervals) provided by the Polar™ ECG were averaged by a moving averaging window of identical size. The range of averaging times (*2s to 16s*) of the Masimo SET® is typical for commercial pulse oximeters [28].

8.3. OFFLINE PROCESSING

Raw body acceleration and PPG data were collected by LabVIEW and stored in a file format readable by Matlab. Processing of SpO_2 and HR data were performed in Matlab.

Statistical analyses were performed using the SAS software environment.

8.3.1. EXTRACTION OF SpO_2 AND HR MEASUREMENTS

Algorithms for SpO_2 and HR extraction algorithms were written in Matlab based on software described by Johnston [12].

SpO_2 Readings

The *SpO_2 Differential* algorithm developed by Johnston [12] incorporated a routine to reject PPG signal derivatives that were equivalent to 0. In an effort to reduce the effects of motion artifacts, the *SpO_2 Differential* algorithm was modified to remove derivative values that were less than a threshold value. The threshold was based on the mean signal derivative value of the AC component of the PPG signals. The modified software was designed to reject outlying signal derivative values since erroneous signal derivatives occurred during motion.

Averaging of HR Readings

HR readings were obtained in software by averaging several IHR measurements. The *Peak Count-Based Averaging* scheme that was devised by Johnston [12] was dependent on IHR peak count. Therefore, fluctuations in HR level caused variations in averaging window size which resulted in inconsistent HR measurements. This averaging routine was modified by implementing the *Time-Based Averaging* algorithm which was based on a constant-length time averaging window. This modification was implemented in order to prevent the HR value from affecting the averaging window.

R and IR Based HR Algorithm

The *Signal Derivative* algorithm devised by Johnston [12] extracted HR readings from PPG signals by processing the AC component of the IR signal. In order to obtain potentially more accurate HR readings during jogging, this algorithm was modified to incorporate the AC component of the R signal. The detection of multiple peaks as well as missed peaks contributes to inaccurate HR readings. The *R and IR Based HR Algorithm* modification was based on the rejection of outlying IHR values measured from either the R or IR signals. For instance, an IHR measurement extracted from the R signal would be incorporated in the average HR reading unless the value differed significantly from the IHR measurement obtained from the IR signal and visa versa.

IHR Threshold

An additional modification was incorporated the calculation of HR in order to extract more accurate HR readings. Similar to the *R and IR Based HR Algorithm*, this algorithm change consisted of calculating more accurate HR readings by removing significantly outlying IHR values. A threshold based on the average HR reading was utilized to classify outlying IHR readings. Therefore, if an IHR value was significantly lower or higher than the average HR reading, the IHR value would not be incorporated in the calculation of HR.

In addition to implementing the modifications to the SpO_2 and HR algorithms, ACC and PPG data were analyzed to determine the efficacy of obtaining more accurate readings by making use of ANC software available in Matlab.

8.3.2. ACCELEROMETER-BASED ADAPTIVE NOISE CANCELLATION

An accelerometry-based adaptive noise cancellation algorithm was implemented

offline in Matlab. Analyses included testing the effects of filter order as well as step-size and forgetting factor parameters of LMS and RLS adaptive algorithms, respectively. Root mean squared errors (RMSE) were calculated as the mean difference between the reference measurement and measurement obtained from the custom pulse oximeter during jogging; RMSE were used as an indication of the performance of the adaptive filter algorithms.

Accelerometer Axis Selection as a Noise Reference Input Signal

Experiments were performed to determine which axis of the ACC could provide the most appropriate noise reference input to reduce the effects of motion artifacts. The orthogonal X, Y, and Z axes, as well as the linear summation (X+Y+Z), were processed as noise reference inputs of the acceleration axes.

Filter Optimization

The step-size (μ) and filter order (M) of the LMS adaptive filter were varied separately to determine the optimal filter parameters. Likewise, the forgetting factor (λ) and filter order (M) were varied to independently determine the optimal parameters of the RLS filter. Adaptive filter order affects the execution time, learning rate, and RMSE. Separate studies were performed to determine the optimal type and order for the adaptive filter algorithms by implementing these algorithms inside the embedded μC.

8.3.3. ACC AND PPG SIGNAL TIME DIFFERENCE

It has been suggested in the literature that significant time differences exist between body acceleration and PPG signals [59]. The effect of time delays between ACC and PPG signals on measurement accuracy was investigated by calculating the cross-correlation

for various time-shifts. To determine the potential effect of time lags between ACC and PPG signals could have on measurement accuracy, SpO_2 and HR measurements were calculated for the time-shifted signals.

8.3.4. ACC LOCATION

In order to obtain a reference signal for the ACC-based ANC algorithm, an ACC was incorporated into the forehead-worn PPG sensor. A study was not performed to determine the effect of ACC placement on various body locations since an inherent assumption of the ACC-based ANC algorithm is that signal corruption is due to local perturbations at the skin-sensor interface.

8.4. SPECTRAL OVERLAP

The adaptive noise canceling process can be modeled as an FIR noise-reject filter with an adapting cutoff frequency. The frequency spectrum of ACC and PPG signals can overlap if stepping frequency coincides with the cardiac frequency. It was suggested by Asada et al that similar acceleration and cardiac spectral bands can cause attenuation of the cardiac frequency and lead to inaccurate readings [60]. Since it was expected that body acceleration matching the subject's cardiac frequency would cause deterioration in the SNR of the recorded PPG signals, we investigated the effect of cardiac and motion frequency overlap.

Spectral Overlap Simulation

In order to simulate frequency overlap conditions, sine waves were created and processed to mimic body acceleration and PPG signals offline in Matlab using custom ANC

routines. Various degrees of spectral overlap were studied by simulating body acceleration and PPG signals over a range of frequencies. To determine the effects of spectral overlap simulations, the spectral content of the sine waves were determined before and after ANC processing.

Spectral Overlap Experimentation

Experimental trials that possessed body acceleration and PPG signals with overlapping spectral bands were processed by adaptive filters in Matlab and measurements were extracted from the adapted signals to determine the effect of spectral overlap during running trials. Measurement accuracy was compared before and after applying the ANC algorithm.

8.5 REAL-TIME ADAPTIVE NOISE CANCELLATION

In order to determine the feasibility of implementing an ACC-based ANC algorithm in an embedded μC, the LMS and RLS adaptive algorithms were implemented within the TI-MSP430 and execution times were measured. Two methods were considered: (1) utilizing Simulink and Real-Time Workshop® software (Matlab™) to generate the C code for implementing the algorithms, and (2) developing custom written LMS and RLS algorithms based on the discrete-time functions commonly available in the literature.

Real-Time Workshop (Matlab™)

A potential approach to implement an ANC algorithm in an embedded μC is to utilize Simulink and Real-Time Workshop® software. Generally, since the LMS and RLS adaptive algorithms are comprised of basic discrete-time operations, it is simpler to

design custom adaptive functions in the C programming language than to employ functions generated via Real-Time Workshop®.

Custom LMS and RLS Algorithms

Custom ANC functions were implemented in Matlab based on the LMS and RLS algorithms. The outputs of the custom functions were compared to the outputs of the Matlab functions in order to verify that the custom routines provided the same functionality as the Matlab routines. Since the focus of this work is on real-time processing, the custom algorithms were rewritten in the C programming language and implemented within the TI-MSP430 microcontroller (μC) environment to determine the feasibility of implementing adaptive algorithm software in a real-time embedded μC.

9. RESULTS

9.1. PRELIMINARY RESULTS

In order to determine the effects of physiological changes on SpO_2 and HR accuracies, stationary cycling experiments were conducted. Representative PPG signals acquired during cycling, as shown in Fig. 9.1, were processed in Matlab. Fig. 9.1 shows that PPG signals obtained during rest had slightly greater amplitudes than signals obtained during cycling. This result could have been caused by differences in breathing during bicycling as compared to breathing during resting. Also, due to body activity associated with cycling, these PPG signals had a higher frequency content than signals obtained during rest.

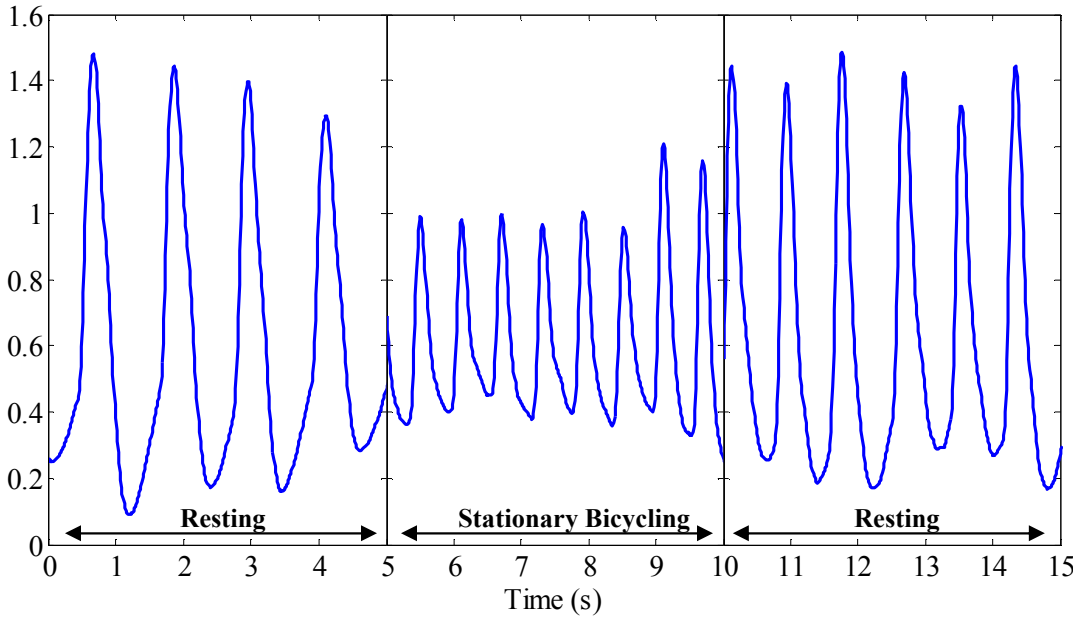

Figure 9.1. *Representative IR PPG signals before, during, and after stationary bicycling.*

Fig. 9.2 shows representative FFT spectra of body acceleration and PPG signals. This result indicated that the frequency spectra of the PPG signals acquired during bicycling were similar to the frequency content during rest, shown in Fig. 3.7. Compared to

jogging, there was a low degree of movement during cycling, although the FFT spectra of the ACC signals show a frequency band centered near 1Hz coinciding with the rate of body acceleration. Due to limited body movement, the FFT spectra indicated that the ACC signals have a relatively low SNR. In addition, Fig. 9.2 shows that the FFT spectra of the PPG signals did not change after processing using the ANC algorithm. This occurred because the PPG signals were not compromised by motion.

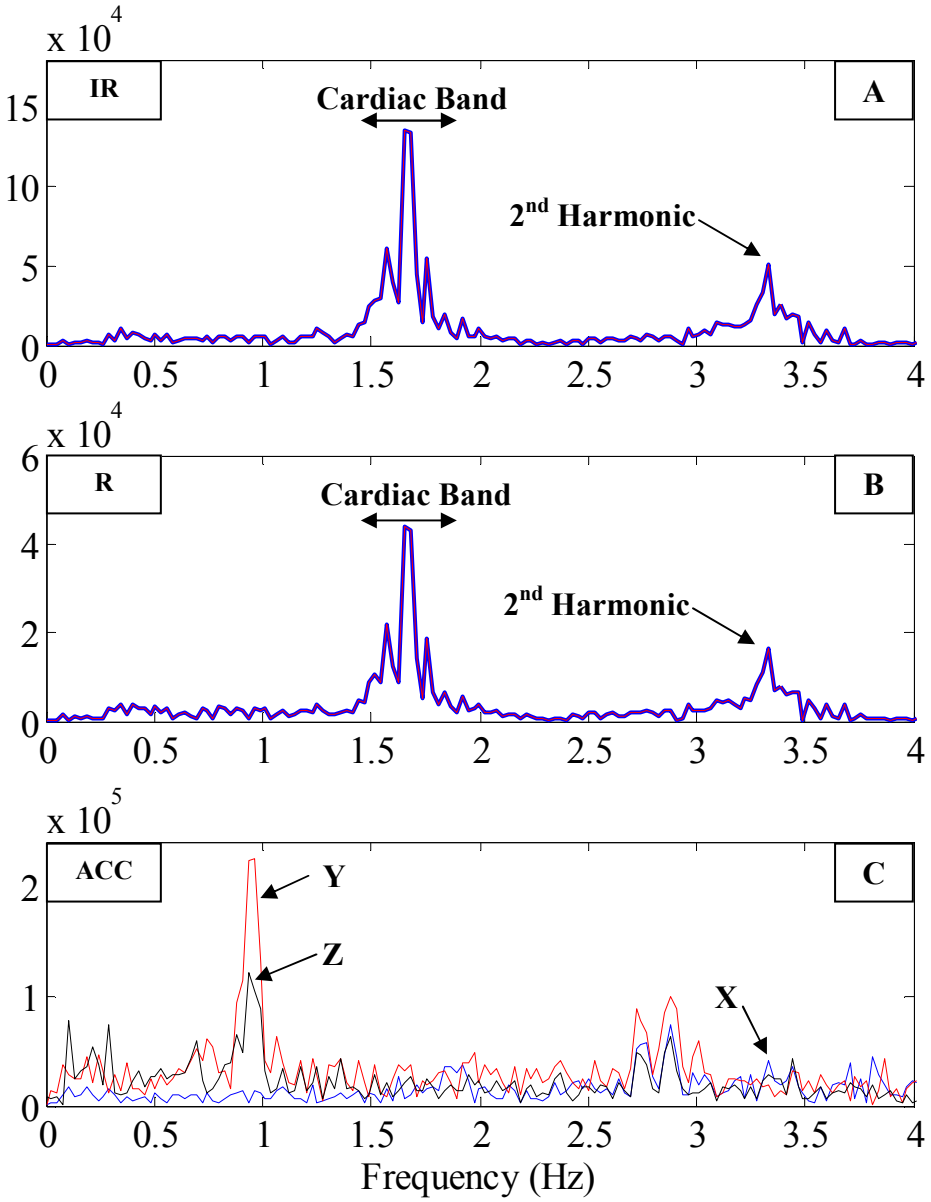

Figure 9.2. *(A) Representative FFT spectra of IR PPG, (B) R PPG, and (C) corresponding ACC signals during stationary bicycling.*

9.2 ALGORITHM MODIFICATIONS

In order to extract more accurate SpO_2 and HR measurements during jogging the algorithms developed by Johnston [12] were modified. The modifications described in the Background section were implemented in Matlab. These modifications were integrated with ACC-based ANC software as described in Section 8.2.3.

9.2.1. EXTRACTION OF SpO_2 MEASUREMENTS

In order to remove signal derivatives associated with motion artifacts, an adaptive signal differential threshold was incorporated into the SpO_2 algorithm devised by Johnston [12]. Fig. 9.3 shows a typical resting PPG signal, its corresponding derivatives. The *SpO_2 Differential Threshold* algorithm, shown in Fig. 9.3 (D), was designed to be adjustable based on past signal derivatives; derivative values that do not meet the threshold were discarded.

Fig. 9.4 shows a typical PPG signal and its corresponding derivatives acquired during jogging. SpO_2 measurements extracted from the PPG signals acquired during jogging are shown in Fig. 9.5. These measurements were obtained using the algorithm developed by Johnston [12] and the *SpO_2 Differential Threshold* described in the Background section. Fig. 9.5A provides an example of an experimental trial during which SpO_2 readings increased slightly during jogging (*with the exception of the hypoxia period*). Conversely, Fig. 9.5B shows an example of an experimental trial during which SpO_2 readings decreased during the jogging activity.

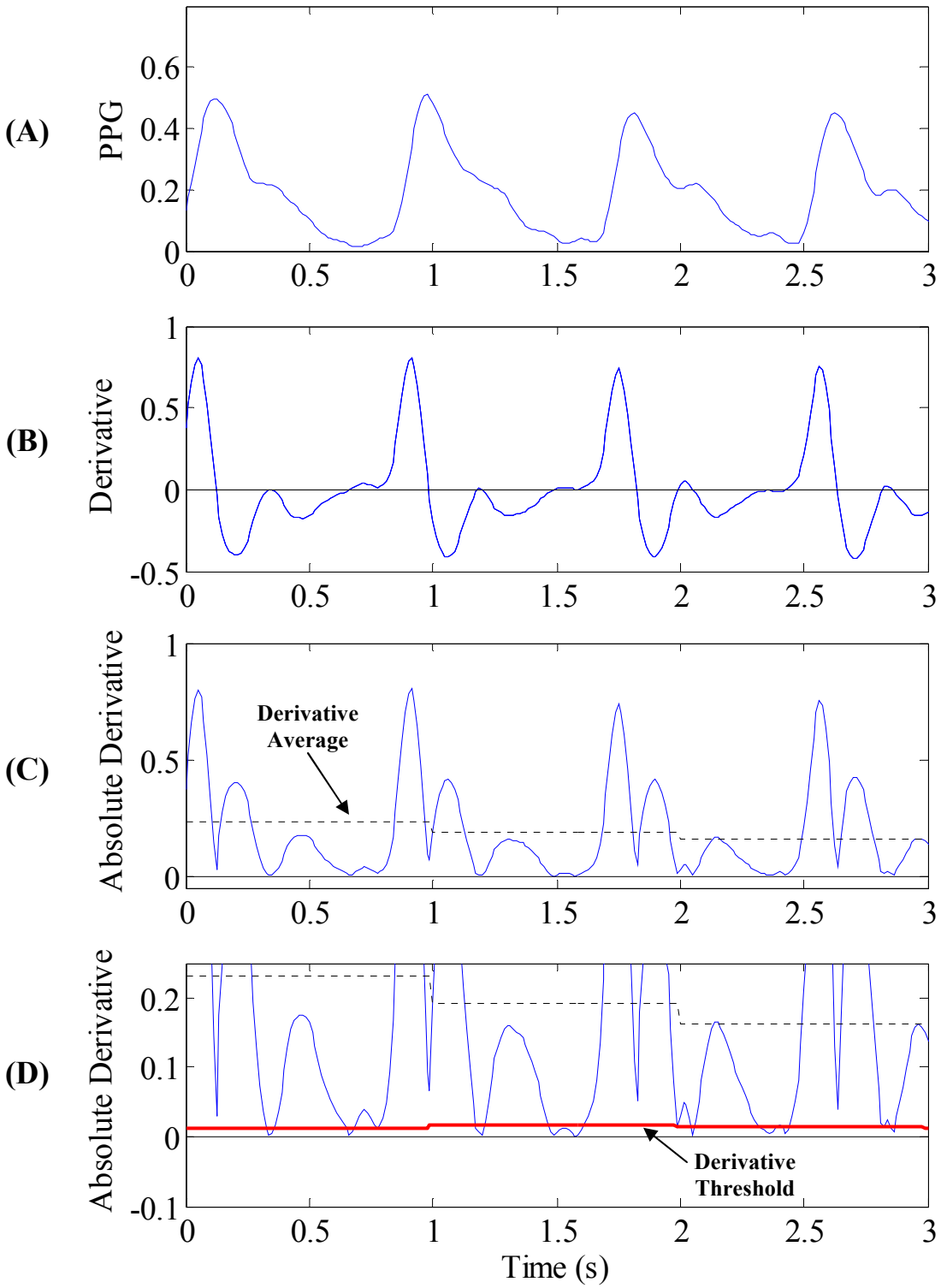

Figure 9.3. *(A) Typical resting PPG signal, (B) corresponding derivative, and (C) absolute derivative. The absolute derivative and the adapting derivative threshold are shown in (D).*

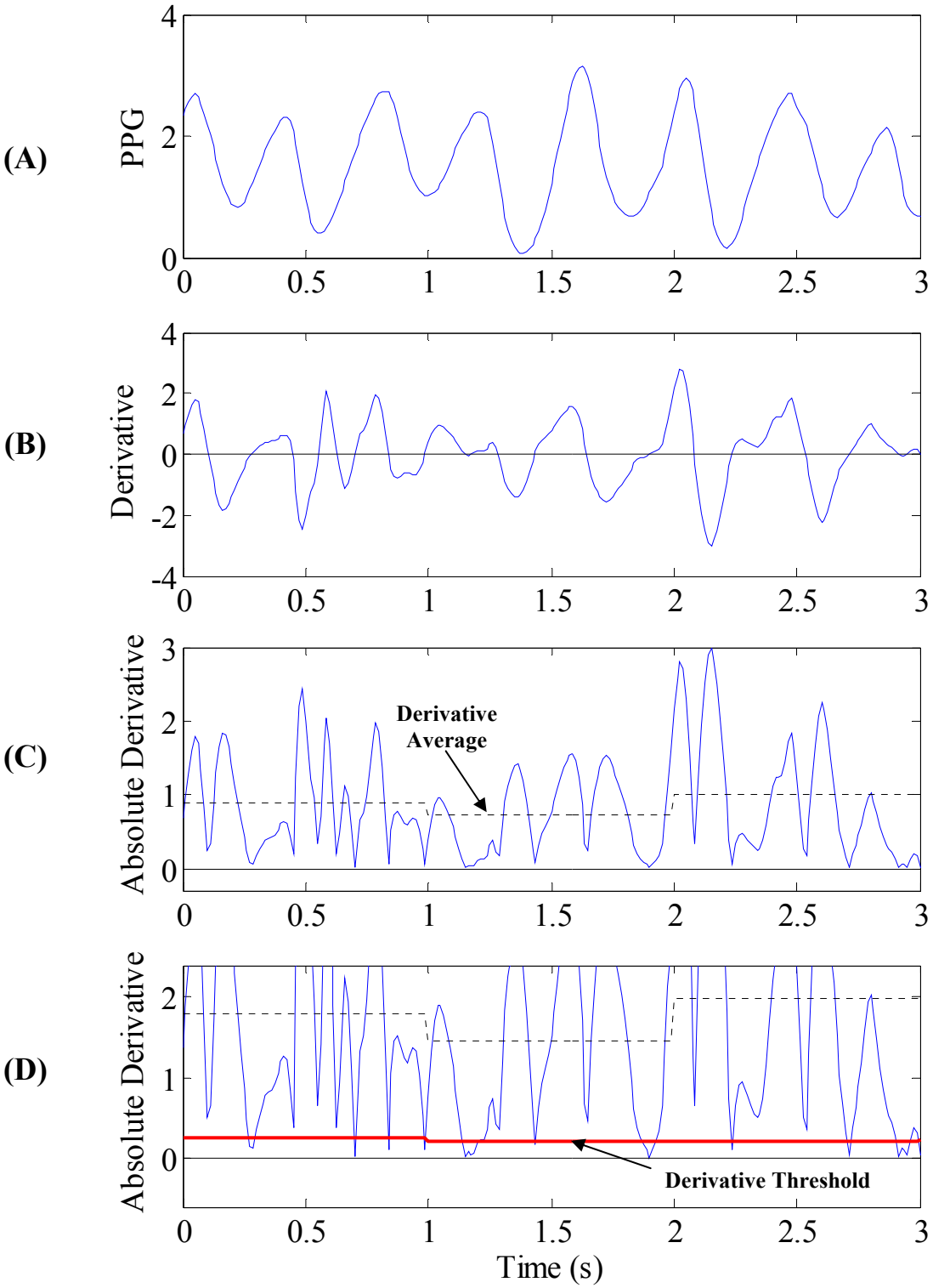

Figure 9.4. *(A) Typical PPG signal during jogging, (B) corresponding derivative, and (C) absolute derivative. The absolute derivative and the adapting derivative threshold are shown in (D).*

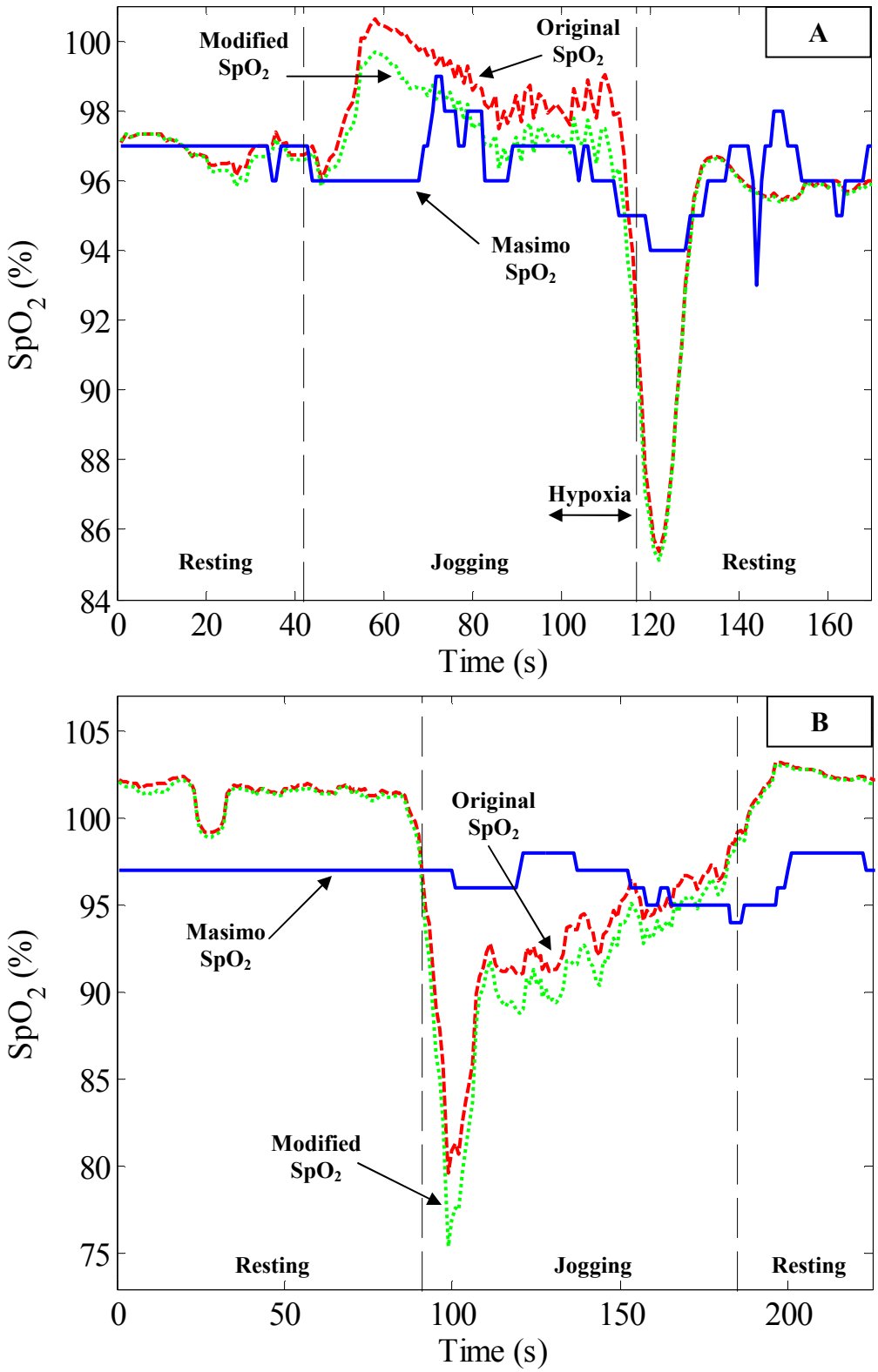

Figure 9.5. *Representative SpO_2 measurements. (A) An example of a jogging trial during which the calculated SpO_2 approached 100%. (B) An example of a jogging trial during which the calculated SpO_2 approached 85%.*

Generally, compared to the algorithm devised by Johnston, the modified SpO_2 algorithm produced lower SpO_2 measurements. Since SpO_2 readings decreased (*approached 85%*) during jogging, the additional drop in values associated with the *SpO_2 Differential Threshold* caused less accurate measurements to be obtained during jogging. Lower SpO_2 values were due to the rejection of derivative values that did not meet the threshold which adapted based on prior signal derivatives.

9.2.2. EXTRACTION OF HR MEASUREMENTS

Time-Based Averaging

The *Peak Count-Based Averaging* routine designed by Johnston [12] was based on calculating the mean of 10 IHR values. Since this averaging scheme would incorporate the 10 most recent IHR values, the major drawback was that the length of time represented by the HR measurement changed depending on the heart rate. Conversely, the *Time-Based Averaging* scheme described in the Background section incorporated a time window of constant length. Therefore, HR calculated using this method consistently represented 10s of heart beats.

Fig. 9.6 shows HR measurements obtained from *Peak Count-Based Averaging* according to Johnston [12], *Time-Based Averaging*, and Polar™ HR measurements acquired concurrently during rest. The results show that the *Peak Count-Based Averaging* window is affected by the value of the HR. For example, the *Peak Count-Based Averaging* scheme incorporated 10 past IHR values, although the modified averaging scheme incorporated the past 10s of IHR values. Therefore, as shown in Fig. 9.6A, the averaging schemes provided similar measurements for an average HR of 60bpm. Conversely, Fig. 9.6B shows that during more rapid HR, where 10 beats represents less

time (*the Peak Count-Based Averaging routine provides 6s window an average HR of 95bpm*), the measured HR values differed significantly. In this example, since the *Peak Count-Based Averaging* scheme averaged less IHR values, the average HR responded too quickly to changes in HR. Therefore, HR readings were more instantaneous and did not indicate a more accurate average HR measurement.

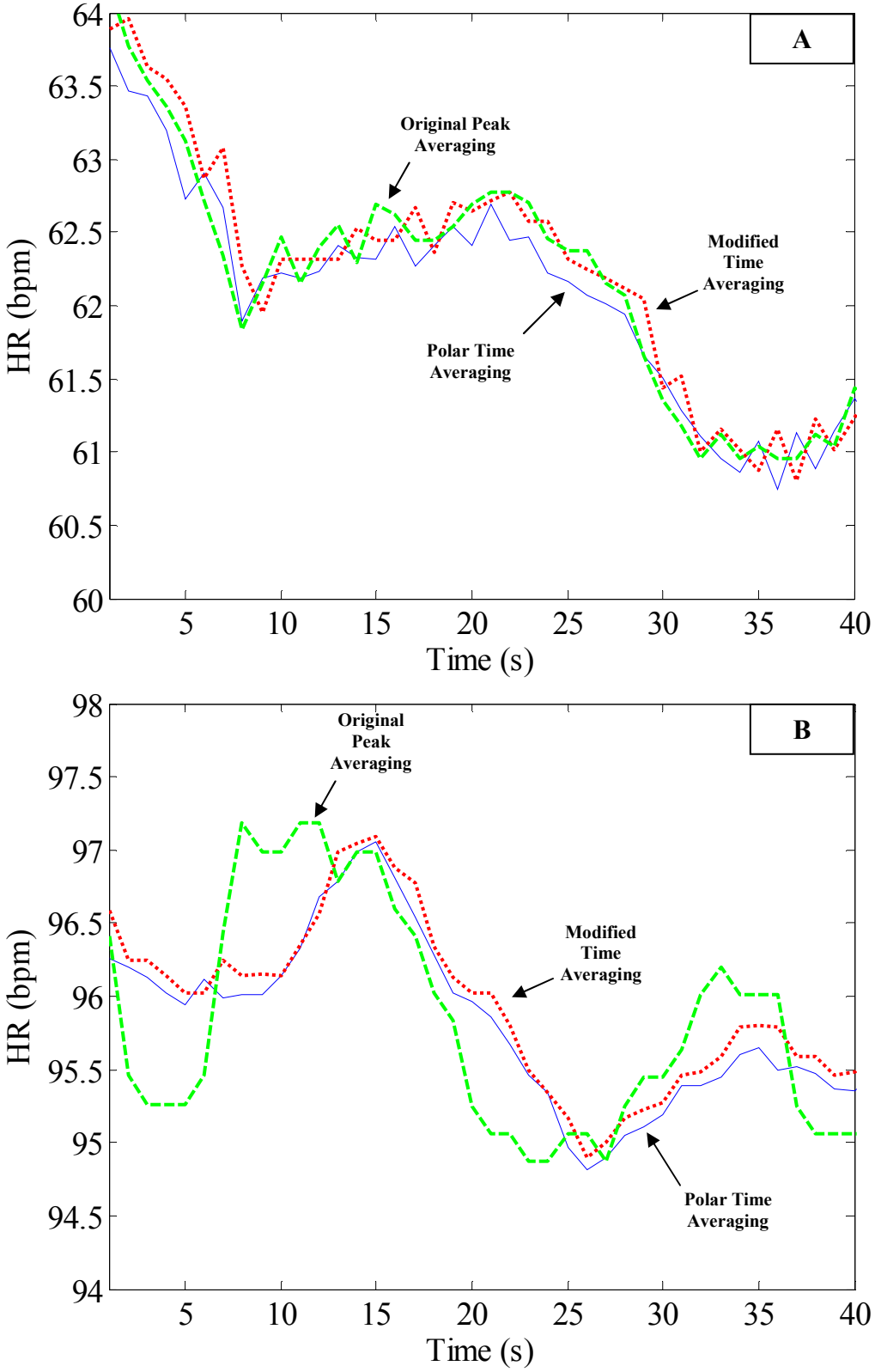

***Figure 9.6**. HR measurements extracted during rest using Peak Count-Based Averaging (dashed) and Time-Based Averaging (dotted) routines. HR readings of 60bpm (A) and 95bpm (B) are shown.*

Extraction of HR from R and IR PPG Signals

Heavy respiration during jogging caused significant changes in the amplitude of the PPG which lead to missed peak identification in the IR signal, as shown in Fig. 9.7A. In this example, missed peaks caused erroneous IHR values to be incorporated into the calculation of HR. Since respiration did not affect the R signal to the same degree as the IR signal, missed peaks occurred less frequently (*shown in Fig. 9.7B*). Therefore, to acquire more accurate HR during jogging, the algorithm devised by Johnston [12] was modified to incorporate IHR values extracted from the R signal.

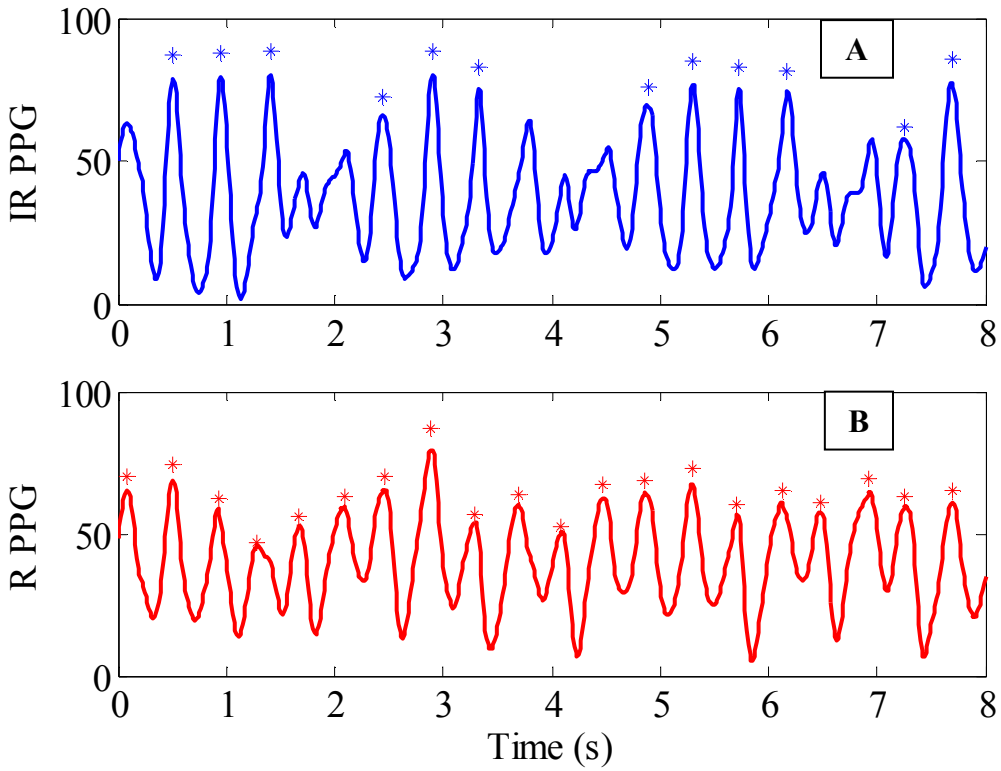

Figure 9.7. *(A) Typical IR and (B) R PPGs acquired during jogging. * indicate automatic software-detected peaks.*

The R PPG signal also provided a means of verifying the IHR values extracted from the IR signal. IHR values extracted from the R PPG that were greater than 200% or less than 50% of the IR IHR values were not incorporated into the calculation of HR. The range of values greater than 200% and less than 50% were selected in order to remove

outlying IHR values due to the detection of multiple and missed peaks, respectively. Fig. 9.8 shows IHR values extracted from each PPG signal. The rejected IHR values are indicated by asterisks. Generally, this modification to the algorithm helped to reject erroneous IHR values.

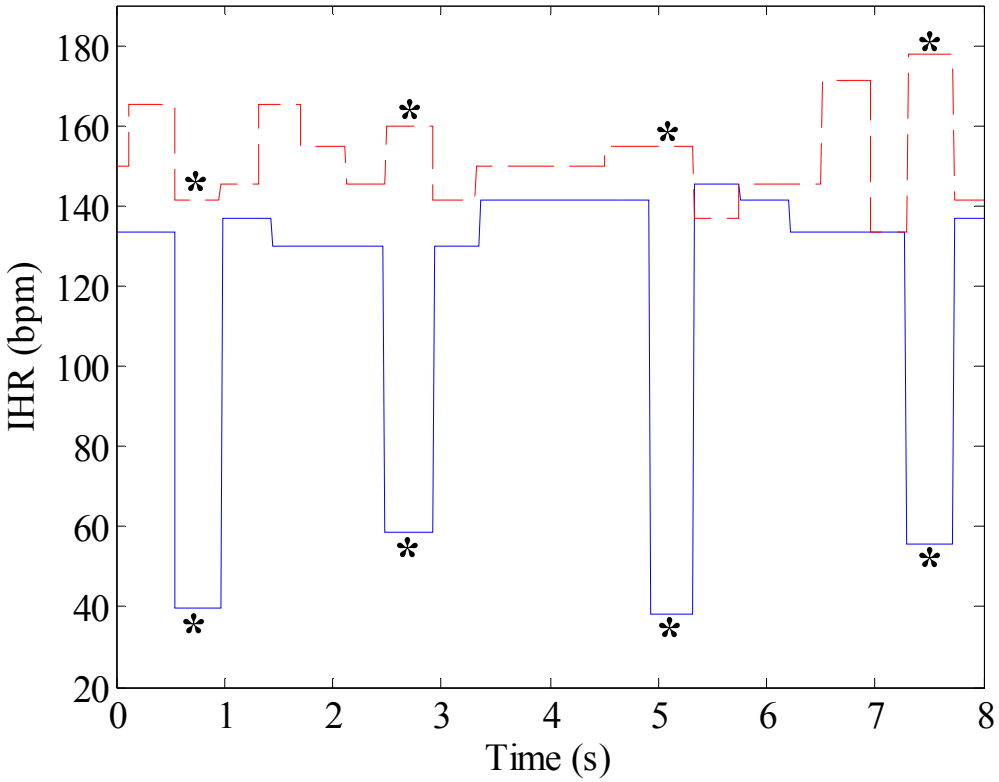

Figure 9.8. *IHR measurements extracted from the IR (solid) and R (dashed) PPG signals. * indicate rejected IHR measurements.*

IHR Threshold

The *IHR Threshold Routine* was incorporated into the algorithm to reject IHR measurements that were outside the range of recent HR readings. To obtain more accurate HR measurements, IHR values extracted from R and IR signals were compared to a threshold based on the average HR measurement. Similar to the *Extraction of HR from R and IR Signals*, the *IHR Threshold* modification rejected IHR values that were greater than 175% and less than 50% of the average HR (*this range was selected based*

on analysis of PPG signals acquired during jogging). For example, at the onset of jogging, R and IR PPG signals (*Fig. 9.9*) typically provided high-valued outlying IHR measurements due to the detection of multiple erroneous peak-to-peak intervals. The rejection of outlying IHR measurements contributed to more accurate HR readings, especially during the onset of jogging. Note that the rejection of high-valued IHR measurements extracted from the R signal occurred frequently at the beginning of jogging and ceased shortly thereafter.

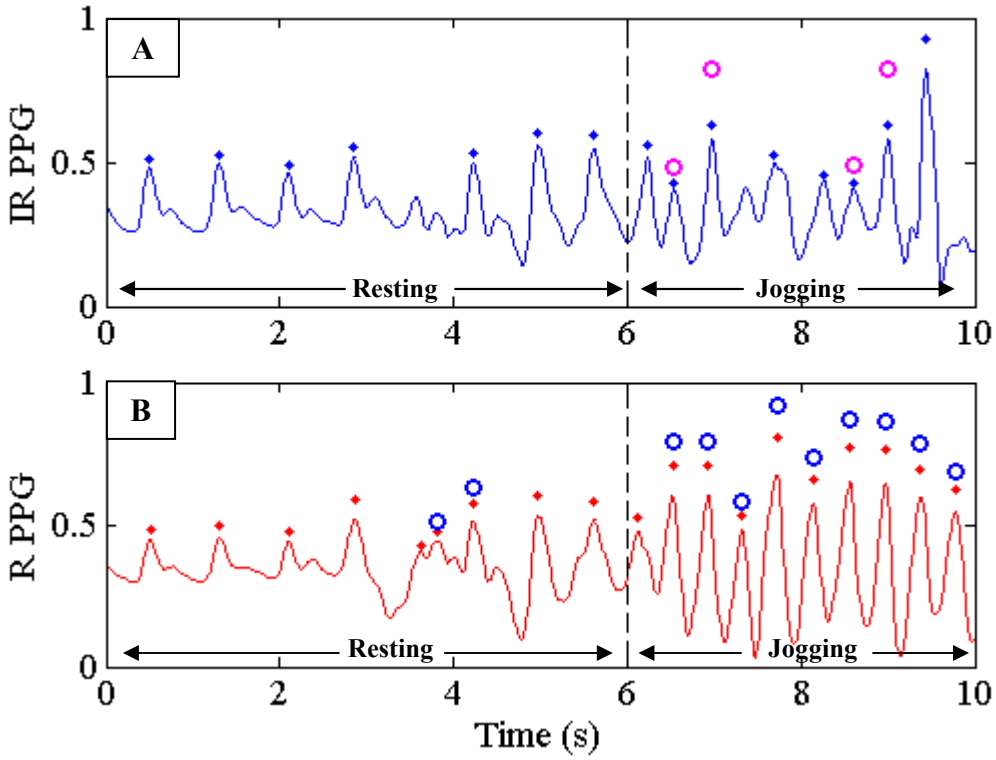

Figure 9.9. *(A) Typical IR and (B) R PPG signals. ♦ indicate detected peaks and ○ indicate high outlying IHR measurements.*

Fig. 9.10 demonstrates the rejection of low outlying IHR measurements calculated from missed peaks in the IR signal. The peak-to-peak intervals in Fig. 9.10 were rejected since the algorithm detected low outlying IHR values associated with missed peaks. By removing low outlying IHR values, the HR calculation algorithm provided more accurate

HR readings during jogging. Missed intervals and the detection of multiple peaks were typical in all PPG signals acquired during jogging.

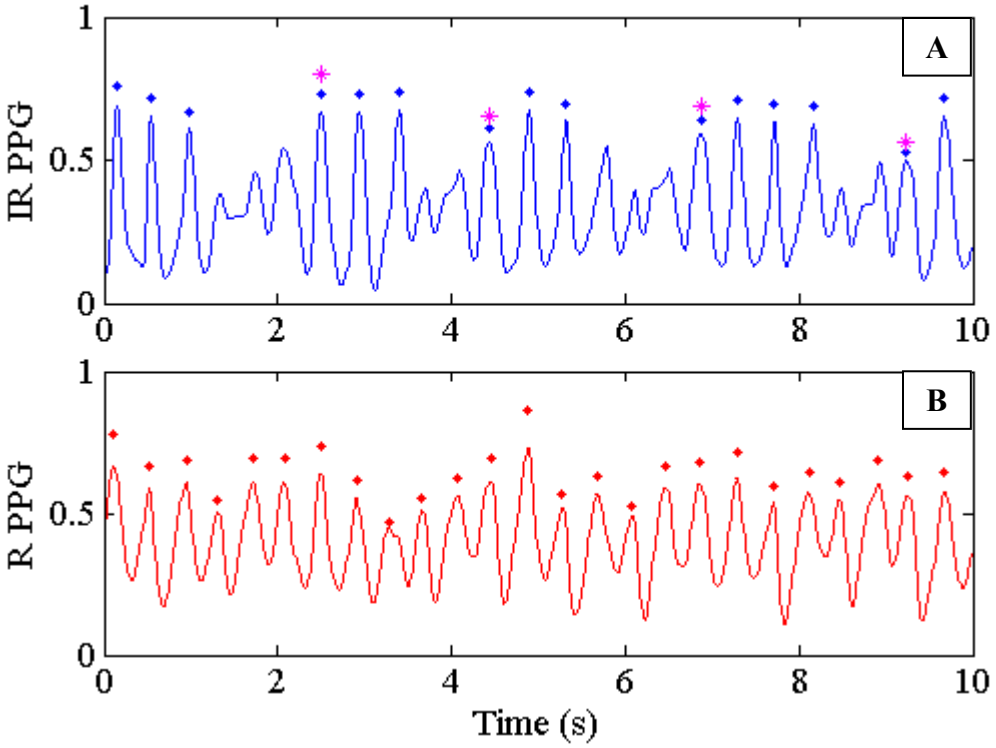

Figure 9.10. *(A) Typical IR and (B) R PPG signals. ♦ indicate detected peaks and * indicate low outlying IHR measurements due to missed peaks.*

Despite the implementation of several modifications to the SpO_2 and HR algorithms, we found that measurement accuracy did not improve during jogging. This indicated that the effects of motion artifacts were not reduced by the modifications made to the algorithms. As described in the Limitations to Pulse Oximetry (*Section 3.7*), the PPG signals acquired during jogging are compromised by the frequency of motion. Since the modifications to the algorithms did not alter the spectral content of the signals, inaccurate measurements were extracted during jogging.

Fig. 9.11 shows representative HR readings obtained during jogging. This figure demonstrates that the modifications made to the algorithm rejected some of the erroneous HR readings during jogging. The large fluctuations in HR readings obtained from the

finger-worn Masimo sensor did not respond adequately to the corresponding changes in physiology during jogging.

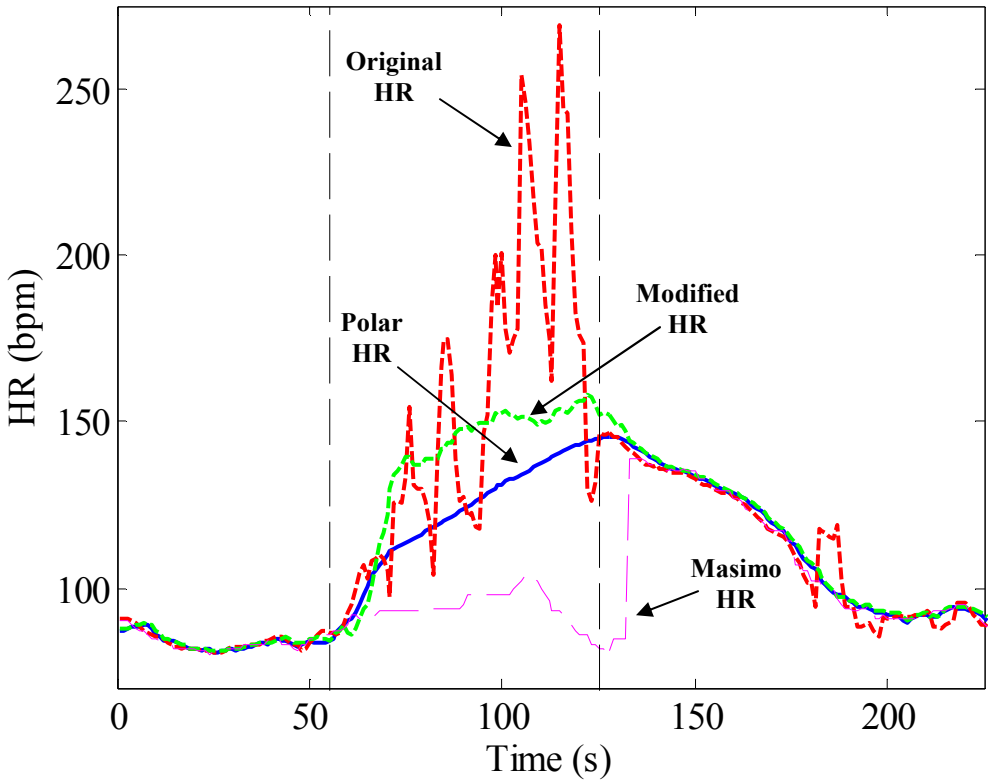

Figure 9.11. *Representative HR measurements obtained during jogging.*

9.3. ADAPTIVE NOISE CANCELLATION

During jogging, changes in the morphology of PPG signals cause a reduction in the accuracy of SpO_2 and HR obtained by signal processing algorithms developed by Johnston [12]. To evaluate the effectiveness of the ACC-based ANC algorithm, body acceleration and PPG data were processed using ANC algorithms in Matlab. Representative body acceleration, raw PPG signals acquired during jogging, and adaptively filtered PPG signals are shown in Fig. 9.12. The adaptively filtered PPG signals (*Fig. 9.12B, D*) show that PPG peaks can be more easily identified as compared to the peaks raw signals (*Fig. 9.12A, C*). For example, several portions of the adaptively

filtered IR signal appear more like typical, clean PPG signals (*Fig. 9.12B; t = 1.5s, 3.5s, 5.5s, 8s*).

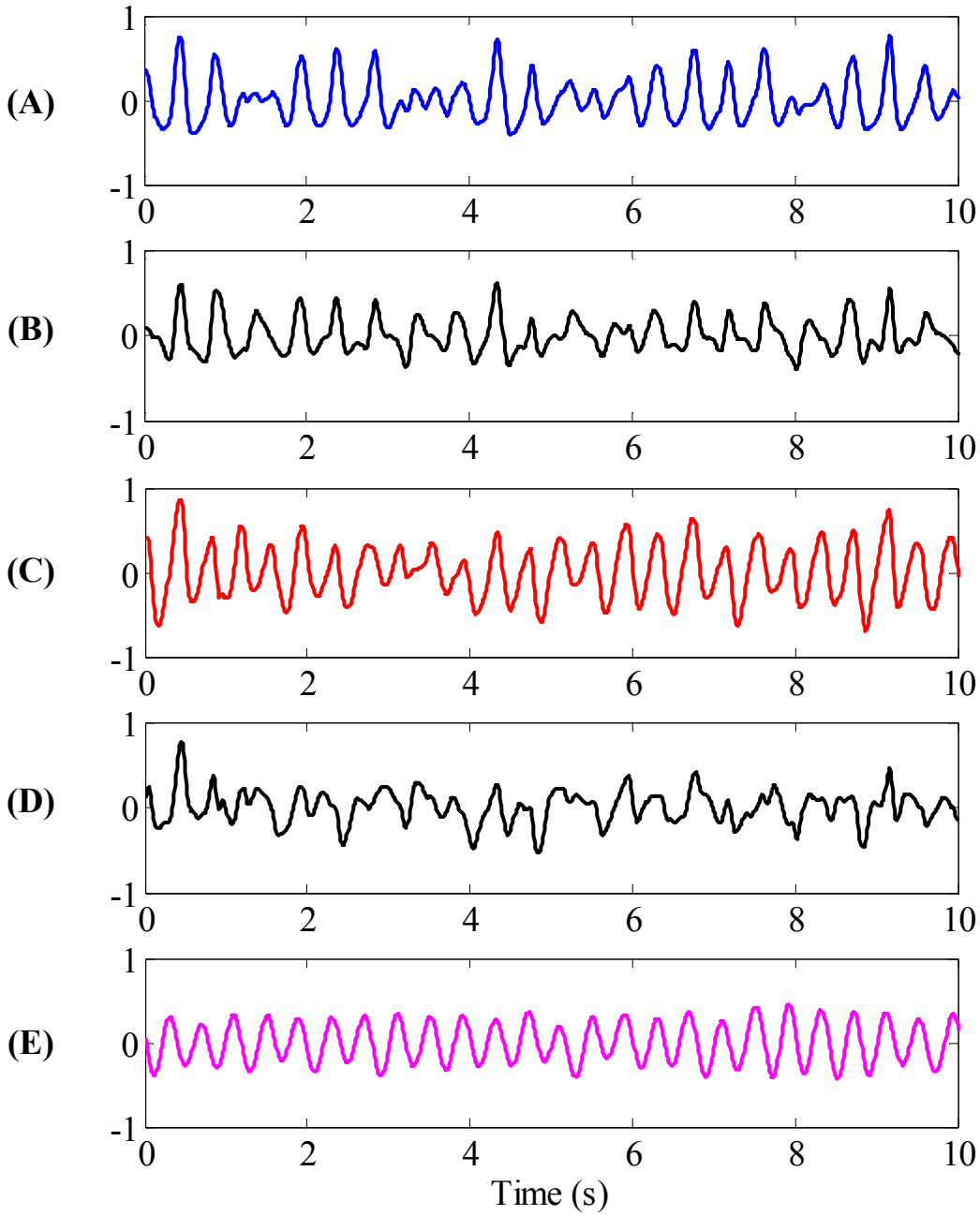

Figure 9.12. *(A) Typical IR PPG signals before and (B) after processing by the ANC algorithm. (C) Typical R PPG signal before and (D) after processing by the ANC algorithm. (E) corresponds to the reference noise obtained simultaneously from the ACC during treadmill jogging (X+Y+Z).*

Fig. 9.13 shows representative FFT spectra of body acceleration and PPG signals

before and after processing by the ANC algorithm. The FFT signals shown in Fig 9.13 correspond to the body acceleration and PPG signals depicted in Fig. 9.12. The spectral band centered at 2Hz corresponds to the cardiac frequency during jogging (*Fig. 9.13A, B*). The spectral band centered at 2.45Hz corresponds to the frequency of body acceleration. This figure also demonstrates that the frequency of motion can be significantly attenuated by the ACC-based ANC algorithm. Fig. 9.13C indicates that the movement occurred primarily in the vertical (X) plane of motion although body acceleration was also measured by the horizontal (Y) and anterior-posterior (Z) planes of the ACC.

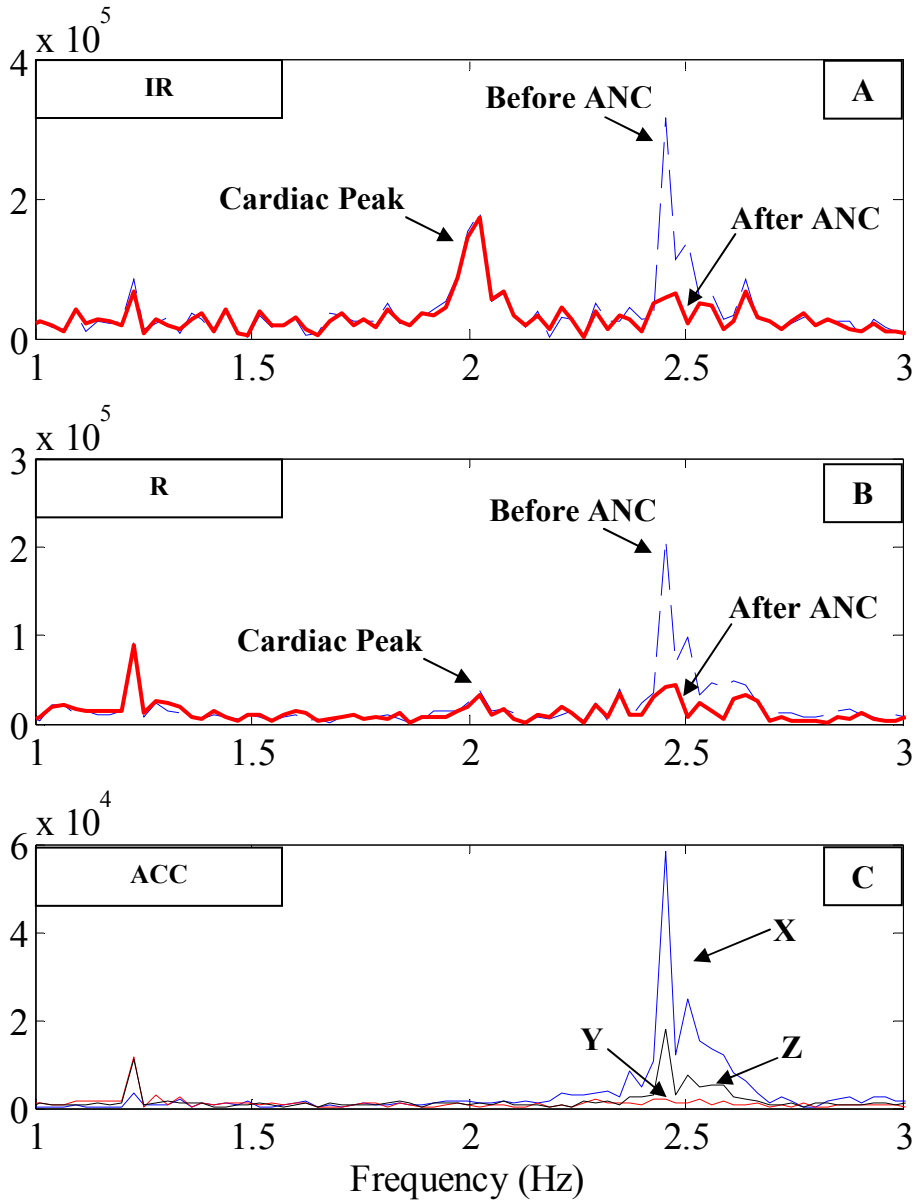

Figure 9.13. *(A) FFT spectra of the IR PPG, (B) R PPG and (C) corresponding ACC signals during treadmill jogging.*

9.3.1. LMS Step-Size Selection

The LMS algorithm step-size, μ, was varied to determine its potential effect on the accuracy of SpO_2 and HR measurements. The Matlab function mumax was utilized in order to determine the relative range of μ. The selection of μ by mumax was based on the statistics of the ACC and PPG data (*μ was varied between 0.002 and 0.05*). Fig. 9.14 shows calculated mean SpO_2 and HR RMSE ±1 standard deviation (SD) for all trials. A

32^{nd} order LMS filter was chosen for this study.

This study was performed to determine a range of μ that could be used to implement an LMS algorithm. Generally, the results show that the SpO_2 and HR measurements extracted from the adaptive filter algorithm have a lower RMSE and SD than the non-adaptive algorithm ($\mu = 0$). For SpO_2, the results show that the reduction in RMSE occurred over the entire range of μ, although the reduction in SpO_2 measurement error was relatively constant for $\mu > 0.35$. Similarly, the RMSE for HR was reduced over the entire range of μ although RMSE increased for $\mu > 0.03$. This suggests that an LMS algorithm with constant μ could be implemented to improve measurement accuracy during jogging. $\mu = 0.016$ was selected for further analysis since this value obtained optimal reduction in RMSE and SD.

9.3.2. RLS FORGETTING FACTOR SELECTION

The RLS algorithm forgetting factor, λ, was varied to determine its potential effect on the accuracy of SpO_2 and HR measurements. This study was performed to determine the feasibility of implementing an RLS algorithm with a constant λ. Since the literature suggested that λ is typically near 1 [53], the parameter was varied between 0.9 and 1.

Fig. 9.15 and 9.16 show the average RMSE ±1 SD for SpO_2 and HR for all trials. A 16^{th} order RLS filter was chosen for this study. The results indicate that $0.98 < \lambda < 1$ provided the lowest RMSE and SD. This suggests that an RLS algorithm with constant λ could be implemented to improve measurement accuracy during jogging. $\lambda = 0.99$ was selected for further analyses since this value obtained optimal reduction in the RMSE.

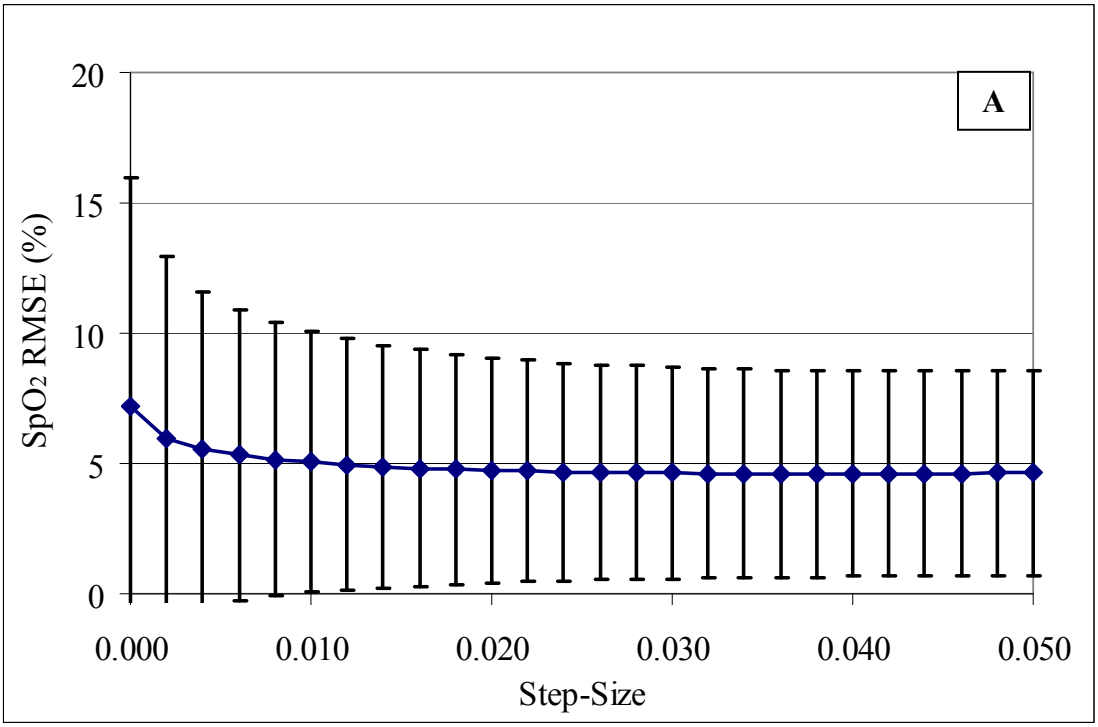

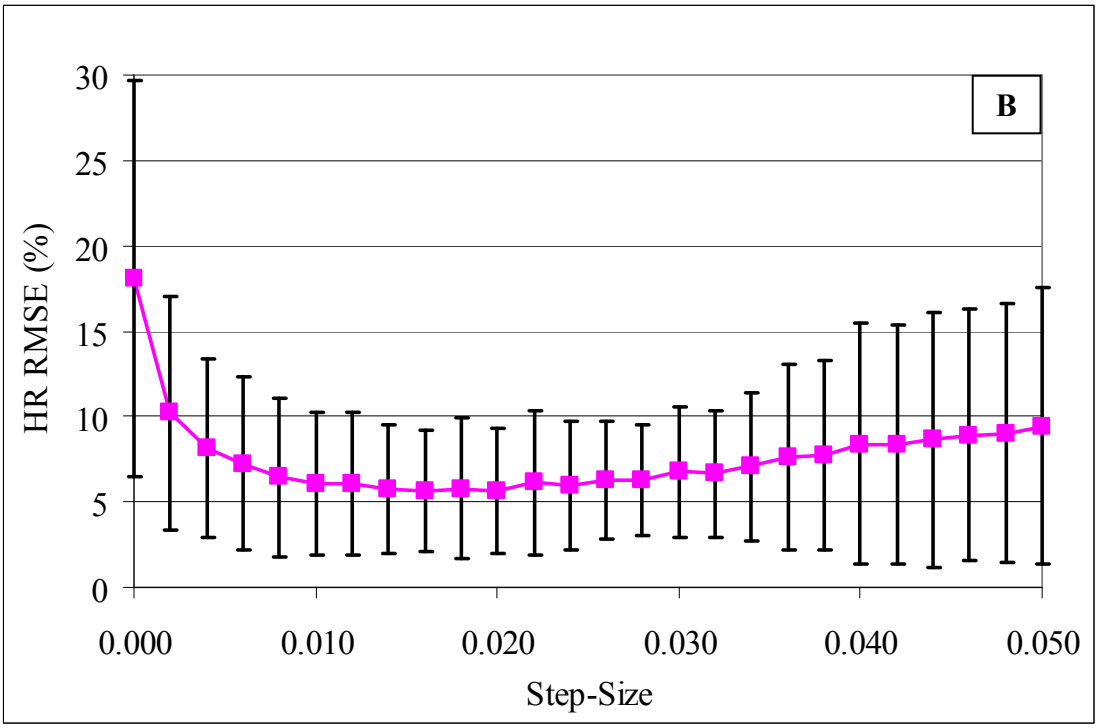

Figure 9.14. *(A) Average SpO_2 and (B) HR RMSE for the LMS adaptive filter algorithm for varying μ (filter order M = 32). Error bars indicate ±1 SD. Data reflect 32 trials. μ = 0 represents measurements extracted from the non-adapted PPG signals.*

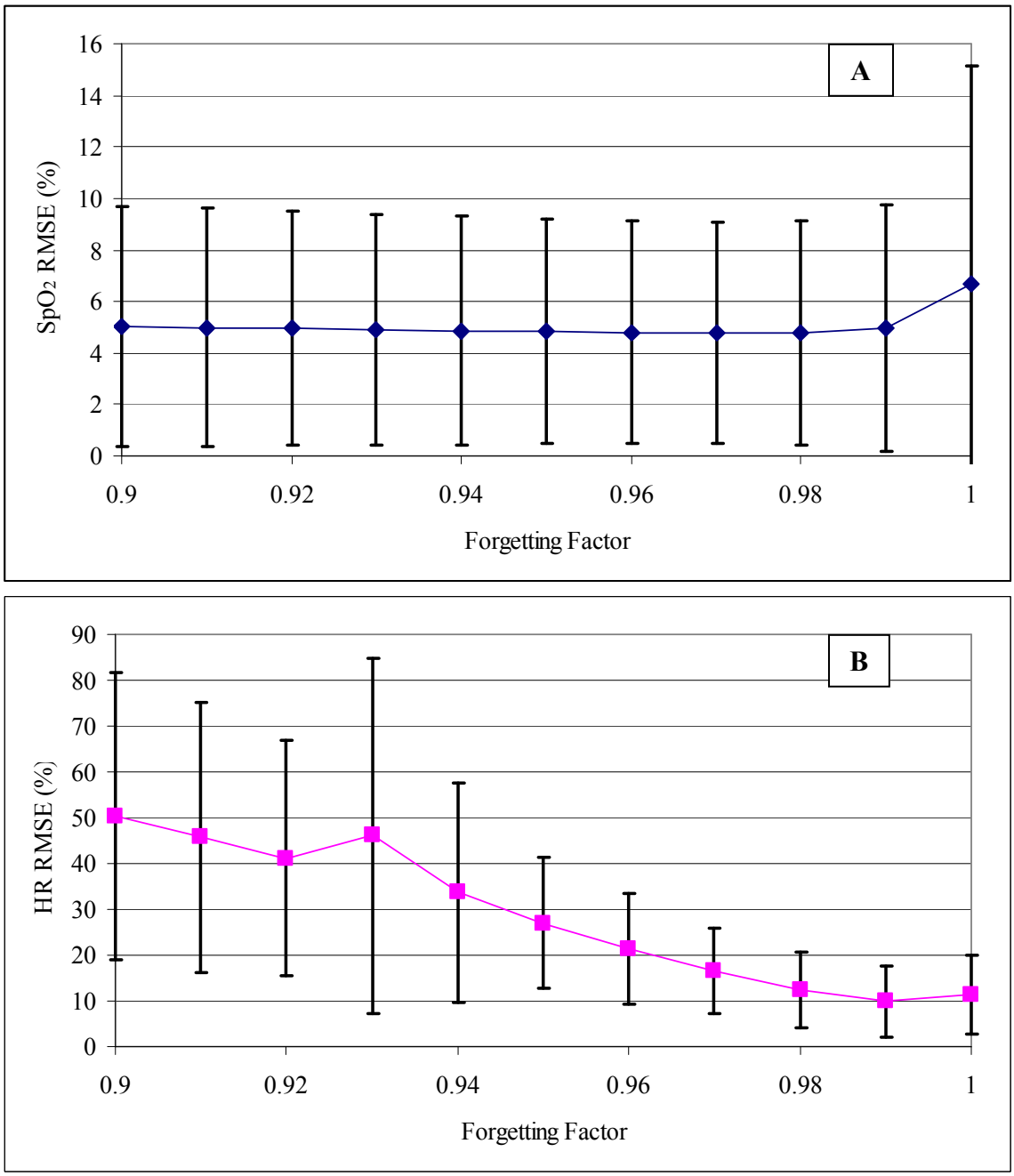

Figure 9.15. *(A) Average SpO_2 and (B) HR RMSE for $0.9 < \lambda < 1$. RLS order $M = 16$. Error bars indicate ±1 SD. Data reflect 32 jogging trials.*

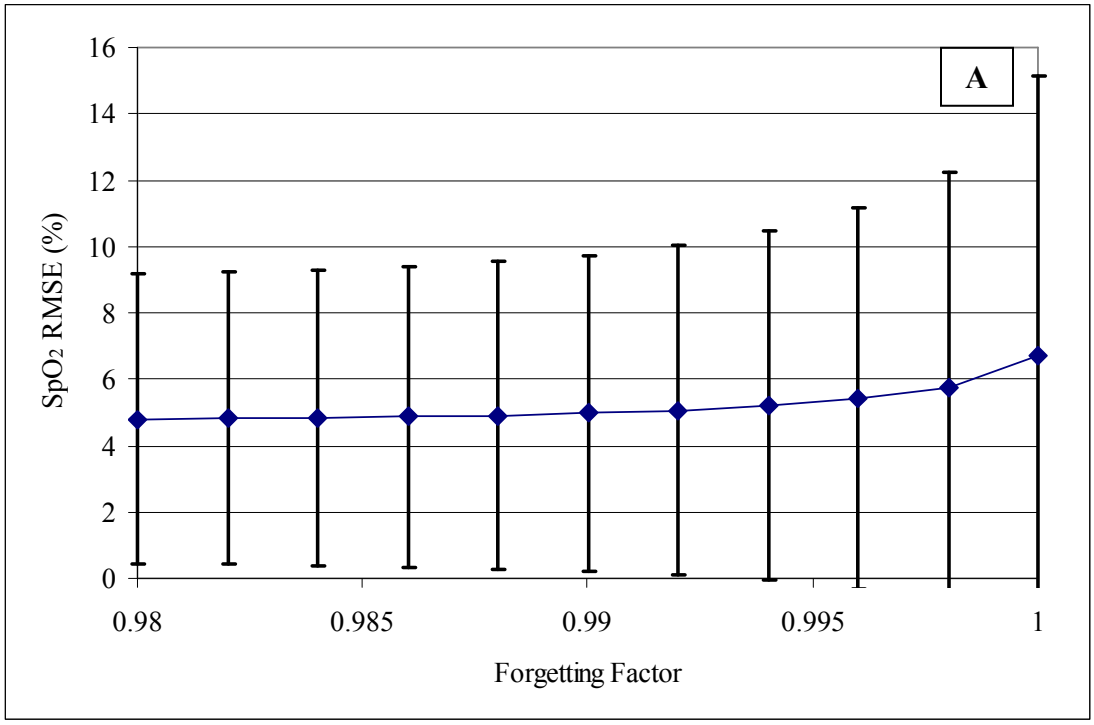

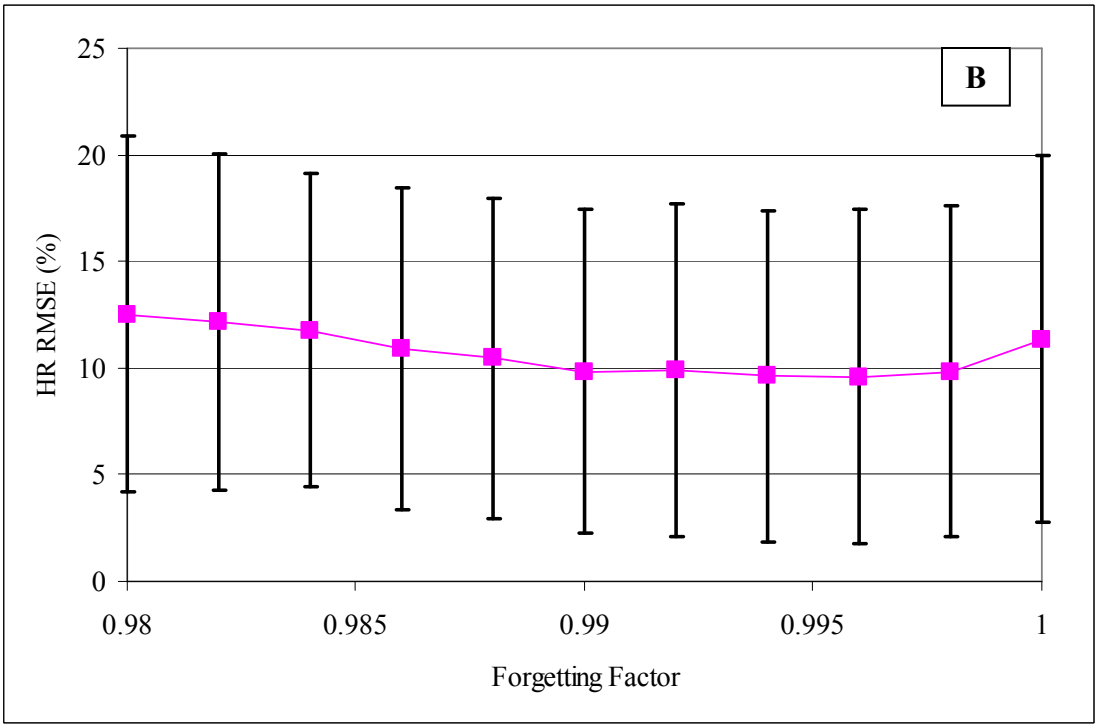

Figure 9.16. *(A) Average SpO_2 and (B) HR RMSE for $0.98 < \lambda < 1$. RLS order $M = 16$. Error bars indicate ±1 SD. Data reflect 32 jogging trials.*

9.3.3. SELECTION OF FILTER ORDER

The filter order, *M*, was varied to determine its potential effect on the accuracy of SpO_2 and HR measurements obtained by LMS and RLS algorithms. This study was performed to compare the measurement accuracy obtained by the adaptive algorithms. Fig. 9.17 shows the average RMSE ±1 SD for varied *M* for all trials. LMS ($\mu = 0.016$) and RLS ($\lambda = 0.99$) algorithms were chosen for this study.

The results indicate that SpO_2 and HR measurements extracted from the adaptive filter had a lower RMSE and SD than the non-adaptive algorithm ($M = 0$). For example, for SpO_2, using a 24^{th} order filter, the LMS and RLS algorithms provided a mean percent reduction of the RMSE corresponding to 21.8% and 23.3%, respectively. Similarly, for HR, the LMS and RLS algorithms provided a mean percent reduction in RMSE corresponding to 58.9% and 35.5%, respectively. This indicates that LMS and RLS algorithms could provide a similar degree of improvement in measurement of SpO_2 although the LMS could provide a more significant improvement in measurement of HR.

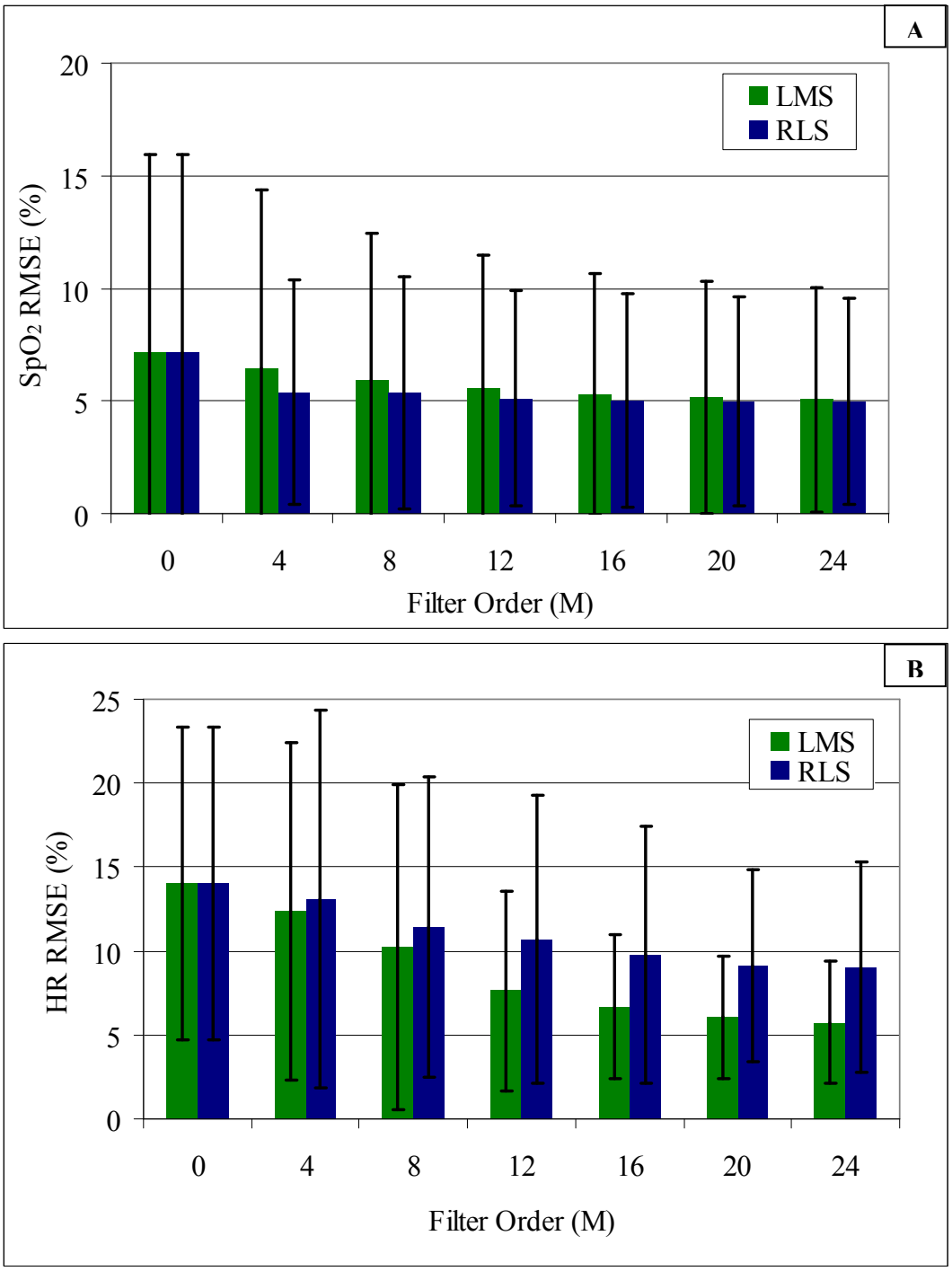

Figure 9.17. *(A) Average SpO_2 and (B) HR RMSE obtained using the LMS (light) and RLS (dark) algorithms for filter order. The error bars indicate ±1 SD. The data reflect 32 jogging trials. M = 0 represents measurements extracted from non-adapted PPG signals.*

9.4. ANALYSIS METHODS

Fig. 9.18 shows the mean difference between SpO_2 and HR measurements obtained from the non-adaptive and LMS algorithms. The differences between the non-adaptive and measurements obtained from the RLS algorithm are shown in Fig. 9.19. The data indicate that the differences between the measurements extracted using the non-adaptive and adaptive algorithms varied significantly for each individual. The one-way analysis of variance (ANOVA) test was used to determine the statistical significance for the difference between the non-adaptive and adaptive algorithms. Due to the high variation in measurement differences among individuals, the ANOVA included a model to account for differences between individuals.

The results of the ANOVA included the estimate error, standard error of the estimate (SEE), *p* value, and 95% confidence interval (CI_{95}). To facilitate comparisons between the non-adaptive and adaptive methods, the error of the estimate represents the mean difference between measurements obtained by each method, the SEE value represents the standard deviation of the estimate, the *p* value indicates the level of significance of the test, and the CI_{95} indicates the range representing 95% of the differences between measurements.

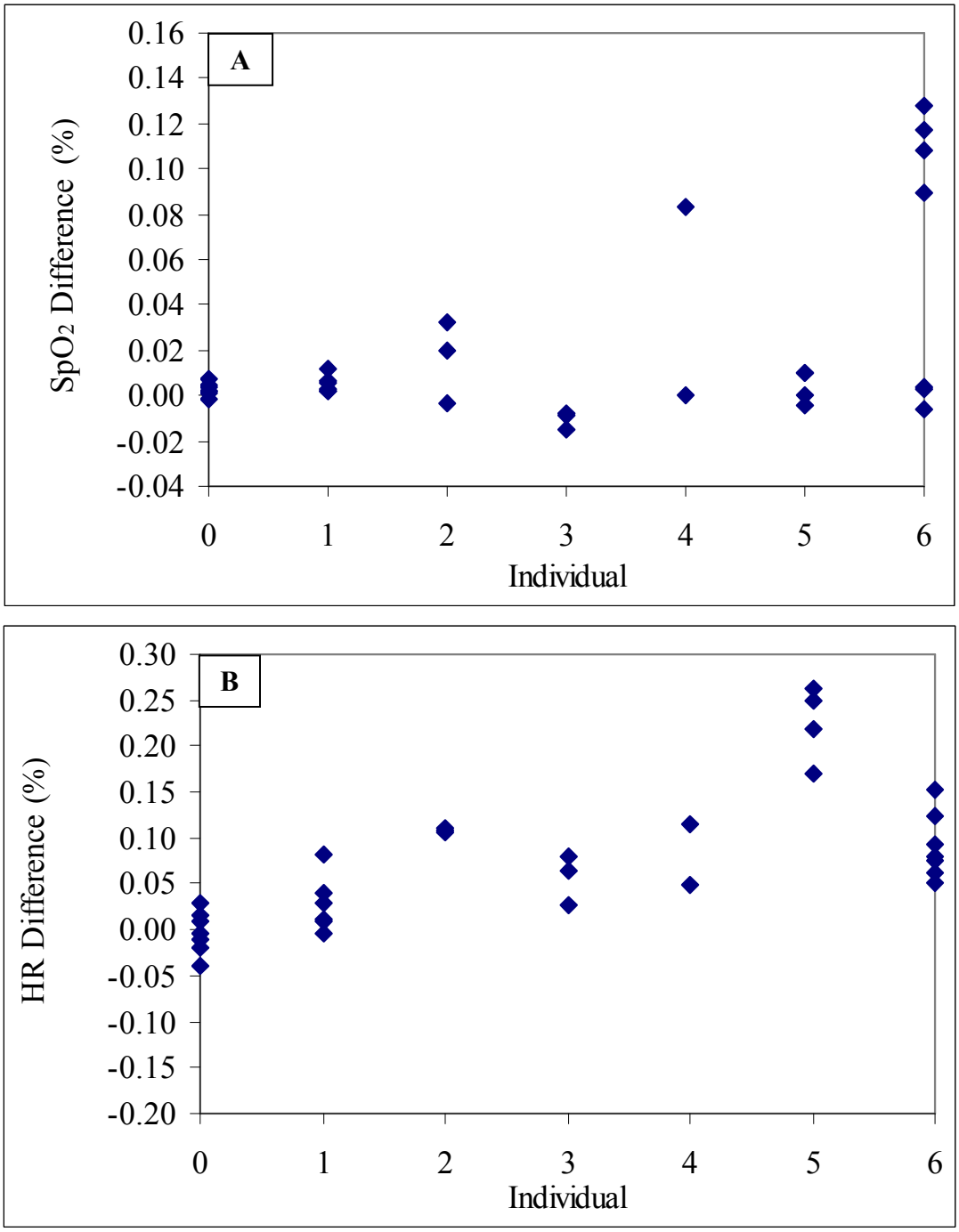

Figure 9.18. *(A) Percent differences between SpO_2 and (B) HR extracted by the non-adaptive and adaptive LMS algorithms.*

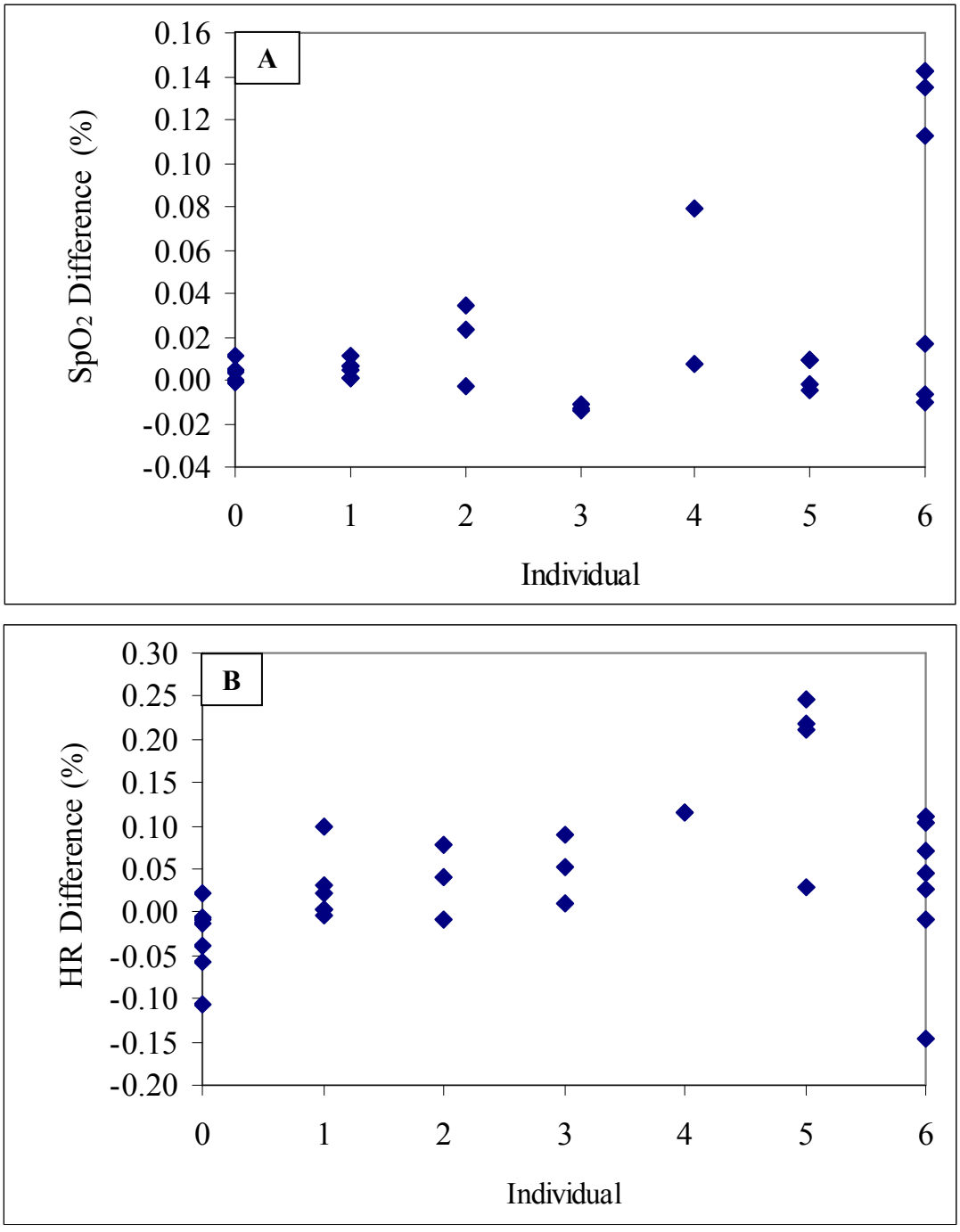

Figure 9.19. *(A) Percent differences between SpO_2 and (B) HR extracted by the non-adaptive and adaptive RLS algorithms.*

Fig. 9.20 shows a flowchart of the data path used to obtain SpO_2, HR, body orientation, and activity. Raw data were filtered in software using LPF and BPF routines. The AC and DC components of body acceleration signals were processed by Orientation and Activity algorithms, respectively. In addition to providing activity information, the summation of the AC components of the body acceleration signals was used as a noise reference input to the ANC algorithm. The AC component of the PPG signals was processed by the ANC algorithms in order to attenuate the motion spectrum from the corrupted signals. To obtain SpO_2 readings, adaptively filtered AC components and raw DC components of PPG signals were processed by the SpO_2 algorithm. Similarly, adaptively filtered AC components of PPG signals were processed by the HR algorithm to acquire HR readings. All processing was completed in Matlab.

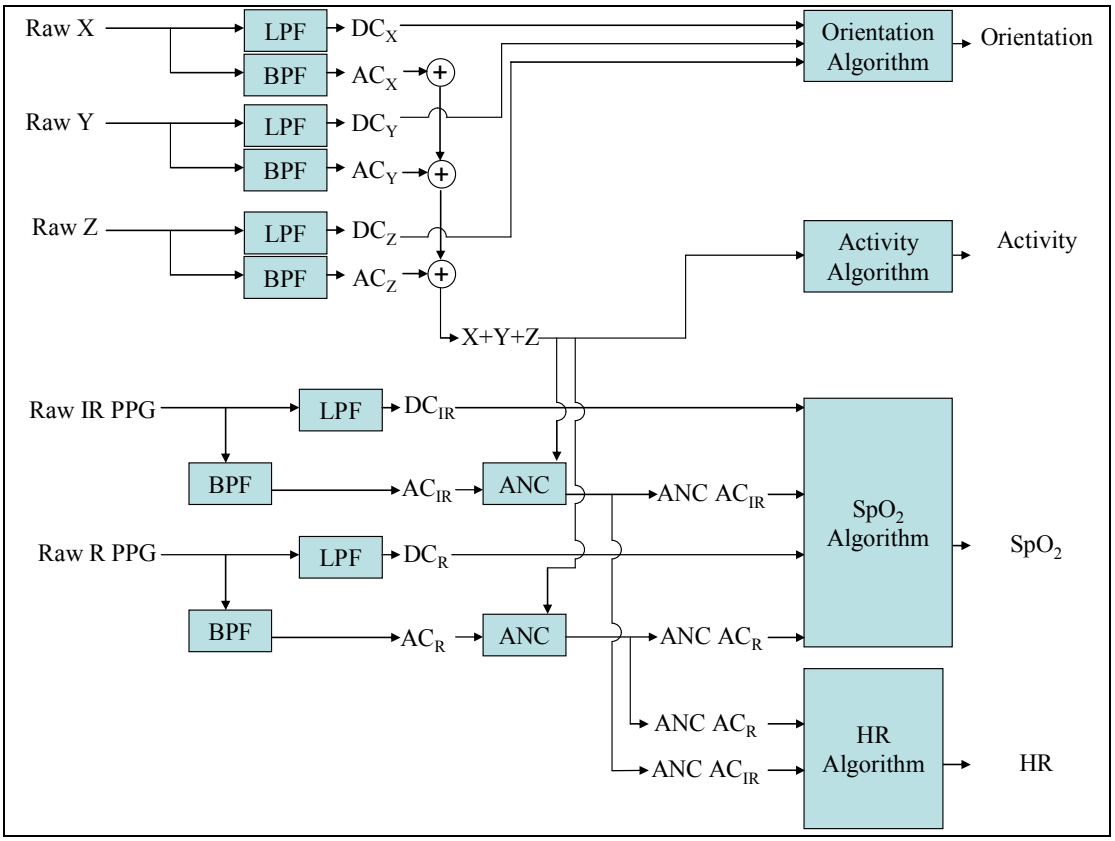

Figure 9.20. *Data path for ACC and PPG signals.*

9.4.1. SpO_2 DIFFERENTIAL THRESHOLD

SpO_2 measurements were extracted from PPG signals that were adaptively filtered by the LMS and RLS filters. Measurements were compared using the SpO_2 algorithm described by Johnston [12] and the modified SpO_2 algorithm implemented in this thesis. This analysis was performed to determine the level of significance of the difference in RMSE obtained from the SpO_2 algorithms. The estimate error was calculated as the subtraction of the SpO_2 measurement error obtained by the algorithm devised by Johnston from the error obtained by the algorithm that incorporated the *SpO_2 Differential Threshold* modification. Table 9.1 shows the results of the one-way ANOVA. The results indicate that the algorithm devised by Johnston provided slightly more accurate measurements than the modified algorithm; the result obtained using the LMS algorithm was considered significant at the 0.05 level although the results obtained using the RLS algorithm was not considered significant ($p = 0.128$).

Table 9.1. *Mean percent differences in SpO_2 extracted from the adaptively filtered PPG signals by using the SpO_2 algorithm devised by Johnston [12] and the modified algorithm.*

	Mean Percent Difference in SpO_2 (%)			**95% Confidence Interval**	
	Estimate	SE	*p*	Lower	Upper
LMS ($\mu = 0.016$, M = 16)	-0.41	0.156	0.015	-0.732	-0.088
RLS ($\lambda = 0.99$, M = 16)	-0.254	0.161	0.128*	-0.585	0.078†

* *p* value is not considered significant † confidence interval includes the zero estimate

Fig. 9.21 shows an experimental trial during which the SpO_2 measurements had a high degree of inaccuracy during jogging. In this example, the ACC-based ANC algorithm provided more accurate measurements than the non-adaptively filtered signals. The results show that the measurements obtained using the *SpO_2 Differential Threshold* were less accurate than measurements extracted using the SpO_2 algorithm devised by Johnston [12]. This suggests that the *SpO_2 Differential Threshold* algorithm should not be

implemented for the calculation of SpO_2 readings.

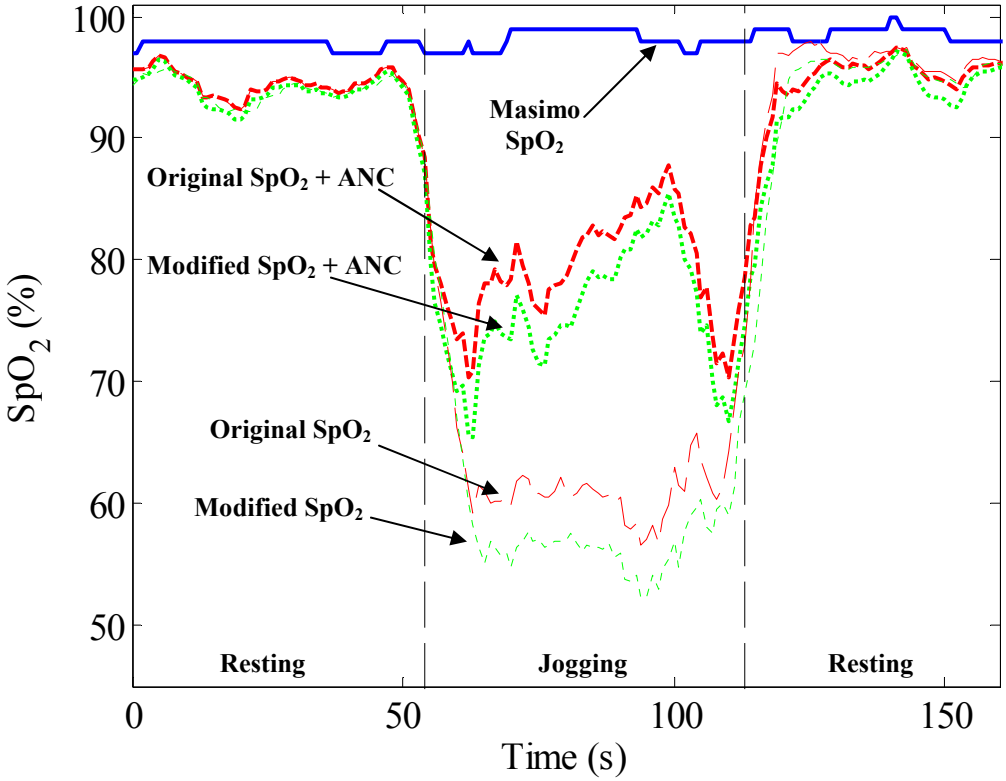

Fig. 9.21. *SpO_2 measurements obtained with and without ANC using the algorithm developed by Johnston [12] and the SpO_2 Differential Threshold.*

Fig. 9.22 shows the AC and DC signals corresponding to the experimental trial shown in Fig. 9.21. This figure shows that relatively large changes occurred in the DC signals during jogging. Since DC signals were not processed by the ACC-based ANC algorithm, changes in PPG morphology due to the effects of motion were not removed from the signals. This suggests that signal components due to movement present in the DC signals contributed partially to the calculation of erroneous measurements.

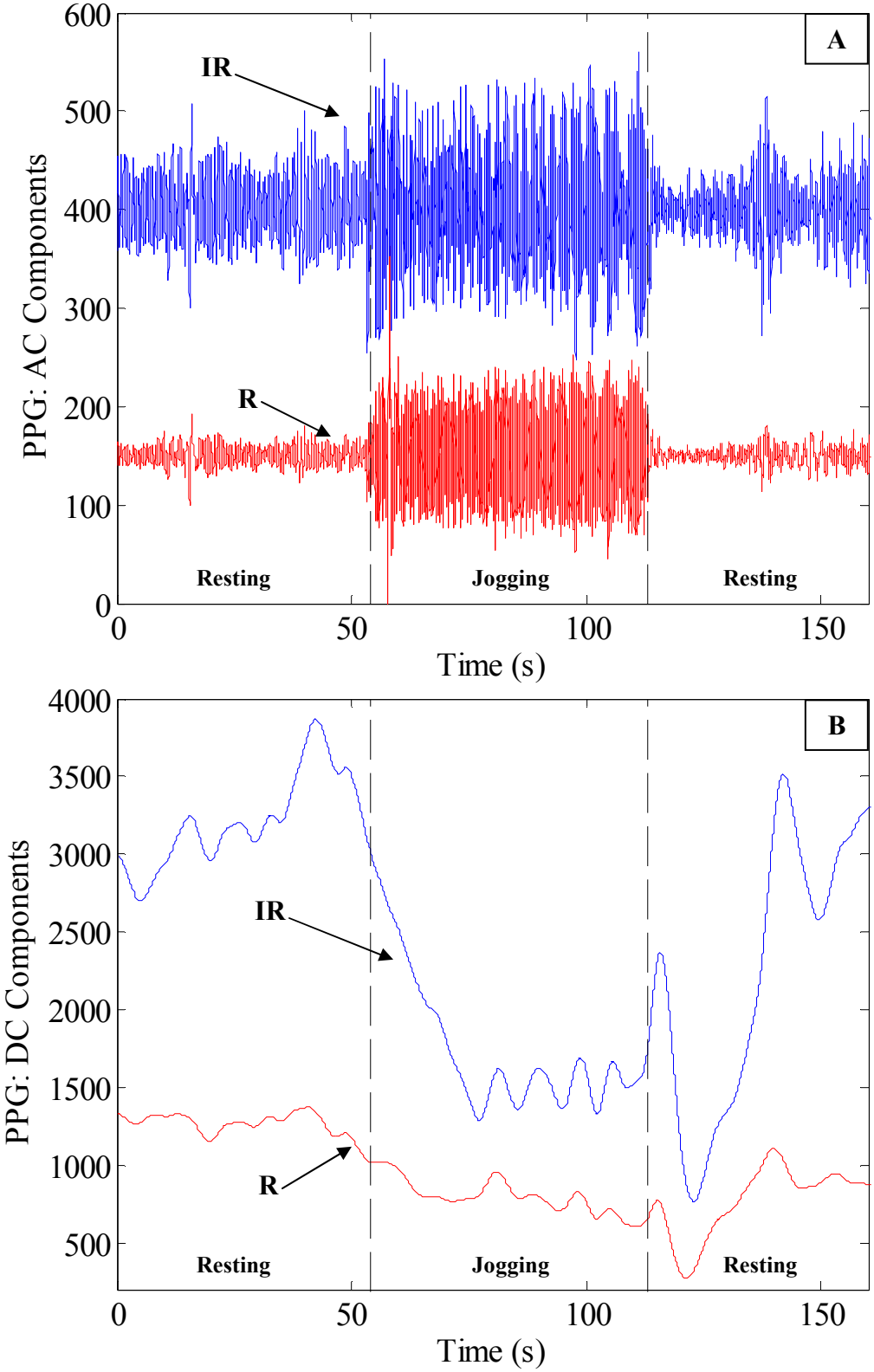

Fig. 9.22. *(A) AC_R and AC_{IR} and (B) DC_R and DC_{IR} signals obtained during jogging.*

9.4.2. HR AVERAGING

HR measurements were extracted from adaptively filtered PPG signals acquired during jogging. This study was performed to determine the effectiveness of the *Time-Based Averaging* scheme for providing improved accuracy of HR measurements during jogging. Differences were calculated between HR measurements extracted by using the HR algorithm described by Johnston [12] and HR measurements extracted by *Time-Based Averaging*. The error of the estimate is shown in Table 9.2. The results indicate that *Time-Based Averaging* provided more accurate HR measurements during jogging. The difference obtained by utilizing the LMS algorithm was considered significant at the 0.05 level although the difference obtained from the RLS algorithm was not considered significant ($p = 0.115$).

Table 9.2. *Mean percent differences in HR extracted from the adaptively filtered PPG signals by using the HR algorithm devised by Johnston [12] and the modified averaging algorithm.*

	Mean Percent Difference in HR (%)			**95% Confidence Interval**	
	Estimate	SE	*p*	Lower	Upper
LMS (μ = 0.016, M = 16)	3.951	0.469	< .0001	2.985	4.917
RLS (λ = 0.99, M = 16)	1.625	0.995	0.115*	-0.424	3.673†

* *p* value is not considered significant † confidence interval includes the zero estimate

9.4.3. EXTRACTION OF HR FROM R AND IR SIGNALS

The HR algorithm developed by Johnston [12] utilized the IR PPG for the extraction of HR measurements. In order to calculate more accurate measurements, this algorithm was modified to incorporate peak identification of the R signal. A threshold was implemented to remove IHR values extracted from the IR signal that varied from IHR values extracted from the R signal, as well as the contrary case. Using adaptively filtered PPG signals, estimate errors were obtained from the algorithm developed by Johnston

and the modified algorithm (*Table 9.3*). Results indicate that this modification to the algorithm provided improved HR accuracy; improvements were considered significant for the measurements obtained from both the LMS and RLS algorithms ($p < 0.0001$).

Table 9.3. *Mean percent differences in HR extracted from the adaptively filtered PPG signals by using the HR algorithm developed by Johnston [12] and the algorithm modified to incorporate R and IR IHR values.*

	Mean Percent Difference in HR			**95% Confidence Interval**	
	Estimate	SE	*p*	Lower	Upper
LMS (μ = 0.016, M = 16)	10.745	1.768	< .0001	7.104	14.387
RLS (λ = 0.99, M = 16)	34.138	3.232	< .0001	27.483	40.793

9.4.4. IHR THRESHOLD

The *IHR Threshold* modification consisted of the removal of IHR values that deviated significantly from the average HR reading. Deviations were considered significant if an IHR measurement was greater than 175% or less than 50% of the present average HR reading. This range was found to be effective for the data analyzed for this thesis.

The algorithm developed by Johnston [12] and the *IHR Threshold* were compared by differences in estimate error (*Table 9.4*). Results indicate that this modification provided improvements in HR measurement accuracy; improvements were considered significant for the measurements obtained from both the LMS and RLS algorithms ($p < 0.0001$).

Table 9.4. *Mean percent differences in HR extracted from the adaptively filtered PPG signals by using the HR algorithm designed by Johnston [12] and the algorithm modified to incorporate R and IR IHR values as well as the IHR threshold function.*

	Mean Percent Difference in HR			**95% Confidence Interval**	
	Estimate	SE	*p*	Lower	Upper
LMS (μ = 0.016, M = 16)	20.518	2.826	< .0001	14.697	26.338
RLS (λ = 0.99, M = 16)	63.166	5.362	< .0001	52.122	74.209

Fig. 9.23 shows the effectiveness of the *IHR Threshold* algorithm to reject erroneous, high valued IHR values extracted from PPG signals, particularly during the onset of

jogging. Similarly, the *IHR Threshold* algorithm rejected several high valued IHR values extracted from adaptively filtered PPG signals (*Fig. 9.23B*). This result indicates that this modification to the algorithm devised by Johnston [12] is effective in providing more accurate HR readings from adaptively filtered signals.

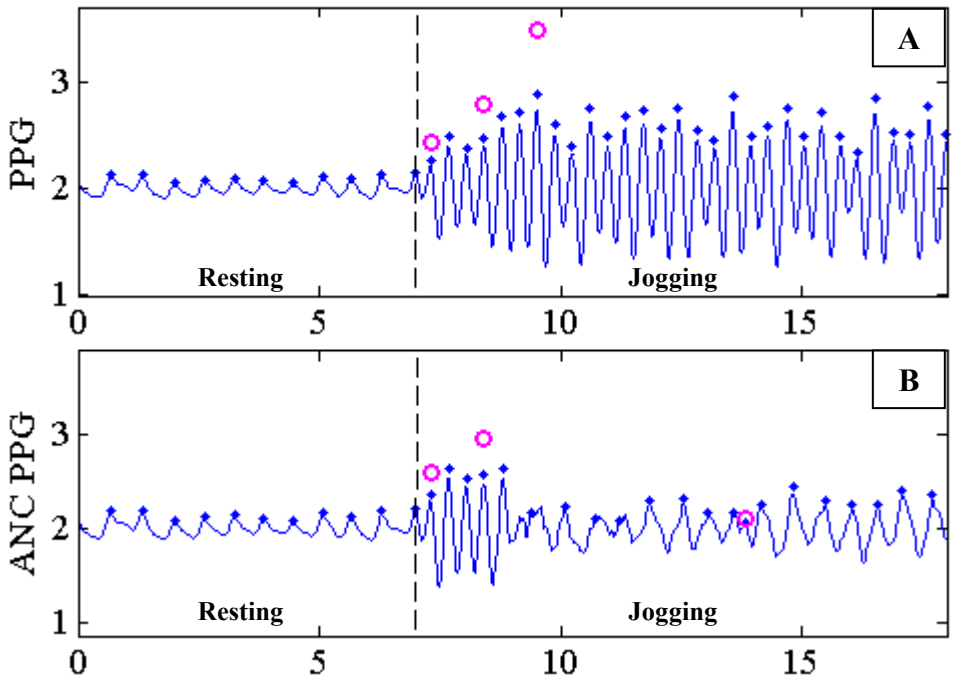

Fig. 9.23. *(A) AC_{IR} obtained during jogging without ANC and (B) with ANC algorithm.* ♦ *indicate detected peaks.* ○ *indicate high outlying IHR measurements.*

Fig. 9.24 shows PPG signals obtained before and after processing using an ANC algorithm. As was demonstrated by Fig. 9.12, this figure also shows that the adaptively filtered signals provided more noticeable peaks for peak identification. As described previously, respiration during jogging caused missed peak identification in PPG signals. Fig. 9.24 demonstrates that more consistent peak identification resulted in fewer missed peaks. Although fewer PPG peaks were missed in adaptively filtered signals, it is shown that the *IHR Threshold* was effective in rejecting missed peaks that occurred during some periods of jogging. Therefore, the *IHR Threshold* was effective in removing low outlying

IHR values from adaptively filtered signals.

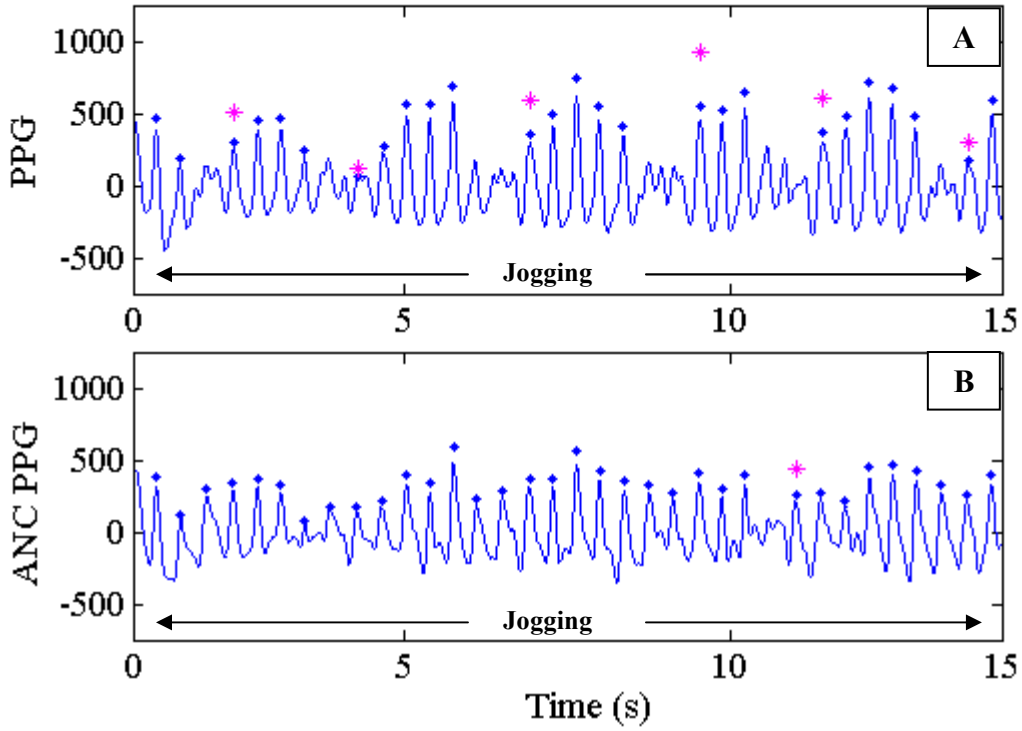

Fig. 9.24. *(A) AC_{IR} obtained during jogging without ANC and (B) with the ANC algorithm. ♦ indicate detected peaks and * indicate low outlying IHR measurements.*

Fig. 9.25 shows a representative adaptively filtered PPG during jogging. Although it was shown that the ACC-based ANC algorithm is effective in attenuating the frequency of motion in PPG signals (*Fig. 9.13*), the effects of motion artifacts are still present to a certain degree. This figure indicates that the rejection of both low and high outlying IHR values was typical for adaptively filtered PPG signals acquired during jogging. Therefore, the *IHR Threshold* modification was effective in improving HR measurements extracted from adaptively filtered PPG signals acquired during jogging.

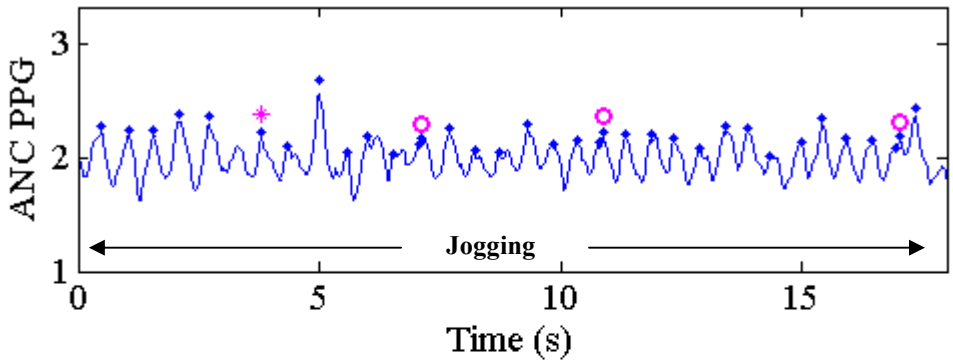

Fig. 9.25. *AC_{IR} obtained during jogging with the ANC algorithm. ♦ indicate detected peaks. ○ and * indicate high and low outlying IHR measurements, respectively.*

Fig. 9.26 shows HR readings obtained using the algorithm devised by Johnston [12] with readings obtained using the algorithm developed for this thesis. This plot shows that the modified HR algorithm incorporating ACC-based ANC provided the most accurate readings. Note that processing the signals obtained by using the ACC-based ANC algorithm in conjunction with the routine devised by Johnston [12] did not provide accurate readings during jogging.

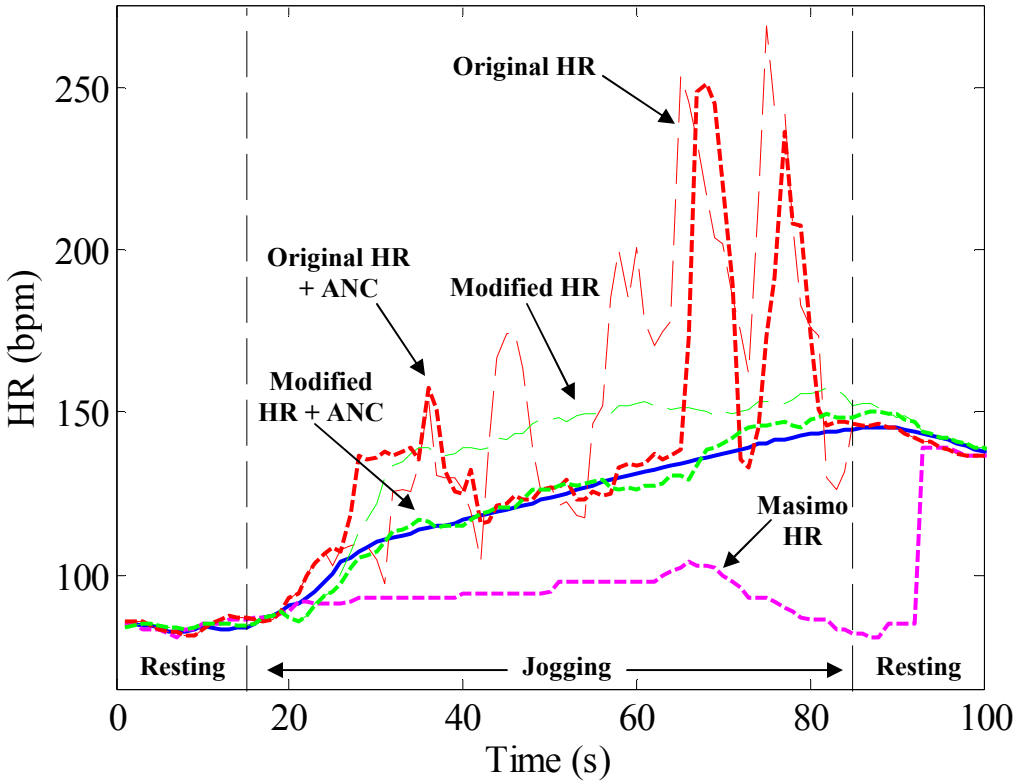

Fig. 9.26. *HR measurements obtained with and without ANC using the algorithm developed by Johnston [12] and the modified HR algorithm.*

9.5. ACCELEROMETER AXIS SELECTION

SpO_2 and HR were extracted from signals that were processed by an LMS algorithm using body acceleration signals. This study was performed to determine the potential effect of ACC axis selection on measurement accuracy. Measurements extracted from the adapted PPG signals during preliminary experimentation are summarized in Table 9.5. The data show that improvements in SpO_2 and HR were obtained by utilizing each acceleration axis separately as well as the summed combination of the accelerometer axes ($X+Y+Z$). The data given in Table 9.5 correspond to the mean result obtained during five trials performed by one individual.

Additionally, the data indicate that HR readings obtained from the Masimo SET® were not consistent with the readings acquired from the Polar™ monitor (*Table 9.5*). This

inconsistency suggests that the Masimo SET® would not be reliable for obtaining accurate readings during jogging.

Table 9.5. *Percent SpO_2 and HR differences (RMSE ± SD) during jogging (N = 300).*

	Masimo SET®		**Polar™**
	SpO_2	**HR**	**HR**
Not Corrected	2.5 ± 1.5	59.7 ± 22.7	6.6 ± 3.6
ANC (X)	1.9 ± 1.2	54.4 ± 19.4	1.8 ± 1.4
ANC (Y)	2.3 ± 1.4	57.5 ± 22.2	5.2 ± 3.5
ANC (Z)	2.3 ± 1.5	56.8 ± 20.9	4.0 ± 2.8
ANC (X+Y+Z)	2.0 ± 1.3	58.0 ± 21.8	2.7 ± 1.7

The results summarized in Table 9.6 show that for all data and an X-axis noise reference input signal, the mean difference in SpO_2 and HR measurements between the non-adaptive and adaptive LMS algorithms is equal to -2.02% and -8.47%, respectively ($p < 0.05$). Similar results were obtained for the tri-axial (X+Y+Z) reference signal; the mean differences in SpO_2 and HR measurements were equal to -1.75% and -8.40%, respectively ($p < 0.05$). These results indicate that using the X-axis and X+Y+Z axis signals as noise reference inputs provided significant improvement in measurement accuracy during jogging.

Table 9.6. *Mean percent differences in SpO_2 (top) and HR (bottom) measurements extracted from the adaptive LMS algorithm for each noise reference input signal.*

	Mean Percent Difference in SpO_2			**95% Confidence Interval**	
	Estimate	SE	*p*	Lower	Upper
X	-2.02	0.73	0.01	-3.52	-0.52
Y	-0.45	0.16	0.01	-0.78	-0.12
Z	-1.09	0.51	0.04	-2.14	-0.04
X+Y+Z	-1.75	0.63	0.01	-3.05	-0.44

	Mean Percent Difference in HR			**95% Confidence Interval**	
	Estimate	SE	*p*	Lower	Upper
X	-8.47	0.97	< .0001	-10.47	-6.46
Y	-1.80	0.30	< .0001	-2.42	-1.18
Z	-5.20	0.78	< .0001	-6.80	-3.59
X+Y+Z	-8.40	0.60	< .0001	-9.64	-7.15

Similar to the results shown for the LMS algorithm, Table 9.7 demonstrate that the RLS algorithm provided improvements in the accuracy of SpO_2 and HR measurements. The mean differences in SpO_2 and HR measurements between the non-adaptive and adaptive RLS algorithms were -1.94% and -5.79%, respectively. The improvement in SpO_2 measurement obtained using the RLS algorithm is comparable to the improvement obtained using the LMS algorithm. In contrast, the improvements in HR obtained from the LMS algorithm are more significant than those obtained using the RLS algorithm.

Table 9.7. *Mean percent differences in SpO_2 (top) and HR (bottom) measurements extracted from the RLS adaptive algorithm utilizing the X+Y+Z noise reference input.*

	Mean Percent Difference in SpO_2			**95% Confidence Interval**	
	Estimate	SE	*p*	Lower	Upper
X+Y+Z	-1.94	0.73	0.01	-3.45	-0.43

	Mean Percent Difference in HR			**95% Confidence Interval**	
	Estimate	SE	*p*	Lower	Upper
X+Y+Z	-5.79	1.24	<.0001	-8.35	-3.24

9.6. TIME DIFFERENCES IN BODY ACCELERATION AND PPG SIGNALS

Results shown by Asada et al suggested that a significant time delay exists between body acceleration and PPG signals acquired from a finger-worn PPG sensor during treadmill jogging [59]. Since the degree of time delay between body acceleration and PPG signals acquired from the forehead has not been shown, an experiment was performed to determine the potential degree of time delay. The effects that implementing a time delay had on measurements were found in order to evaluate the clinical significance of the delay.

Representative data from one jogging trial given in Figure 9.27 show that the degree of correlation between ACC and PPG signals depended on the time delay. Therefore, RMSE and SD were determined over a range of time delays (*Fig. 9.28*). These results indicate that the effect of time delay on measurement error is not considered clinically significant.

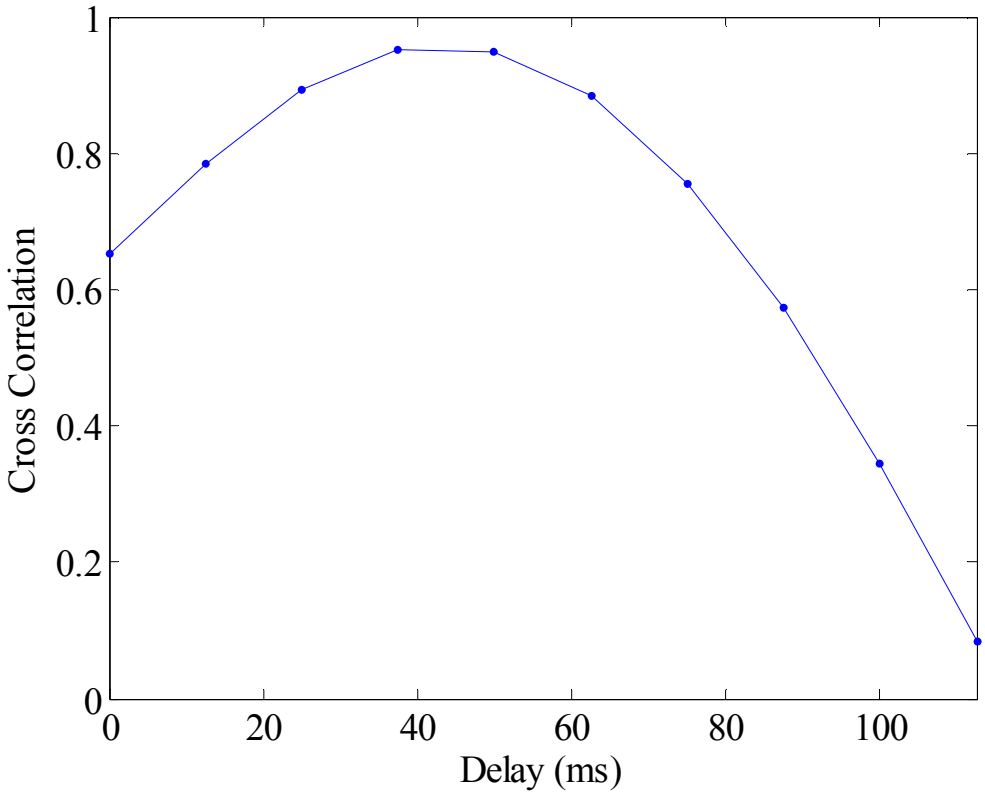

Figure 9.27. *Degree of correlation between ACC and PPG signals for time delays.*

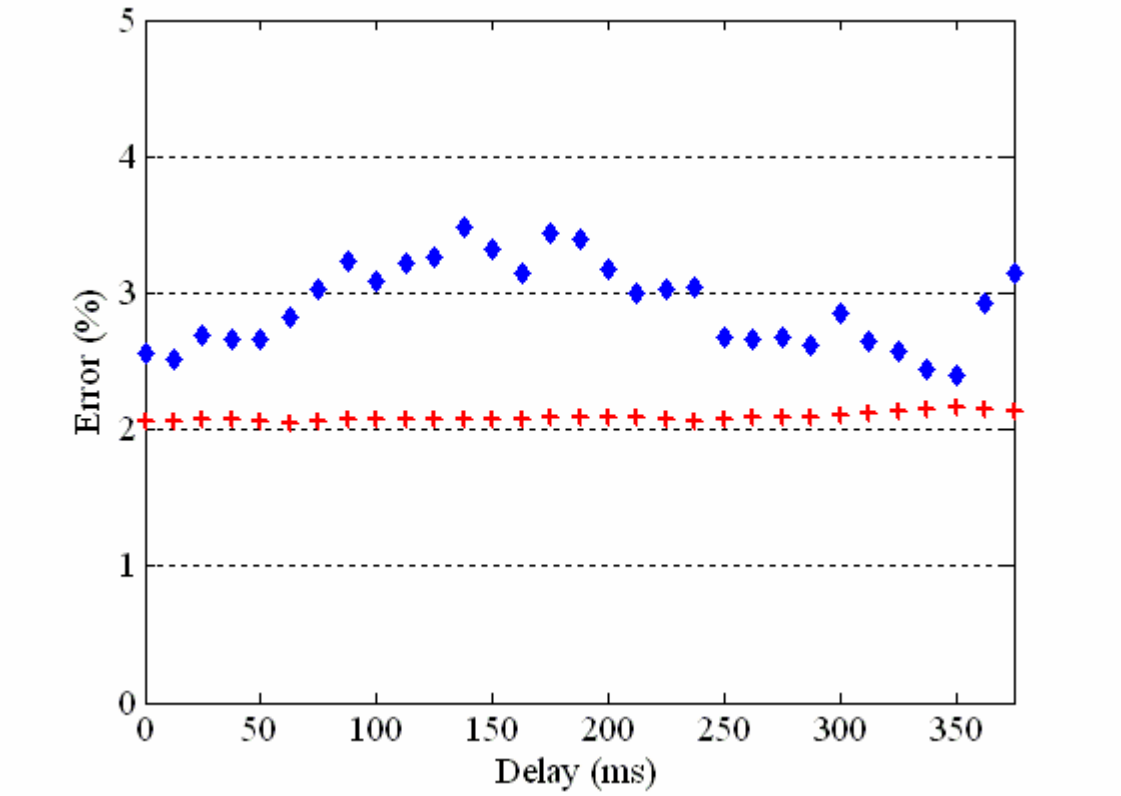

Figure 9.28. *Measurement errors for time delays. SpO_2 and HR errors indicated by + and ♦, respectively.*

9.7. SPECTRAL OVERLAP

MATLAB SIMULATION

Body acceleration and PPG signals were simulated in Matlab using sinusoidal waveforms that shared a common frequency band (*i.e.* $f_{PPG} = 2Hz$, $f_{ACC} = 2.1Hz$). Fig. 9.29 and Fig. 9.30 show frequency spectra of simulated ACC and PPG signals. In these examples, jogging was simulated during which the frequency of activity coincided to varying degrees with the cardiac frequency. Generally, the results showed that the ANC algorithm did not remove the cardiac frequency from the simulated PPG signal unless the spectral overlap between body acceleration and the cardiac rate was within 0.1Hz (*Fig. 9.29*).

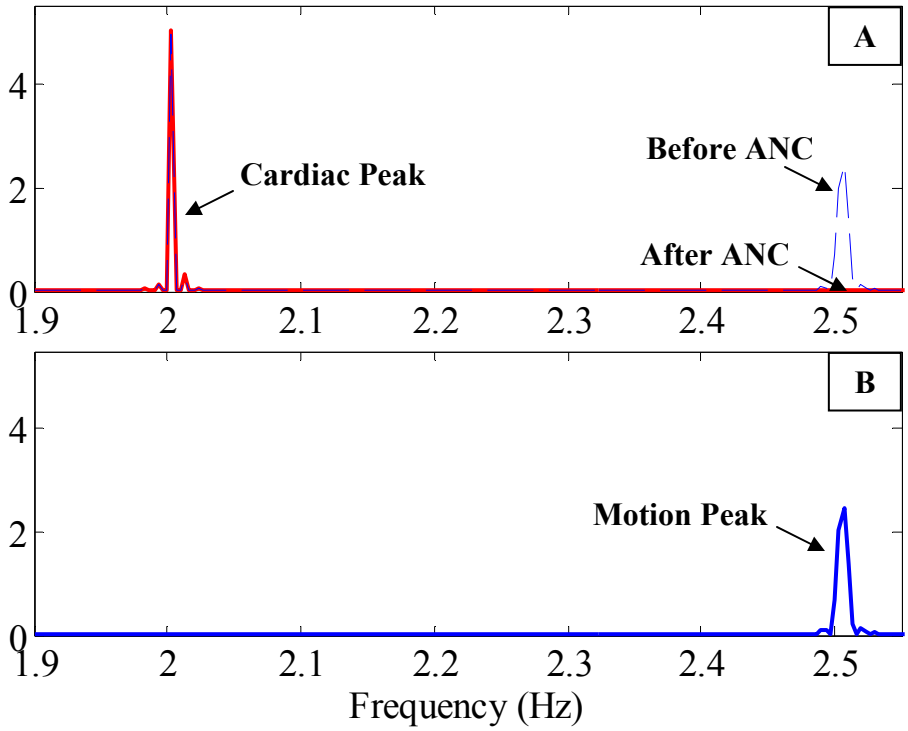

Figure 9.29. *(A) Frequency spectra of simulated PPG and (B) ACC signals consisting of separate frequency bands. All data generated in Matlab.*

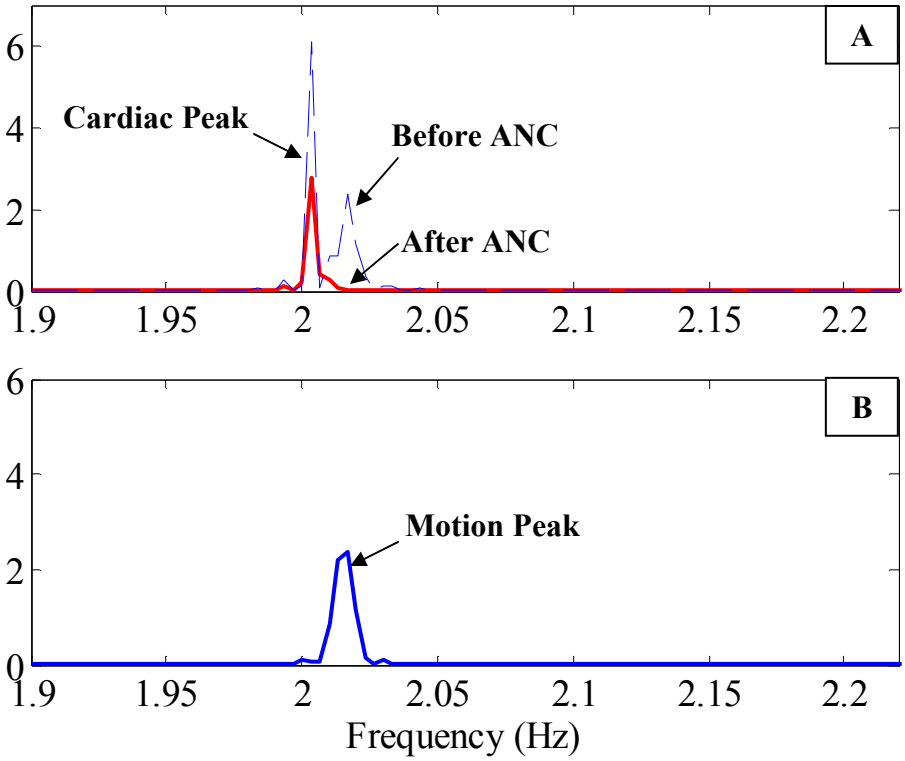

Figure 9.30. *(A) Frequency spectra of simulated PPG and (B) ACC signals consisting of overlapping frequency bands. All data generated in Matlab.*

Spectral Overlap during Jogging Trials

Experimental trials were analyzed during which the cardiac and frequency spectral components overlapped. These data were analyzed separately since these trials provided signals with significant overlap of the body acceleration and cardiac frequencies. Since some researchers suggested that spectral overlap could reduce the effectiveness of an ACC-based ANC algorithm [60], the RMSE and SD were obtained from the trials consisting of spectral overlap.

The spectral overlap data consisted of eight indoor and treadmill jogging trials (*two participants*). Fig. 9.31 shows representative frequency spectra of jogging PPG and ACC signals consisting of spectral overlap. This demonstrates that the ACC-based ANC algorithm attenuates to a certain degree the frequency of body acceleration contained in the PPG signals. This result indicates that the cardiac spectral band is not completely

attenuated by the ANC algorithm.

Fig. 9.32 shows SpO_2 and HR measurements extracted from PPG signals processed by the LMS and RLS algorithms. We noticed that measurement accuracy obtained from PPG signals acquired during spectral overlap was similar to accuracy obtained by processing without the ANC algorithm (M = 0). Additionally, the SpO_2 and HR measurement error is relatively low compared to measurements extracted from signals that did not consist of spectral overlap (*Fig. 9.17*). This suggests that spectral overlap will not cause reduction in SpO_2 and HR measurement accuracy obtained from PPG signals processed by an ACC-based ANC algorithm.

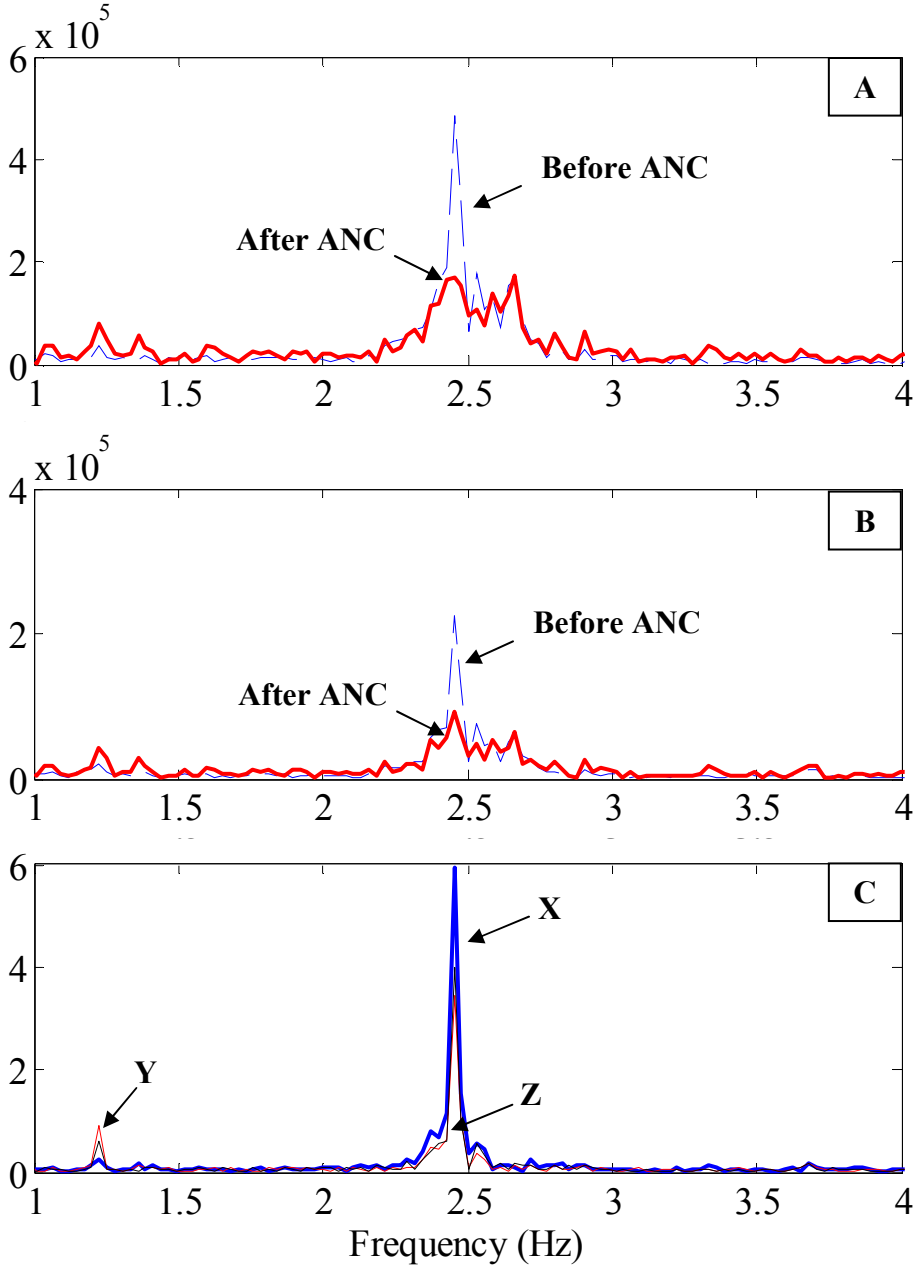

Figure 9.31. *(A) FFT spectra of IR, (B) R and (C) ACC signals consisting of spectral overlap during jogging.*

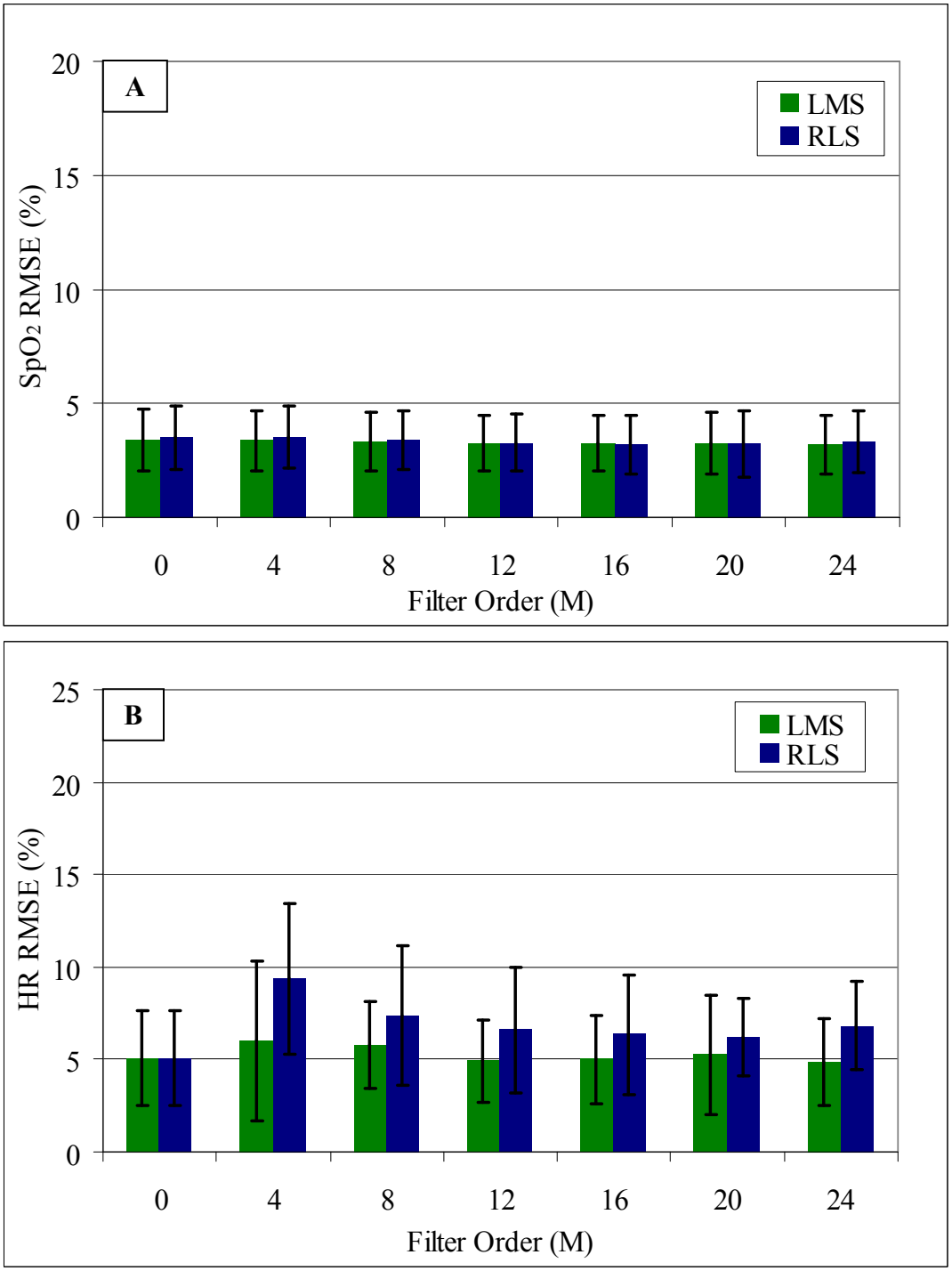

Figure 9.32. *(A) Average SpO_2 and (B) HR RMSE obtained using the LMS (light) and RLS (dark) algorithms for varied filter order. The error bars indicate ±1 SD. The data reflect 8 jogging trials during which there was partial cardiac and motion spectral overlap. M = 0 represents measurements extracted from non-adapted PPG signals.*

9.8. REAL-TIME ADAPTIVE NOISE CANCELLATION

Since the focus of this thesis is real-time physiological monitoring, a study was performed to determine the feasibility of implementing ACC-based ANC software algorithms within the embedded TI-MSP430 μC. Custom-written LMS and RLS algorithms were implemented within the embedded TI-MSP430 μC. To determine the effect of filter order on the execution time of the algorithms, the ACC-based ANC software was implemented in the TI-MSP430 over a range of filter orders. Fig. 9.32 shows the corresponding execution times of the TI-MSP430.

Briefly, Fig. 9.33 shows that the execution time of the adaptive algorithms increase with filter order. The execution time of the LMS increases at a relatively slow rate compared to that of the RLS algorithm. Three difference clock speeds are shown (*80kHz, 1MHz, 8MHz*). These times represent low, medium, and high ranges of the clock within the TI-MSP430 μC.

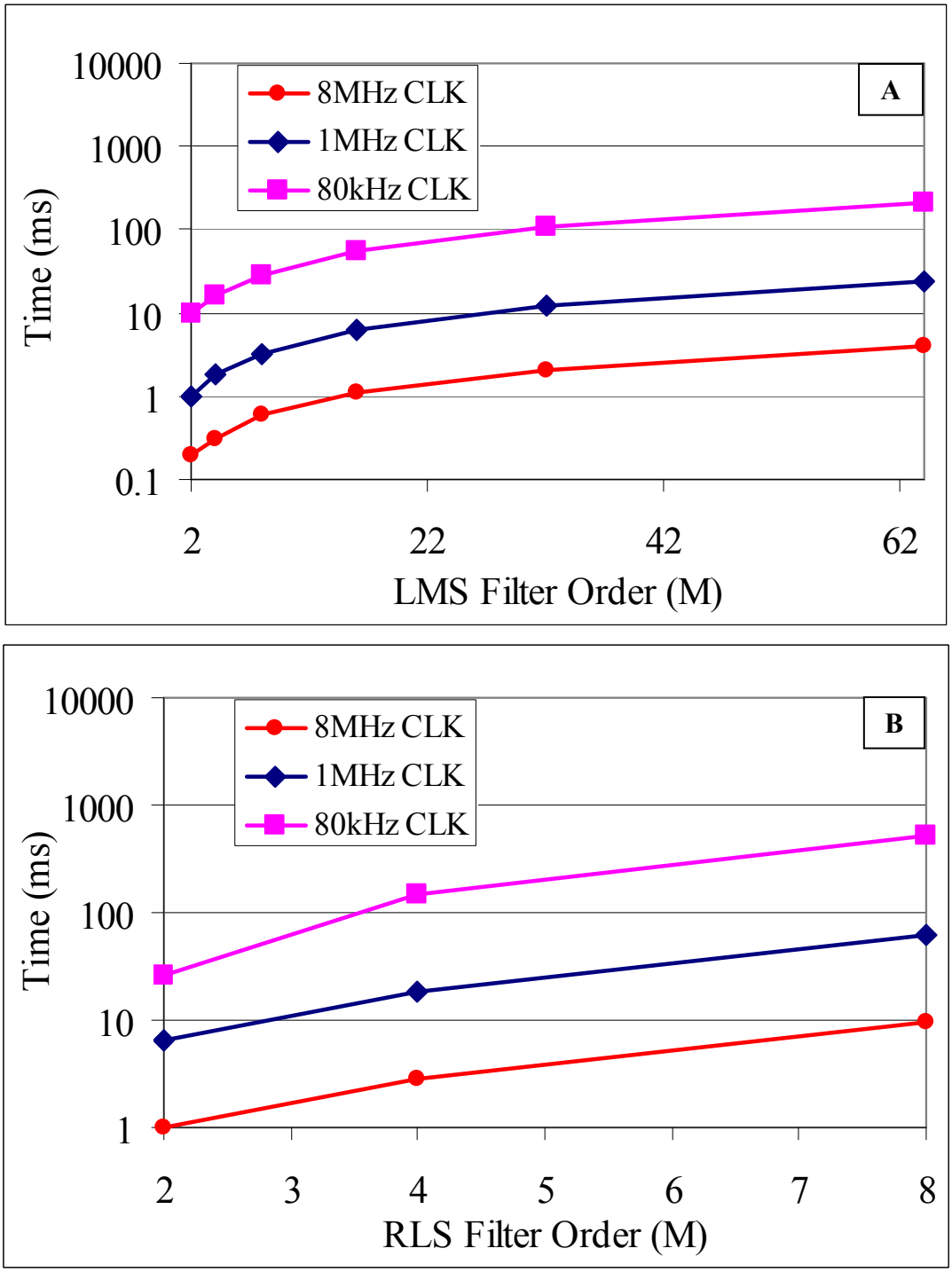

Figure 9.33. *(A) Execution times of the LMS and (B) RLS algorithms in the TI-MSP430 embedded μC.*

10. DISCUSSION

The results from the stationary cycling experiments showed that increased breathing rate did not contribute to measurement inaccuracies during exercise. This suggested that the effects of motion artifacts were caused by body movements rather than physiological changes associated with jogging. Results from *in* vivo jogging experiments confirmed that an ACC-based ANC algorithm could reduce considerably the RMSE of HR readings although the reduction in RMSE of SpO_2 readings was less significant. Since these studies were limited to 32 jogging trials, additional investigation will be required to determine the feasibility to extract more accurate readings from PPG signals acquired during activity in the field. Further, an assessment of the RAM and processing requirements associated with ACC-based ANC algorithms suggested that it would be feasible to implement ACC-based ANC software within the embedded TI-MSP430 μC.

10.1. PRELIMINARY EXPERIMENTS

Experiments showed that the morphology of PPG signals obtained during stationary cycling and resting were similar (*Fig. 9.1*). The primary difference was the amplitude of the PPG signals. Despite this change in amplitude, PPG signals obtained during resting and bicycling appeared very similar in terms of the ability to identify the primary features in the signals.

The spectral content of PPG signals obtained during stationary bicycling was composed primarily of the cardiac spectral band and its harmonics (*Fig. 9.2*). In contrast to Figure 3.7, the PPG signals obtained during cycling only contained a spectral band at the cardiac frequency. This is likely due to the decreased motion associated with cycling.

Therefore, the differences in PPG amplitude were most likely attributed to changes in physiology that occurred during cycling, such as increased breathing rate. This suggests that accurate SpO_2 and HR readings could potentially be acquired from PPG signals during stationary cycling.

Additionally, we noticed that the frequency spectra of the ACC signals acquired during bicycling (*Fig. 9.2C*) consisted of a lower SNR than the ACC signals acquired during jogging (*Fig. 9.13C*). This indicated that the degree of body acceleration that occurred during stationary cycling was significantly smaller compared to treadmill jogging, consistent with decreased motion in cycling. Therefore, the PPG signals associated with cycling were not affected by motion artifacts but rather by changes in physiology, whereas PPG signals associated with treadmill jogging were affected by changes in physiology as well as motion artifacts.

10.2. ALGORITHM MODIFICATIONS

10.2.1. EXTRACTION OF SpO_2 MEASUREMENTS

SpO_2 measurements obtained from the algorithm developed by Johnston [12] were slightly higher than the Masimo reference SpO_2 during jogging (*Fig. 9.5A*). Accordingly, the *SpO_2 Differential Threshold* algorithm was designed to remove derivatives that did not meet the calculated threshold value in order to produce more accurate SpO_2 readings. The removal of low value signal derivatives by the modified algorithm helped to improve the accuracy during jogging.

The algorithm devised by Johnston [12] and the *SpO_2 Differential Threshold* algorithm produced SpO_2 readings that increased steadily during the onset of jogging ($45s < t < 60s$). Although there was a slight time lag, the Masimo reference produced a

similar result (*70s < t < 85s*). Also, the readings obtained using the Masimo reference source and the custom algorithms showed similarly stable trends for 80s < t < 120s. These similarities suggest that the readings obtained were partly due to physiological effects. For instance, the increased SpO_2 values during the onset of jogging could have been a result of physiological changes associated with increased breathing.

The *SpO_2 Differential Threshold* algorithm and the algorithm devised by Johnston [12] detected hypoxic drops in SpO_2 during breath-holding (*100s < t < 116s*). Although the Masimo sensor was held still during hypoxia, the SpO_2 readings did not respond to the same extent as the readings from the custom pulse oximeter. While this could be due to differences in physiology between the forehead and fingers, this indicates that the algorithms incorporated into the custom pulse oximeter were effective in measuring significant changes in SpO_2 during jogging.

Generally, during subsequent data collection, SpO_2 measurements decreased considerably during free, non-treadmill jogging (*Fig. 9.5B*). Although this differed from the results shown in Fig. 9.5A, this result was not surprising since SpO_2 readings typically approach 85% due to pronounced movement artifacts. During persistent motion artifacts, R and IR PPG signals are obtained with similar amplitudes. This produces an ***R*** value near 1 which in turn yields SpO_2 readings near 85% [20]. Since the *SpO_2 Differential Threshold* algorithm produced lower SpO_2 measurements during jogging, this modification provided less accurate measurements. Therefore, the *SpO_2 Differential Threshold* algorithm was not incorporated into the calculation of SpO_2 for measurements obtained from the ACC-based ANC algorithms.

It should be noted that the SpO_2 readings obtained from the finger-worn Masimo

sensor did not approach 85% during jogging. Since the Masimo sensor was worn on a finger that remained still during jogging, this suggests that the drop in SpO_2 was due to the effects of motion artifacts rather than changes in blood oxygenation. Also, we noticed differences in the SpO_2 readings (> *4%*) obtained from the custom and the reference pulse oximeters during the resting portions of Fig. 9.5B. We believe that this was due to differences in SpO_2 calibration.

In addition, we think that the relatively large drop in SpO_2 at the beginning of jogging (*88s* < *t* < *112s*) in Fig. 9.5B could be due to movement artifacts during jogging. We believe that this drop was not due to physiology since the subject was breathing throughout the jogging exercise. Generally, although the SpO_2 readings in Fig. 9.5B were not equal to 85% throughout the jogging period, these variations were not likely due to changes in blood oxygenation level. Since these readings were extracted during intense activity, we believe that the trends in SpO_2 readings can be attributed to the effects of motion artifacts. Also, Fig. 9.5B illustrates that the Masimo reference SpO_2 was relatively stable during the beginning of jogging. As shown in Fig. 9.22, these types of drops in SpO_2 could be attributed to large changes in the DC component of PPG signals.

10.2.2. EXTRACTION OF HR MEASUREMENTS

Time-Based Averaging

In general, the HR measurements extracted using the *Time-Based Averaging* approach provided more accurate readings since the Polar HR readings were also calculated using an averaging routine based on a constant length window. HR measurements acquired during rest using the *Peak Count-Based Averaging* algorithm devised by Johnston [12] provided less accurate readings compared to the *Time-Based Averaging* algorithm for an

average HR of 95bpm (*Fig. 9.6*). The less accurate readings obtained for higher average HR values in the *Peak Count-Based Averaging* algorithm likely result from a shorter averaging time, since it incorporated 10 beats. Table 10.1 summarizes the changes in the time averaging window for elevated HR values. This demonstrates that the amount of time represented by the HR reading can vary considerably even during resting conditions. The time represented by the *Peak Count-Based Averaging* algorithm varies much more during activity since, for example, HR can reach levels as high as 240bpm, representing a 2.5s window.

From a clinical perspective, the *Time-Based Averaging* approach would be more appropriate than a routine based on the number of peaks since the amount of time corresponding to readings extracted using an averaging method with a constant averaging length would provide more consistent results. Typically, commercially available pulse oximeters provide different averaging settings [28]. This provides a range of response times that can be utilized during patient monitoring. Since a constant response time is desired in these applications, we suggest that the *Time-Based Averaging* algorithm should be utilized for the calculation of HR values.

Table 10.1. *HR averaging time for the Peak Count-Based Averaging algorithm during rest.*

Resting HR (bpm)	Peak Count-Based Averaging (s)
50	12.0
60	10.0
70	8.6
80	7.5
90	6.7
100	6.0
110	5.5
120	5.0

Extraction of HR from R and IR PPG Signals

As described in Section 9.2.2, the *Extraction of HR from R and IR PPG Signals* modification made to the HR algorithm did not incorporate outlying IHR values into the calculation of HR. IHR values were extracted separately from R and IR PPG signals. Values that differed significantly (*greater than 200% or less than 50%*) were considered outliers and were removed from the calculation of the HR reading. As shown in Fig. 9.8, the IHR values rejected during jogging included the low outlying values extracted from the IR signal as well as values extracted from the R signal. In this example, the values extracted from the IR signal deviated significantly from the mean HR reading whereas the values extracted from the R signal were comparable to the mean HR reading. This shows that accurate IHR measurements derived from the R signal were identified as erroneous and discarded (*false negatives*) from the calculation. Therefore, to reduce the amount of false negatives removed from the HR reading, the *IHR Threshold* modification was implemented.

It was shown that the signal derivatives associated with the R signal provided more consistent peak detection during jogging since the morphology of the R signal was generally less affected by amplitude changes due to respiration than the IR signal. Despite more consistent peak identification in the R signal, we found that the *Extraction of HR from R and IR PPG Signals* routine did not completely reduce the effects of motion artifacts during jogging. The frequency band associated with motion dominated the spectral content of the PPG signals during jogging (*Fig. 3.7*). Since this algorithm did not reduce the spectral content due to motion, this algorithm modification did not sufficiently minimize the underlying effects contributed by motion artifacts.

The range of values used to reject IHR measurements from the calculation of HR was

selected in order to remove IHR values due to extraneous peak detection and missed peaks. For the sample studies performed in this thesis, the range used to reject IHR values (*greater than 200% or less than 50%*) was appropriate for measurements acquired during jogging.

IHR Threshold

The *IHR Threshold* routine was effective in removing erroneous high and low IHR values from the calculation of HR averages. The rejection of erroneously high IHR values (*Fig. 9.9*) provided more accurate HR measurements during jogging since erroneous multiple peaks were detected and removed by the algorithm. Similar to the range used by the *Extraction of HR from R and IR PPG Signals* algorithm, this algorithm modification utilized a range (*greater than 175% or less than 50%*) to reject IHR measurements from the HR calculation. This particular range was selected in order to remove IHR values due to extraneous peak detection and missed peaks since it was appropriate for measurements acquired during jogging. Likewise, the rejection of erroneously low IHR values (*Fig. 9.10*) provided more accurate HR measurements during jogging since heavy respiration associated with jogging resulted in missed peaks. A potential short-coming of this study was that an additional test was not performed to determine the feasibility of modifying the range to reject erroneous high and low IHR readings in order to improve the sensitivity and specificity of the algorithm. Future studies should be performed to evaluate the range used to reject high and low IHR readings during jogging.

Fig. 9.11 showed that despite several modifications to the HR algorithm, HR measurements remained inaccurate during jogging. Specifically, this figure indicated that the HR readings obtained with the modified algorithm were consistently greater than the

Polar® reference measurements. Analysis showed that these HR readings were higher since the motion spectral component in the PPG signal was at a higher frequency than the cardiac spectral component (*Fig. 3.7*). This confirms that an advanced signal processing solution to attenuate the motion spectral band is required to reduce the effects of motion artifacts.

10.3. ADAPTIVE NOISE CANCELLATION

PPG Signal Morphology

Raw IR and R PPG signals acquired during jogging, as shown in Fig. 9.12, had an inconsistent morphology due to the effects of motion artifacts. For example, inspection of the raw IR signal (*Fig. 9.12A*) showed that it was difficult to discern true portions of the PPG signal from portions that were consequences of the induced motion artifacts. Conversely, the morphology of the adaptively filtered IR signal (*Fig. 9.12B*) appeared to have more consistently shaped peaks. Similarly, the morphology of the R signal was changed significantly after being processed by the ANC filter. Qualitatively, Fig. 9.12 showed that the noisy portions of the IR signal (*Fig. 9.12A*) appeared to be corrected such that peaks were identified more easily in the adaptively filtered signal (*Fig. 9.12B*). This is illustrated in Fig. 10.1. Also, the morphology of the adaptively filtered R signal was comparable to the corrected IR signal, although we noticed that the peaks were generally sharper in the corrected IR signal.

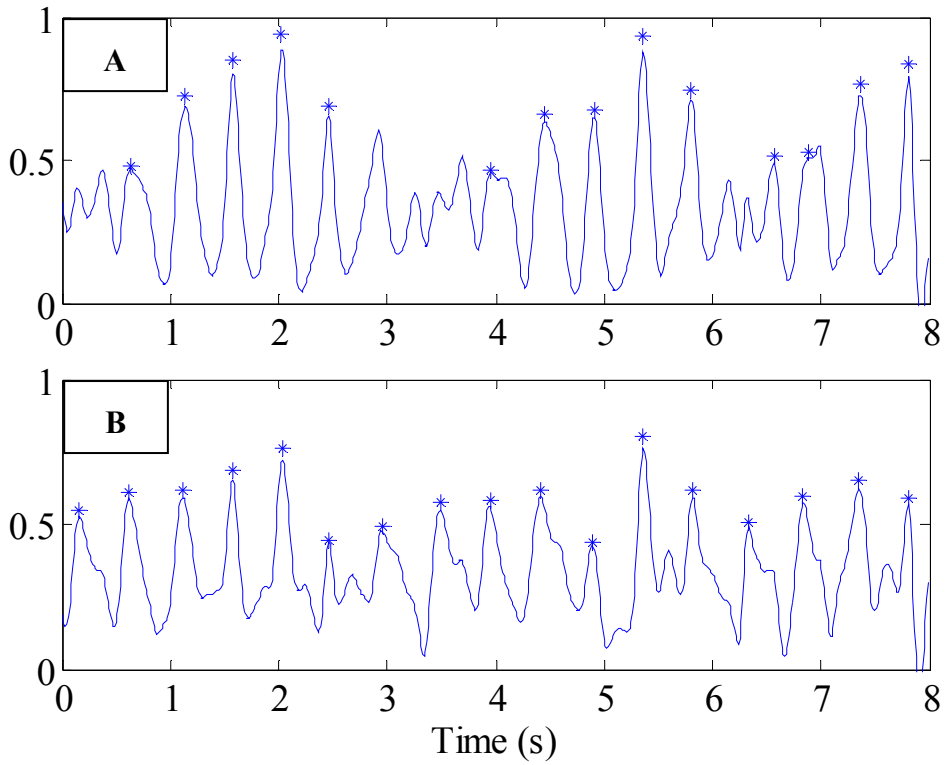

Figure 10.1. *IR PPG signals during jogging. (A) Noisy IR signals before applying ANC. (B) Adaptively filtered IR signals. * indicate automatic software-detected peaks.*

Frequency spectra of PPG signals obtained during jogging, as depicted in Fig. 9.13, revealed that PPG signals acquired during jogging were dominated by frequencies corresponding with body acceleration. Hence, the contribution of body acceleration to the spectral content of the PPG signal was the primary cause for reduced measurement accuracy during jogging. Fig. 9.13 also showed that the ACC-based ANC algorithm was effective in removing the frequency associated with body acceleration, which increased the SNR of the PPG signals obtained during jogging. The ANC algorithm functioned effectively as a band-rejection filter and attenuated the frequency spectrum corresponding to body acceleration. It should be kept in mind that since the frequency band of body acceleration was not known *a priori*, an ordinary band-reject filter with a fixed rejection band would not have been as effective in attenuating the spectral content due to body

acceleration.

As discussed in Section 9.1., despite the modifications made to the SpO_2 and HR extraction algorithms developed by Johnston [12], no considerable improvements were found in measurement accuracy during jogging. Therefore, an ACC-based ANC algorithm was studied since other researchers have suggested that this method could potentially improve measurement accuracy during jogging [16, 42, 47-51].

To address the feasibility of improving the performance of the custom pulse oximeter during jogging, the effectiveness of ACC-based ANC algorithms was investigated. The ACC-based ANC approach was effective in removing the frequency of motion from the corrupted PPG signals (*Fig. 9.13*). This result demonstrated that body acceleration signals, which were obtained from the forehead-worn SM by the integrated ACC, were an effective noise reference input signal to the ANC algorithm. Although some authors have presented similar work, this finding was significant since previous research focused on finger-worn PPG sensors [42, 47] which are known to be more prone to motion artifacts [20].

As described in Section 9.2, the parameters of the LMS and RLS algorithms were varied to determine the effect of these values on measurement accuracy during jogging. Studies were conducted to determine optimal values of μ, M, for the LMS algorithm and λ and M for the RLS algorithm.

10.3.1. LMS: STEP-SIZE SELECTION

It is known from the literature that a small valued step-size, μ, is desirable since this provides an LMS filter with relatively low adjustment error [53]. Larger μ values are known to increase the learning rate of the adaptive filter at the expense of increased

adjustment error. Faster adaptation speed could be more desirable for certain applications that do not require low measurement errors [53]. Utilizing an adaptive filter for real-time physiological monitoring would require relatively low adjustment error such that accurate measurements could be obtained [53].

Generally, the findings of this thesis agreed with the literature regarding the selection of a range of relatively small μ values for the implementation of the LMS algorithm [53]. Results for HR calculations showed that $0.01 \leq \mu \leq 0.028$ provided the lowest RMSE and SD values during jogging (*Fig. 9.14*). In addition, the RMSE and SD associated with HR measurements tend to increase for $\mu > 0.032$. Conversely, the RMSE and SD of SpO_2 measurements did not vary significantly as a function of μ, but the minimum RMSE for SpO_2 measurements were obtained for $0.032 \leq \mu \leq 0.046$.

HR measurements were generally more affected by changes in μ since subtle variations in PPG morphology affected peak identification. Conversely, SpO_2 readings were less affected by changes in μ since readings were calculated based on a 1s average window. Therefore, measurements were extracted using LMS filters with the optimal value found for HR readings ($\mu = 0.016$).

Although the effects of μ on SpO_2 and HR errors had not been discussed previously in the literature, some authors reported using μ values comparable to the range reported in this thesis [53]. For real-time implementation of an LMS algorithm, it would not be feasible to vary the μ associated with the adaptive filter based on the ACC and PPG signals since these data would not be known *a priori*. Typically, μ would be set offline in software during the initial implementation of the algorithm. Since the results showed that HR accuracy was mostly affected by μ, the range of values determined in this study (*0.01*

$\leq \mu \leq 0.028$) would be most appropriate for the implementation of an LMS algorithm. Furthermore, since the studies conducted in this thesis were limited to jogging experiments, the potential effects of μ on the accuracy of SpO_2 and HR measurements were not determined for other types of activities.

10.3.2. RLS: FORGETTING FACTOR SELECTION

It is known that the value of λ affects the "memory" of the RLS algorithm (i.e. *the degree to which past data is present in the algorithm*) [53]. Specifically, $0.9999 \leq \lambda \leq 1$ has been typically utilized for RLS algorithms [53]. Some authors have suggested that RLS algorithms using λ within this range could be effective in reducing the effects of motion artifacts in PPG signals during movement [57].

The effect of λ on SpO_2 and HR errors was presented in section 9.2.2. It was found that $\lambda = 0.99$ provided optimal RMSE during jogging. HR measurements extracted from PPG signals adaptively filtered using $0.99 \leq \lambda \leq 0.998$ provided the lowest mean RMSE and SD. Similarly, the RMSE and SD of SpO_2 measurements were minimized for $0.94 \leq \lambda \leq 0.99$. In addition, it was found that the RMSE of SpO_2 increased for $\lambda > 0.99$, as depicted in Fig. 8.12 and 8.13. Therefore, SpO_2 and HR measurements were extracted from RLS filters with $\lambda = 0.99$.

Although some authors have suggested different values of λ for ANC algorithms [57], an analysis of how λ affects SpO_2 and HR measurement accuracy has not been shown previously in the literature. Real-time implementation of an RLS algorithm would require a constant λ to be set in software during initial implementation of the algorithm since ACC and PPG data would not be known *a priori*. Based on the results found in this

thesis, we concluded that $\lambda = 0.99$ would be the most appropriate value for the implementation of an RLS algorithm in real-time.

10.3.3 SELECTION OF FILTER ORDER

The filter order, *M*, of an adaptive filter algorithm affects the required computational time as well as measurement errors. LMS and RLS adaptive algorithms were studied since the software needed to implement these functions consists of relatively simple discrete-time equations [53-56]. In addition, due to the relatively simple implementation, these algorithms appeared extensively in the literature [16, 42, 47-51].

To study the potential effects of *M* on SpO_2 and HR accuracy, *M* was varied using a constant $\mu = 0.016$ and $\lambda = 0.99$ parameter in the LMS and RLS algorithms, respectively. SpO_2 and HR accuracy correlated with the order of the adaptive filter. As shown in Fig. 9.17, improvements in RMSE and SD appeared to settle for $M = 16$. These data also showed that the LMS and RLS filters obtained similar reduction in RMSE as a function of *M*.

We found that RMSE and SD were reduced for higher order adaptive filters (*Fig. 9.17*). This was an expected result since it was shown in the literature that adjustment error decreases for higher order filters [53]. Also, some authors have suggested that filters with $M = 10$ [59] and $M = 20$ [49] could potentially reduce the effects of motion artifacts which is in agreement with the findings of this thesis. Our data indicated that more significant improvement in measurement accuracy can be obtained for increased filter order (*i.e. M = 24*).

Asada et al [59] and Foo et al [49] have suggested that an ANC algorithm could provide significant reduction in the effects of motion artifacts during treadmill jogging.

Generally, the results presented in this thesis agree with results reported by these researchers. The data shown in Fig. 9.17 demonstrate that the LMS and RLS algorithms provided significant reduction in the RMSE and SD of SpO_2 and HR measurements during jogging. Although the improvement in SpO_2 accuracy (*Fig. 9.17A*) was similar for the LMS and RLS algorithms, HR accuracy obtained using the LMS was more significant than that obtained using the RLS algorithm (*Fig. 9.17B*).

Our results indicate that significant reduction in RMSE can be obtained by utilizing an ACC-based ANC algorithm for a forehead-worn PPG sensor. This result was similar to findings by Asada et al [59] and Foo et al [49], although they used finger-worn sensors. This suggests that the assumptions of the ACC-based ANC algorithm regarding body acceleration signals used as a reference to detect motion local to the finger-worn PPG sensor is also appropriate for forehead-worn sensors.

10.4. ANALYSIS METHODS

Mean percent differences were obtained between measurements derived using the ANC algorithms and reference measurements. The results showed that there was a large degree of variation in mean percent differences among participants, as shown in Figs. 9.18 and 9.19. Therefore, an ANOVA was used with a model to account for the differences among participants.

As shown in Section 9.1, the SpO_2 and HR algorithms devised by Johnston [12] were modified in order to obtain more accurate measurements during jogging. For comparison, PPG signals adaptively filtered by the LMS and RLS algorithms using ACC signals as noise reference were processed by the algorithms developed by Johnston as well as the

modified algorithms. The one-way ANOVA was used to determine the significance of the differences between these measurements.

10.4.1. SpO_2 Differential Threshold

The *SpO_2 Differential Threshold* algorithm was implemented to determine whether the rejection of certain SpO_2 derivatives would provide more accurate readings from adaptively filtered PPG signals. However, the mean percent differences of -0.41 and -0.25 obtained by the LMS and RLS algorithms, respectively, indicated that this modification provided less accurate readings. Since the CI_{95} of the difference between the RLS and the reference measurements contained 0, a difference of 0 would be an expected result. This indicates that there is potentially no statistically significant difference between the measurements obtained from RLS-adaptively filtered signals using the SpO_2 algorithm developed by Johnston [12] and the *SpO_2 Differential Threshold* algorithm developed in this thesis.

As shown in Section 9.1.1 and discussed in Section 10.1.1, the *SpO_2 Differential Threshold* algorithm obtained lower SpO_2 values from PPG signals acquired during jogging (*Fig. 9.5*). For non-adaptively filtered PPG signals, this modification generally provided less accurate measurements during jogging. In comparison, the ACC-based ANC algorithm produced more accurate SpO_2 measurements than the non-adaptive algorithm (M = 0) (*Fig. 8.14*). Likewise, in the example shown in Fig. 9.21, the adaptively filtered PPG signals provided SpO_2 measurements that were closer to the reference values during jogging. Generally, the *SpO_2 Differential Threshold* algorithm provided SpO_2 measurements that were less accurate than the algorithm designed by Johnston [12]. Therefore, the SpO_2 algorithm designed by Johnston [12] was

implemented in this thesis and should be utilized for the calculation of SpO_2 readings.

PPG signals acquired during jogging (*Fig. 9.22*) suggested that SpO_2 accuracy may be significantly affected by changes in the DC components of PPG signals. Although this result was not observed in the literature, it was found to occur during a limited number of experiments. This result suggests that potentially more accurate SpO_2 measurements could be obtained if the effects of motion artifacts on the DC components of PPG signals can be minimized.

10.4.2. HR AVERAGING

The *Peak Count-Based Averaging* algorithm [12] provided inaccurate HR readings during rest, as shown in Fig. 9.6B. These inaccuracies were a consequence of varying the response times of the *Peak Count-Based Averaging* routine (*Table 9.1*). The *Time-Based Averaging* algorithm shown in Section 9.1.2 provided HR readings with a constant time response which was therefore independent of HR readings. The data in Table 9.2 showed that the improvement in the RMSE of the measured HR was considered significant using the LMS algorithm ($p < 0.0001$) but was not considered significant using the RLS algorithm ($p = 0.115$). This modification was particularly important for comparison purposes since averaging in commercial pulse oximeters typically consists of averaging readings within fixed time length windows (*typically 2s to 16s*) [22, 28].

10.4.3. EXTRACTION OF HR FROM R AND IR SIGNALS

IHR values extracted from R signals were utilized to improve the accuracy of HR measurements during jogging. Results shown in Section 9.3.3 indicated that by employing the modified HR extraction scheme, 10.75% and 34.14% mean improvement

in HR measurement were obtained from the LMS and RLS algorithms, respectively. These mean differences were significant at the $p = 0.05$ level (*Table 9.3*).

10.4.4. IHR THRESHOLD

The IHR threshold routine was used to reject IHR values that varied significantly from the average HR readings. Data in Section 9.3.4 confirmed that by using the *IHR Threshold* algorithm, 20.52% and 63.17% mean improvement in HR measurement can be obtained from the LMS and RLS algorithms, respectively. These mean differences were significant at the $p = 0.05$ level (*Table 94*).

As described in Section 9.3.4 and 10.1.2, IHR values were rejected from the average HR reading by employing a threshold range of 50% and 175% difference between the R and IR derived IHR values. The results showed that this threshold range was appropriate for adaptively filtered PPG signals since multiple peak detection and missed peaks also occurred in these signals (*Fig. 9.23, 9.24, 9.25*).

The results indicated that the HR extraction algorithms significantly improved measurement accuracy extracted from adaptively filtered PPG signals, as shown in Fig. 9.26. The results associated with these modifications were significant since a limited amount of research exists regarding the feasibility of obtaining more accurate measurements from a wearable pulse oximeter during episodes of motion artifacts. Some researchers suggested that an ACC-based ANC algorithm could improve HR accuracy [49, 59], although details regarding the method of HR extraction were not reported. The results in this thesis indicated that ACC-based ANC, in conjunction with modified measurement extraction algorithms, were effective in obtaining more accurate measurements during jogging.

It should be noted also that inaccurate HR readings were obtained by processing adaptively filtered PPG signals in the *Signal Derivative* algorithm devised by Johnston [12], as shown in Fig. 9.26. This indicates that the algorithm modifications helped to remove erroneous HR calculations from the final HR reading. In contrast, the algorithm developed by Johnston did not incorporate clever routines to reject inaccurate measurements.

In addition, Fig. 9.26 indicated that the HR readings obtained from the Masimo reference pulse oximeter were unresponsive to the changes in HR. We noticed that inaccurate Masimo readings were obtained during several jogging trials despite keeping the finger-worn sensor relatively still during jogging. This suggests that the software incorporated into the Masimo pulse oximeter detected corrupted PPG signals, therefore, limiting the usefulness for field applications.

Jogging Activity

Jogging was the primary type of activity studied in this thesis since this activity induced intense motions which would be typical during some field applications. Other body movements pertinent to soldiers and first responders that can occur in the field (*i.e. crawling, jumping, climbing, etc.*) were not studied. The results from these limited studies indicated that the ACC-based ANC algorithms can provide substantial improvements in SpO_2 and HR accuracies. Despite these improvements, the readings may not be sufficiently reliable for diagnosis purposes during jogging. With this in mind, it should be noted that the primary aim of this work was not to develop a wearable pulse oximeter for jogging, but rather to study the effects of motion artifacts associated with jogging activity. Therefore, improvements in SpO_2 and HR measurement accuracy, as shown in

Fig. 9.17, suggest that ACC-based ANC could provide more accurate readings during other activities typical in the field. However, future studies should be performed to assess the potential for obtaining more accurate readings during other types of activities.

Additionally, a sustained activity was studied in order to characterize the ACC-based ANC algorithms. Since an adaptation process was an inherent component to this algorithm, sustained activity was studied to simplify the analysis of the ANC systems. Practically, since movements in the field can change continually, additional studies should be conducted to evaluate ACC-based ANC algorithms for these types of changing activities.

From a clinical standpoint, the ACC-based ANC algorithm and the modified software provided more accurate readings during jogging. Despite this improvement, it might not be feasible to measure precisely the SpO_2 and HR of a jogger due to the high degree of movement artifacts. Generally, by obtaining certain body orientation and activity information (*i.e. standing and performing high activity*), a medic would be able to infer that the soldier was not injured. Similarly, a medic could rely on body acceleration information as an indication that if an individual remains motionless and is lying on the ground, there is a greater probability that the person may be wounded.

10.5. ACCELEROMETER AXES SELECTION

To determine how each axis may help to improve measurement accuracy, a triaxial ACC was integrated within the forehead-mounted SM. The results indicated that the vertical acceleration signal was the most dominant plane of acceleration during jogging (*Fig. 9.13C*). This suggests that the frequency associated with the vertical displacement

of the SM during jogging contribute significantly to the spectral content of the motion-corrupted PPG signal.

The results described in section 9.4 showed that the X-axis reference signal provided significant improvement in SpO_2 and HR measurements during jogging. It was also shown that the combined X+Y+Z signal provided comparable results (*Table 9.5*). Despite the similarity between the results obtained by the X vs. X+Y+Z signals, the implementation of a triaxial ACC would be more advantageous than a single axis ACC. For example, during sensor misalignment, a single vertical-axis ACC could become misaligned, thus providing an ineffective noise reference signal. Hence, an X+Y+Z signal would be a more effective noise reference.

A practical advantage of a triaxial ACC is that accurate body activity and posture information can be extracted [52]. In addition, utilizing the tilt-sensing component can indicate posture more accurately. For example, Bouten et al have shown that signals from a triaxial ACC could be processed in software to assess the level of activity and posture [52]. In contrast, since a single-axis ACC represents only 1 physical plane of movement, only limited information would be acquired.

For instance, a triaxial ACC would be especially useful during combat since ACC signals could indicate that a soldier is lying down and remains inactive. Thus, a medic would consider the SpO_2 and HR readings acquired during rest to be reliable and therefore assess the health status with greater confidence.

Additionally, Table 10.2 shows that the power consumed by obtaining a single axis of body acceleration is comparable to obtaining three axes of acceleration. The effective duty cycle was calculated as the portion of time during which the ACC draws current

(*0.5mA average current draw*). Since the ACC signals were sampled at 80Hz, a 12.5ms sampling period was used for calculations. For instance, sampling a single axis ACC would require 1ms for ACC turn-on time and 0.2ms for sampling by the μC for an effective duty cycle of 9.6% (*i.e. 1.2ms/12.5ms*). The duty cycles associated with a 2-axis and 3-axis ACC were calculated by allowing 0.2ms of sampling time for each additional axis.

Compared to sampling a single-axis ACC, these data show that usage time is decreased by 14.3% and 31.8% by sampling a dual-axis and tri-axis ACC, respectively. Although a reduction in usage time could limit the effectiveness of a battery-powered device, results indicated that a triaxial ACC provided an effective noise reference to an ANC filter. In addition, it was suggested in the literature [52] that triaxial ACC signals can indicate accurately body activity and orientation. Therefore, despite a slight decrease in usage time, it would be advantageous to utilize a triaxial ACC for remote physiological monitoring.

Table 10.2. *Power consumption of the ACC.*

	ACC Average Current (mA)	**Effective Duty Cycle**	**Battery Capacity (mAh)**	**Usage Time (h)**
1-axis ACC	0.5	0.096	220	4583
2-axis ACC	0.5	0.112	220	3928 (-14.3%)
3-axis ACC	0.5	0.128	200	3125 (-31.8%)

10.6. TIME DIFFERENCES IN BODY ACCELERATION AND PPG SIGNALS

It was suggested in the literature that significant time delays exist between ACC and PPG signals acquired during jogging [59]. Fig. 10.2 shows the cross-correlation between ACC and motion-corrupted PPG signals found by Asada and co-workers [59]. The

results in Section 9.5 showed that body acceleration and PPG signals acquired from the custom pulse oximeter produced a higher cross-correlation value for various time delays which was similar to the findings of Asada et al [59]. It was expected that more accurate measurements would be obtained by implementing a fixed delay between the ACC and PPG signals. Despite this expectation, it was found that a time delay did not significantly affect SpO_2 and HR accuracies (*Fig. 9.28*). Therefore, it was determined that the ACC-based ANC algorithm does not require the implementation of a fixed time delay.

As described previously, a constant delay was implemented in this thesis to simplify the software associated with the ACC-based ANC algorithm. In general, a variable time delay would have complicated the methodology and ultimately the real-time software implementation associated with the pulse oximeter. Since the results did not provide compelling evidence that a time delay significantly affects measurement accuracy, there is no reason to implement a time delay between the ACC and PPG signals.

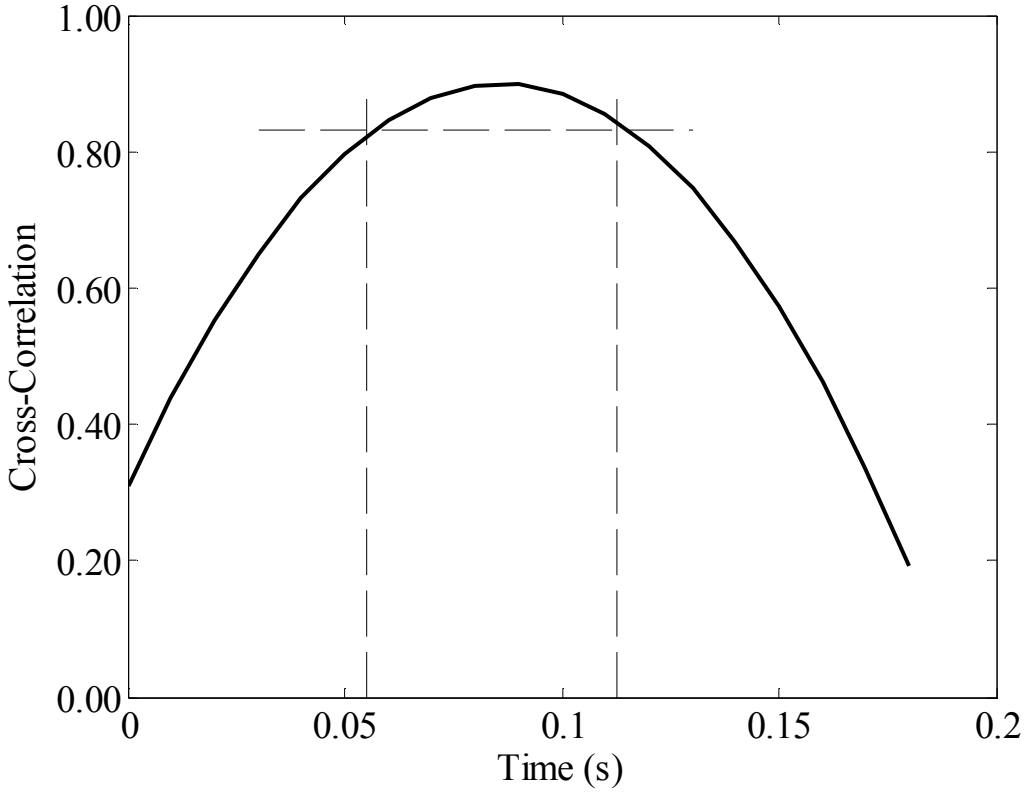

Figure 10.2. *Cross-correlation between body acceleration and PPG signals as a function of time delay [42].*

10.7. SPECTRAL OVERLAP

It was suggested in the literature that spectral overlap between ACC and motion corrupted PPG signals could reduce the effectiveness of the ACC-based ANC algorithm [60]. Consequently, it was expected that the ANC algorithm would attenuate the cardiac spectrum during cases of spectral overlap since the ANC algorithm is essentially a tunable band-reject filter. To test this assertion, ACC and PPG signals consisting of spectral overlap were simulated in Matlab (*Section 9.6.1*). The results showed that the spectral band of the PPG signal was attenuated by about 50% when the spectral band of the ACC signal was within 0.1Hz (*Fig. 9.30*).

To determine the potential effects of spectral overlap during jogging, experiments consisting of spectral overlap were analyzed. It was found that spectral overlap did not

have a significant effect on the accuracy of SpO_2 and HR readings during jogging (*Fig. 9.32*). This supports our Matlab simulations since it was found that the frequency of the desired signal was not attenuated to a significant degree during experimental trials. Practically, PPG signals consist of continually changing frequency components associated with activity, as well as variations in the cardiac and respiration rates. This suggests that there is a low probability that cardiac and body acceleration signals would overlap entirely during jogging. Therefore, we believe that the ACC-based ANC algorithm would be effective in improving SpO_2 and HR accuracy during jogging.

10.8. REAL-TIME ANC

Since this thesis focused on real-time physiological monitoring, we have investigated the feasibility of implementing an ACC-based ANC algorithm within an embedded μC. Each algorithm was investigated for operation in the embedded TI-MSP430 μC. It was found that the LMS and RLS algorithms provided similar improvements in SpO_2 and HR accuracy. Table 10.3 shows the execution time required for the μC to process one sample of the ACC and PPG signals by the LMS and RLS algorithms. The projected execution times for the RLS filter (M = 16, 32, 64) were calculated by extrapolating a 2^{nd} order curve fitted to the data obtained from implementing the algorithm in the embedded TI-MSP430 μC (M = 2, 4, 8).

Table 10.3: *LMS and RLS execution times measured from the embedded TI-MSP430 μC.*

	LMS Execution Time (ms)		
Filter Order (*M*)	80kHz CLK	1MHz CLK	8MHz CLK
2	9.6	1	0.2
4	16	1.8	0.3
8	29	3.2	0.6
16	56	6.2	1.1
32	108	12.2	2
64	208	24	4

	RLS Execution Time (ms)		
Filter Order (*M*)	80kHz CLK	1MHz CLK	8MHz CLK
2	26	6.5	1
4	150	18.5	2.8
8*	510	63	9.4
16‡	2.6E04	1.3E03	182
32‡	4.6E07	4.6E05	6.1E04
64‡	1.5E14	6.0E10	6.9E09

* Due to limitations in system hardware, an 8th order RLS filter was the highest order than could be implemented in the embedded TI-MSP430 μC. ‡ These values represent projected execution times based on the data measured for $2 < M < 8$.

Since the communication protocol of the custom pulse oximeter consists of processing 40 R and IR data samples, the projected execution times for processing 80 samples are shown in Table 10.4. These projected values suggest that the processing requirements of the LMS and RLS algorithms could potentially be a limiting factor in the implementation of the ACC-based ANC algorithm if the TI-MSP430 μC is utilized.

Since the SM and RM transmission cycle consists of 3 transmission bursts once every 500ms, the remaining time (37/40 bursts) can be used for processing. This represents 92.5% of 500ms or 460ms of the processing time in the RM [61]. Since peripheral functions and calculation of measurements requires 150ms, a total of 310ms would be

available for processing associated with the ANC algorithm (these times are bolded in Table 10.4). Due to the substantial amount of processing associated with the RLS adaptive algorithm, it was found that implementation of the algorithm within the embedded μC requires considerable execution time. Therefore, it would be more feasible to implement an LMS type adaptive algorithm.

The effect of clock speed on the power consumption of the μC could limit the order of the filter implemented within the μC. Reduction of measurement error obtained by the ANC filter increases as a function of the filter order (*M*). Since processing time, and therefore power consumption, increases with filter order, the filter order parameter should be minimized. Note that, as shown in Fig. 9.17, the rate of RMSE reduction decreases as *M* approaches 24. Therefore, an evaluation of measurement accuracy and power consumption associated with filter order could potentially determine an optimal clock speed and filter order.

Next, we considered the RAM requirements of the ANC algorithm in order to determine the feasibility of implementing the algorithm within the embedded TI-MSP430 μC. Table 10.5 summarizes the estimated RAM (Kb) required, confirming that the LMS filter would not be limited by RAM usage.

Table 10.4: *Projected LMS and RLS execution times for 80 data samples using the embedded TI-MSP430 μC. The bold numbers represent feasible filter order (M) and μC clock configurations.*

	LMS Execution Time (ms)		
Filter Order (*M*)	80kHz CLK	1MHz CLK	8MHz CLK
2	768	**80**	**16**
4	1280	**144**	**24**
8	2230	**256**	**48**
16	4480	496	**88**
32	8640	976	**160**
64	16640	1920	320

	RLS Execution Time (ms)		
Filter Order (*M*)	80kHz CLK	1MHz CLK	8MHz CLK
2	2080	520	**80**
4	12000	1480	**224**
8*	40800	5040	752
16‡	-	-	-
32‡	-	-	-
64‡	-	-	-

* Due to limitations in system hardware, an 8th order RLS filter was the highest order than could be implemented in the embedded TI-MSP430 μC. ‡ These values exceed feasible time requirements for the present system configuration.

Table 10.5: *Estimated RAM usage for the LMS adaptive filter using the embedded TI-MSP430 μC. Measurements were obtained using a constant clock speed of 1MHz.*

Filter Order (M)	**RAM (Kb)**
2	1.07
4	1.11
8	1.17
16	1.30
24	1.43
32	1.55
64	2.07

11. CONCLUSIONS

Advances in remote physiological monitoring could provide a valuable means for medical personnel and first responders to assess remotely the health status of soldiers, hazmat workers, firefighters, and other individuals operating in dangerous and high-risk environments. A wearable pulse oximeter that provides arterial oxygen saturation (SpO_2), heart rate (HR), heart rate variability (HRV), and respiration rate (RR) readings could be utilized in the field since these readings help to indicate cardiovascular changes, changes physical and mental stresses, changes in autonomic nervous system, and breathing rate, respectively. Unfortunately, commercially available pulse oximeters are limited in terms of measurement reliability during motion. Therefore, the objective of this thesis was to investigate the feasibility of implementing software algorithms to improve measurement accuracy in a custom wearable pulse oximeter. In addition, it was determined whether the TI-MSP430 embedded microcontroller (μC) could support accelerometer (ACC)-based adaptive noise cancellation (ANC).

ACC-based ANC algorithms were studied as a potential means to minimize the effects of motion artifacts in photoplethysmographic (PPG) signals obtained from a forehead-mounted pulse oximeter sensor. A triaxial ACC was integrated into the sensor module (SM) of the wearable pulse oximeter. *In vivo* experiments were conducted to assess the effectiveness of the algorithm during treadmill, indoor and outdoor jogging. Data were processed offline in Matlab to calculate the root mean squared error (RMSE) extracted from PPG signals using Least-Mean-Square (LMS) and Recursive Least-Squares (RLS) ANC algorithms.

Design parameters of the LMS and RLS algorithms were varied in order to determine

their potential effects on measurement accuracy. Since a suitable range of values was established for the step-size (μ), forgetting factor (λ), and filter order (*M*) parameters for all data, the results suggest that it would be feasible to extract more accurate readings using the ANC algorithms during intense motions such as jogging. Similarly, despite differences in jogging between individuals, we found that the summation of body acceleration signals (*X*+*Y*+*Z*) was effective in attenuating the spectral content due to motion from the PPG signals during all jogging trials. Utilizing the appropriate adaptive filter design parameters as well as the combined X+Y+Z noise reference input signal, it was found that the LMS and RLS adaptive noise cancellation algorithms produced similar improvements in SpO_2 and HR accuracy during jogging. Based on these findings, it was concluded that accelerometry-based ANC software was effective to reduce motion artifacts in a forehead-mounted pulse oximeter sensor during jogging.

Potential Causes of Motion Artifacts

The results of this thesis confirmed that jogging activity directly contributes to the effects of motion artifacts in PPG signals. Although changes between the optical coupling of the sensor and the skin may be a potential factor contributing to motion artifacts, the degree to which this appears during jogging remains unclear. Although the studies performed were limited to forehead-worn PPG sensors, it was shown that the ACC noise reference signals provided an accurate estimation of the motion frequency during jogging. This suggests that the physical movement of the sensor, rather than change in blood volume within the vascular tissues, contributed to the effects of motion artifacts.

Accuracy of Arterial Oxygen Saturation during Jogging

As shown in Fig. 9.17, RMSE obtained for SpO_2 measurements averaged over all jogging trials was 5.1 ± 5.0% and 5.0 ± 4.6% for 24^{th} order LMS and RLS adaptive filters, respectively. As compared to RMSE values obtained without ANC, this corresponds to a reduction in RMSE of 22% and 23% using the LMS and RLS algorithms, respectively. Although the frequency of motion was effectively removed from the PPG signals (*Fig. 9.13*), the RMSE obtained for SpO_2 measurements was still relatively high. This suggests that SpO_2 readings may be unreliable during jogging. Additional studies should be performed to assess the feasibility of extracting accurate SpO_2 readings during other types of motion that occur in the field.

Accuracy of Heart Rate Readings during Jogging

Although improvements were shown for both SpO_2 and HR accuracies, the results regarding HR measurements were more promising. For instance, significantly more accurate HR measurements were obtained during jogging from PPG signals extracted using ACC-based ANC algorithms. As shown in Fig. 9.17, RMSE obtained for HR measurements averaged over all jogging trials was 5.8 ± 3.7% and 9.0 ± 6.3% for 24^{th} order LMS and RLS adaptive filters, respectively. As compared to RMSE values without ANC, this corresponds to a reduction in HR RMSE by 59% and 36% using LMS and RLS algorithms, respectively. This suggests that medical personnel could potentially utilize HR readings obtained from the wearable pulse oximeter even during movements typically encountered in the field.

Adaptive Noise Cancellation during Jogging

The experiments performed for this thesis showed that ACC-based ANC can reduce the

effects of motion artifacts in PPG signals obtained from a custom forehead-worn pulse oximeter sensor during jogging. Despite these promising results, note that the effectiveness of the ACC-based ANC algorithm may be limited during certain activities. In particular, since the ANC algorithm adaptively tunes to the noise reference signal, reduction of noise could be limited during motions that are less repetitive compared to jogging. Specifically, movements which produce motion artifacts with frequency content that varies over a wide spectral band could limit the degree to which motion artifacts are removed depending on the adaptation rate of the algorithm. For example, movements whose spectral band rapidly shifts in frequency could reduce the effectiveness of an ANC algorithm with slow adaptation characteristics.

Body Activity during Injury

It is assumed that an individual would be less active during a serious injury, allowing a medic to obtain accurate diagnoses since the effects of motion artifacts would be diminished considerably. By integrating an ACC into the sensor, the custom wearable pulse oximeter, which supplies a medic with physiological readings, can also provide an indication of body activity. The level of body activity provides a medic with additional information regarding the health status of an individual and can be utilized to indicate the degree of measurement accuracy. For example, a medic would have greater confidence in the accuracy of readings when a soldier is motionless or has a low level of body activity. This is significant since low body activity could occur during an injury. In contrast, although measurement accuracy would diminish during higher levels of activity, a medic could consider a highly active subject to be less critically injured.

Memory and Processing Requirements Associated with ANC

To evaluate the effectiveness of ANC algorithms for real-time applications, custom LMS and RLS algorithms were implemented in the embedded TI-MSP430 μC of the receiver module (RM). Due to relatively low processing requirements of the LMS adaptive algorithm, it was determined that this algorithm would be more suitable than the RLS algorithm. In particular, the execution times associated with the LMS algorithm indicated that it would be more suitable for real-time applications within a battery-powered μC.

In order to implement the ACC-based ANC algorithm, the embedded μC must meet several stringent design requirements. A 24^{th}-order LMS algorithm would require 1426 bytes of RAM since the algorithm utilizes several 24-length vectors for storing the filter output, error signals and tap weight vectors associated with the algorithm (*i.e. for an LMS filter of order M, several vectors are required*: $y_{RED}[M]$, $y_{IR}[M]$, $e_{RED}[M]$, $e_{IR}[M]$, $w_{RED}[M]$, and $w_{IR}[M]$). Note that memory requirement includes random access memory (RAM) to store the necessary body acceleration signals used as noise reference inputs. This RAM requirement would not limit the feasibility of implementing this algorithm since 10KB of RAM is available in the TI-MSP430F1611 μC.

Another design consideration includes program memory requirements. The total program memory available in the TI-MSP430F1611 would also be sufficient for implementing ACC-based ANC software routines since the program memory utilized by the adaptive algorithms is 1.2KB and about 2.2 KB for LMS and RLS algorithms, respectively. The program memory required for the SpO_2 and HR measurement algorithms and other support functions is about 8.4KB. Since the TI-MSP430F1611 μC provides 48KB of program memory, no additional memory will be required.

12. FUTURE RECOMMENDATIONS

Evaluation of ACC-Based ANC for Real-Time Conditions

The studies conducted for this thesis consisted of treadmill, indoor and outdoor jogging experiments. Future studies should incorporate experiments with additional activities in order to determine more fully the effectiveness of the ACC-based ANC algorithms. Since the focus of this work is on physiological monitoring and triage of military combatants, firefighters, mountain climbers and other persons operating in dangerous environments, movements typical to these scenarios should be studied.

Since jogging represents one type of movement, studies should be performed to determine the feasibility of improving measurement accuracy during simulated conditions or training missions. Simulations of battlefield scenarios could consist of a combination of resting, jogging and other activities. Also, since we studied the effects of motion during 1-minute jogging trials, it would be useful to determine the feasibility of improving measurement accuracy during longer jogging periods as well as intermittent periods of rest and jogging.

Additional applications that could benefit from motion-resistant pulse oximetry include monitoring firefighters during action and triage of individuals from buildings, athletes during physical training, and injured individuals during patient transport in both the military and clinical settings. In order to address the feasibility of implementing a wearable pulse oximeter for these scenarios, additional studies should be conducted to simulate movements typical during these types of events.

Evaluation of ANC Algorithms in an Embedded Microcontroller

Results presented in this thesis demonstrated that ACC-based ANC algorithms reduced

the RMSE of SpO_2 and HR measured during jogging. It was also demonstrated that the LMS algorithm consists of fewer computations than the RLS algorithm. This has important implications for real-time wearable physiological monitoring which requires optimal processing of software algorithms. Other adaptive filter algorithms that could be considered for ACC-based ANC include the varying step-size LMS (VSLMS), normalized LMS (NLMS), the block NLMS and the fast block NLMS [55]. Although these algorithms could provide potential advantages, such as shorter convergence time and lower RMSE, these algorithms may also increase the execution time. Therefore, to assess measurement accuracy, these algorithms should be evaluated offline in Matlab since this software environment would provide greater algorithm design flexibility and greater ease of implementation than an embedded μC environment. Additionally, the RAM and execution times associated with these algorithms should be measured by implementing these functions in C within an embedded μC environment.

ANC Filter Weight Updating

The ANC filters implemented in this thesis incorporated a filter weight updating scheme that recalculated filter weights during each iteration (*i.e. 80 updates per second*). Implementing this scheme can be advantageous since the filter coefficients adapt continuously to the input noise. A disadvantage of this scheme is that it requires the μC to perform continually calculations associated with the iterations of the ANC filtering process.

A reduction in processing performed by the μC would increase the battery life of the wearable device, so alternative updating algorithms should be investigated. ANC systems found in the literature suggest that filter weight updating schemes could be modified to

perform filter weight adjustment less frequently [62]. This would be useful for real-time applications since fewer computations could provide a reduction of the power cost of the software algorithms. One modification to the filter weight updating scheme could consist of implementing a software routine to reduce the recalculation of the filter weights based on the ACC and PPG data. During a constant activity, the filter weights would remain relatively constant between iterations. Constant activity could be detected in software by processing the ACC signals. For instance, if the amplitude of the ACC signals is within a certain range in a given period of time, the ANC filter could utilize an algorithm with fewer filter weight updates. Such a software routine would update filter weights less frequently when software algorithms detect a sustained activity. Therefore, the power consumed could be preserved by eliminating unnecessary repeated recalculation of filter weights.

Guarding Against Spectral Overlap

It was shown that the SpO_2 and HR readings were not affected significantly during experimental trials that consisted of spectral overlap (*Fig. 9.32*). It was reasoned that during these trials the cardiac spectral bands of the PPG signals were not attenuated since the ACC and PPG frequencies changed continuously over time. Additionally, results from simulations suggest that the ANC algorithm would not attenuate the cardiac frequency unless the frequencies of the ACC and PPG signals differed by 0.1Hz or less (*Fig. 9.30*).

Although the data suggest that the occurrence of spectral overlap does not limit the effectiveness of the ANC software, these studies were limited to 7 individuals performing 1-minute jogging. It is reasonable to consider that more significant spectral overlap could

occur during future studies.

A technique known as Laguerre Expansion has been suggested as a potential method to correct for the spectral overlap between ACC and PPG signals [60]. However, similar results were obtained using standard RLS and the Laguerre RLS [60]. Therefore, since study of the Laguerre Expansion was limited [60], additional investigation should be conducted to verify the usefulness of this method. In addition, software routines should be designed and tested in order to determine the feasibility of detecting spectral overlap.

For example, a potential method that could be tested would be to calculate the spectrum of the AC component of the ACC signals by a time domain algorithm (*i.e. by making use of a peak-detection based routine*). Software could compare the frequencies of ACC and adaptively filtered PPG signals and omit displaying the readings when significant spectral overlap is detected.

Steady-State and Transient Studies of Arterial Oxygen Saturation during Rest

An important part of the development of a wearable pulse oximeter is determining the measurement accuracy of SpO_2 during rest. Studies conducted for this thesis were limited to three trials of transient conditions which consisted of one individual performing a hypoxic episode during rest and three trials that contained hyperventilation periods during rest. Future work should consist of conducting a more complete study during steady-state and transient resting conditions.

In order to determine the accuracy of SpO_2 readings during steady-state conditions, participants must inspire various gas mixtures composed of controlled amounts of oxygen [63]. A minimum of 20 trials should be conducted in order to test against the 0.05 significance level. Participants would be fitted with the forehead-worn custom pulse

oximeter and the Masimo SET™ forehead-worn sensor as reference. Additionally, arterial blood samples should be analyzed by a reference co-oximeter in order to calibrate properly the software embedded within the custom pulse oximeter [63].

To study the effects of transient conditions on SpO_2 readings acquired from the custom pulse oximeter, additional experiments should be performed consisting of hypoxic episodes while resting similar to the experiments performed in this thesis. Data collection should consist of two periods made up of 1 minute of rest and 30 seconds of hypoxia. This study would help to determine the differences in response times between the software associated with the Masimo SET™ and the custom pulse oximeter. Generally, this study would indicate the ability of the custom algorithms to track instantaneous changes in SpO_2 readings. Preferably, this study should be done before determining the accuracy of SpO_2 during motion.

Improving SpO_2 Measurement Accuracy during Jogging

ANC algorithms were implemented to determine whether this software could reduce the effects of motion artifacts in the AC component of PPG signals. It was shown that the ANC algorithms were effective in attenuating the frequency attributed to motion (*Fig. 9.13*) which enabled the calculation of more accurate SpO_2 and HR readings during jogging (*Fig. 9.17*). As illustrated in Fig. 9.20, the DC component of the PPG signal was obtained by applying a LPF to the raw PPG data. Although the frequency of stepping motion was removed from the DC component of the PPG signals by the use of a LPF, low frequency changes due to motion remained in the DC signals. This suggests that additional signal processing algorithms could be designed to improve the reliability of SpO_2 measurements during movements.

Changes in the DC value associated with motion could be detected and corrected for in software. For example, utilizing the DC values obtained before the onset of motion could provide improvements in SpO_2 measurement accuracy during jogging. It is feasible that other signal processing methods could be designed and tested to improve the accuracy of SpO_2 measurements during activity. Therefore, the data collected for this thesis should be analyzed further to determine the feasibility of reducing the effects of motion artifacts on the DC component of PPG signals acquired during activity.

The Effects of Motion Artifacts on Heart Rate Variability and Respiration Rate

It has been shown by Johnston that HRV [64] and RR [65] readings can be extracted from PPG signals acquired from the custom pulse oximeter during rest. HRV in particular may benefit a medic since HRV data can be utilized to predict changes in sympathetic nervous tone, which could enhance the diagnostic usage of the wearable pulse oximeter. Since it was shown that the ANC algorithm provided significant improvements in the accuracy of HR measurements, potentially more accurate HRV readings could be acquired during motions that typically occur in the field. Future studies should be conducted to extract HRV readings from the data collected for the experiments for this thesis. Reference HR readings acquired from the Polar ECG monitor could be utilized as a HRV reference source.

Determining the feasibility of obtaining more accurate RR readings by implementing ANC algorithms is a potential area for future work. Studies performed by Johnston [12] indicated that software algorithms could provide RR readings with clinically acceptable accuracy during rest. Studies should be conducted to determine the accuracy of these algorithms during jogging.

REFERENCES

[1] R. Zajtchuk and G. R. Sullivan, "Battlefield Trauma Care: Focus on Advanced Technology," *Military Medicine*, vol. 160, pp. 1 – 7, 1995.

[2] R. W. Hoyt, J. Reifman, T. S. Coster and M. J. Buller, "Combat Medical Informatics: Present and Future," presented at AMIA Annual Symposium, 2002.

[3] E. Jovanov, A. O'Donnel, A. Morgan, B. Priddy and R. Hormigo, "Prolonged Telemetric Monitoring of Heart Rate Variability Using Wireless Intelligent Sensors and a Mobile Gateway," presented at 2nd Joint EMBS/BMES Conference, 2002.

[4] M. Nogawa, T. Kaiwa and S. Takatani, "A Novel Hybrid Reflectance Pulse Oximeter Sensor with Improved Linearity and General Applicability to Various Portions of the Body," presented at 20th Annual International Conference of the IEEE EMBS, 1998.

[5] P. B. Crilly, "An Integrated Pulse Oximeter System for Telemedicine Applications," presented at IEEE Instrumentation and Measurement Technology Conference," 1997.

[6] S. M. Wendelken, S. P. McGrath and G. T. Blike, "Agent Based Casualty Care – A Medical Expert System for Modern Triage," [Online Article], 2007, [Jun 27 2007], Available at HTTP: http://www.ists.dartmouth.edu/projects/frsensors/artemis/papers/abccare-suzanne.pdf.

[7] S. Wendelken, S. McGrath, G. Blike, M. Akay, "The Feasibility of Using a Forehead Reflectance Pulse Oximeter for Automated Remote Triage," presented at 30th Annual Northeast Bioengineering Conference, pp. 180 – 181, 2004.

[8] H. H. Asada, P. Shaltis, A. Reisner, S. Rhee and R. C. Hutchinson, "Mobile Monitoring with Wearable Photoplethysmographic Biosensors," *IEEE Engineering in Medicine and Biology Magazine*, pp. 28 – 40, 2003.

[9] B. Yang and S. Rhee, "Development of the Ring Sensor for Healthcare Automation," *Robotics and Autonomous Systems*, vol. 30, pp. 273 – 281, 2000.

[10] K. E. Friedl and J. H. Allen, "USARIEM: Physiological Research for the Warfighter," *Army Medical Department Journal*, pp. 33 – 43, 2004.

[11] G. S. F. Ling, B. K. Day, P. Rhee and J. M. Ecklund, "In Search of Technological Solutions to Battlefield Management of Combat Casualties," presented at SPIE Conference on Battlefield Biomedical Technologies, vol. 3712, pp. 1 – 8, 1999.

[12] W. S. Johnston, "Development of a Signal Processing Library for Extraction of

SpO_2, HR, HRV, and RR from Photoplethysmographic Waveforms," M.S. Thesis, Department of Biomedical Engineering, Worcester Polytechnic Institute, Worcester, MA, 2006.

[13] Y. Mendelson, "Pulse Oximetry: Theory and Applications for Noninvasive Monitoring," *Clinical Chemistry*, vol. 38, no. 9, pp. 1601 – 1607, 1992.

[14] S. M. Wendelken, "Using a Forehead Reflectance Pulse Oximeter to Detect Changes in Sympathetic Tone," M.S. Thesis, Thayer School of Engineering, Dartmouth College, Hanover, NH, 2004.

[15] S. M. Wendelken, S. P. McGrath and G. T. Blike, "A Medical Assessment Algorithm for Automated Remote Triage," presented at 25th Annual EMBS Conference, 2003.

[16] P. Gibbs and H. H. Asada, "Reducing Motion Artifact in Wearable Sensors Using MEMS Accelerometers for Active Noise Cancellation," presented at American Control Conference, pp. 1581 – 1586, 2005.

[17] A. Nagre and Y. Mendelson, "Effects of Motion Artifacts on Pulse Oximeter Readings from Different Facial Regions," presented at 31st IEEE Annual Northeast Bioengineering Conference, pp. 220 – 222, 2005.

[18] S. Rhee, B. Yang and H. H. Asada, "Artifact-Resistant Power-Efficient Design of Finger-Ring Plethysmographic Sensors," *IEEE Transactions on Biomedical Engineering*, vol. 48, no. 7, pp. 795 – 805, 2001.

[19] American Telemedicine Association, "ATA Defining Telemedicine," [Online Article], 2007, [Aug 29 2007], Available at HTTP: http://www.americantelemed.org/news/definition.html

[20] J. F. Kelleher, "Pulse Oximetry," *Journal of Clinical Monitoring*, vol. 5, pp. 37 – 62, 1989.

[21] W. S. Johnston, P. C. Branche, C. J. Pujary and Y. Mendelson, "Effects of Motion Artifacts on Helmet-Mounted Pulse Oximeter Sensors," presented at 30th IEEE Annual Northeast Bioengineering Conference, pp. 214 – 215, 2004.

[22] Radical Signal Extraction Pulse Oximeter Operator's Manual, Masimo, 2004.

[23] T. L. Rusch, R. Sankar and J. E. Scharf, "Signal Processing Methods for Pulse Oximetry," *Computations in Biology and Medicine*, vol. 26, no. 2, pp. 143 – 159, 1996.

[24] J. E. Scharf and T. L. Rusch, "Optimization of Portable Pulse Oximetry through Fourier Analysis," presented at 12th Southern Biomedical Engineering

Conference, pp. 233 – 235, 1993.

[25] T. L. Rusch, J. E. Scharf and R. Sankar, "Alternate Pulse Oximetry Algorithms for SpO_2 Computation," presented at 16th Annual International Conference of the IEEE EMBS, pp. 848 – 849, 1994.

[26] Task Force of the European Society of Cardiology and the North American Society of Pacing and Electrophysiology, "Heart Rate Variability: Standards of Measurement, Physiological Interpretation, and Clinical Use," *Circulation*, vol. 93, pp. 1043 – 1065, 1996.

[27] Y. Mendelson, R. J. Duckworth and G. Comtois, "A Wearable Reflectance Pulse Oximeter for Remote Physiological Monitoring," presented at 28th Annual International Conference of the IEEE EMBS, pp. 912 – 915, 2006.

[28] J. E. Sinex, "Pulse Oximetry: Principles and Limitations," *American Journal of Emergency Medicine*, vol. 17, no. 1, pp.59 – 66, 1999.

[29] J. W. Salyer, "Neonatal and Pediatric Pulse Oximetry," *Respiratory Care*, vol. 48, no. 4, pp. 386 – 398, 2003.

[30] H. Gehring, C. Hornberger, H. Matz, E. Konecny and P. Schmucker, "The Effects of Motion Artifact and Low Perfusion on the Performance of a New Generation of Pulse Oximeters in Volunteers Undergoing Hypoxemia," *Respiratory Care*, vol. 47, no. 1, pp. 48 – 60, 2002.

[31] R. M. Tobin, J. A. Pologe and P. B. Batchelder, "A Characterization of Motion Affecting Pulse Oximetry in 350 Patients," *Anesthesia and Analgesia*, vol. 94, pp. S54 – 60, 2002.

[32] M. R. Neuman and N. Wang, "Motion Artifact in Pulse Oximetry," presented at Annual International Conference of the IEEE EMBS, vol. 12, no. 5, pp. 2007 – 2008,1990.

[33] Masimo, "Signal Extraction Technology," Technical Bulletin 1, 2006.

[34] G. Comtois and Y. Mendelson, "A Wearable Wireless Reflectance Pulse Oximeter for Remote Triage Applications," presented at 32nd Annual Northeast Bioengineering Conference, pp. 53 – 54, 2006.

[35] G. Comtois and Y. Mendelson, "A Noise Reference Input to an Adaptive Filter Algorithm for Signal Processing in a Wearable Pulse Oximeter," presented at 33rd Northeast Bioengineering Conference, pp. 106 – 107, 2007.

[36] Y. Mendelson and G. Comtois, "Accelerometry-based Adaptive Noise Cancellation for Remote Physiological Monitoring by a Wearable Pulse

Oximeter," presented at 3rd IASTED International Conference on Telehealth, 2007.

[37] B. S. Kim and S. K. Yoo, "Motion Artifact Reduction in Photoplethysmography Using Independent Component Analysis," *IEEE Transactions on Biomedical Engineering*, vol. 53, no. 3, pp. 566 – 568, 2006.

[38] P. F. Stetson, "Independent Component Analysis of Pulse Oximetry Signals," presented at 26th Annual International Conference of the IEEE EMBS, pp. 231 – 234, 2004.

[39] A. Hyvärinen, J. Karhunen and E. Oja, "Independent Component Analysis," USA: John Wiley & Sons, 2001.

[40] I. T. Jolliffe, "Principal Component Analysis," NJ, USA: Springer-Verlag, Inc. 2002.

[41] M. J. Hayes and P. R. Smith, "Quantitative Evaluation of Photoplethysmographic Artefact Reduction for Pulse Oximetry," presented at EUROPTO Conference on Medical Sensors and Fiber Optic Sensors IV, 1998.

[42] H. H. Asada, H. Jiang and P. Gibbs, "Active Noise Cancellation Using MEMS Accelerometers for Motion-Tolerant Wearable Bio-Sensors, presented at 26th Annual International Conference of the IEEE EMBS, pp. 2157 – 2160, 2004.

[43] D. R. Prytherch, D. H. Evans, M. J. Smith and D. S. Macpherson, "On-line Classification of Arterial Stenosis Severity Using Principal Component Analysis Applied to Doppler Ultrasound Signals," *Clinical Physics of Physiological Measurements*, vol. 3, no. 3, pp. 191 – 200, 1982.

[44] M. J. Hayes and P. R. Smith, "Artifact Reduction in Photoplethysmography," *Applied Optics*, vol. 37, no. 31, pp. 7437 – 7446, 1998.

[45] M. J. Hayes and P. R. Smith, "A New Method for Pulse Oximetry Possessing Inherent Insensitivity to Artifact," *IEEE Transactions on Biomedical Engineering*, vol. 48, no. 4, pp. 452 – 461, 2001.

[46] K. Hamaguri and T. Sakai, "Multi-wavelength Oximeter Having a Means for Disregarding a Poor Signal," U.S. Patent 4,714,341, 1987.

[47] J. Y. A. Foo, S. J. Wilson, G. R. Williams, M. Harris and D. M. Cooper, "Motion Artifact Reduction of the Photoplethysmographic Signal in Pulse Transit Time Measurement," *Australasian Physical & Engineering Sciences in Medicine*, vol. 27, no. 4, pp. 165 – 173, 2004.

[48] J. Y. A. Foo, W. Leong, S. J. Wilson and J. Homer, "Adaptive Algorithms to

Optimise Photoplethysmographic Signals in Heart Rate Estimation," presented at IASTED International Conference, pp. 331 – 334, 2005

[49] J. Y. A. Foo and S. J. Wilson, "A Computational System to Optimise Noise Rejection in Photoplethysmography Signals during Motion or Poor Perfusion States," *Medicine, Biology and Engineering Computing*, vol. 44, pp. 140 – 145, 2006.

[50] P. Gibbs and H. H. Asada, "Reducing Motion Artifact in Wearable Sensors Using MEMS Accelerometers for Active Noise Cancellation," presented at American Control Conference, pp. 1581 – 1586, 2005.

[51] L. B. Wood and H. H. Asada, "Noise Cancellation Model Validation for Reduced Motion Artifact Wearable PPG Sensors Using MEMS Accelerometers," presented at 28th IEEE EMBS Annual International Conference, pp. 3525 – 3528, 2006.

[52] C. V. C. Bouten, K. T. M. Koekkoek, M. Verduin, R. Kodde and J. D. Janssen, "A Triaxial Accelerometer and Portable Data Processing Unit for the Assessment of Daily Physical Activity," *IEEE Transactions on Biomedical Engineering*, vol. 44, no. 3, pp. 136 – 147, 1997.

[53] S. Haykin, "Adaptive Filter Theory," NJ, USA: Prentice Hall, 2002.

[54] B. Widrow, J. R. Glover Jr., J. M. McCool, J. Kaunitz, et al., "Adaptive Noise Cancelling: Principles and Applications," *Proceedings of the IEEE*, vol. 63, no. 12, pp. 1692 – 1716, 1975.

[55] S. C. Douglas, "Introduction to Adaptive Filters," *Digital Signal Processing Handbook*, Ed. V. K. Madisetti and D. B. Williams, Boca Raton: CRC Press LLC, 1999.

[56] D. L. Jones, "The LMS Adaptive Filter Algorithm," [Online Article], 2007, [Feb 16 2004], Available at HTTP: http://cnx.org/content/m11829/latest/

[57] A. R. Relente and L. G. Sison, "Characterization and Adaptive Filtering of Motion Artifacts in Pulse Oximetry Using Accelerometers," presented at 2nd Joint EMBS/BMES Conference, pp. 1769 – 1770, 2002.

[58] Y. Lau, Zahir M. Hussian, and Richard Harris, "Performance of Adaptive Filtering Algorithms: A Comparative Study," submitted to the Centre for Advanced Technology in Telecommunications, RMIT University, Melbourne, Victoria, Australia.

[59] H. H. Asada, H. Jiang and P. Gibbs, "Active Noise Cancellation Using MEMS Accelerometers for Motion-Tolerant Wearable Bio-Sensors," presented at 26th Annual International Conference of the IEEE EMBS, pp. 2157 – 2160, 2004.

[60] L. B. Wood and H. H. Asada, "Active Motion Artifact Reduction for Wearable Sensors Using Laguerre Expansion and Signal Separation," presented at 27th Annual International Conference of the IEEE EMBS, pp. 3571 – 3574, 2005.

[61] Pulse Oximeter Specifications, Rev. 1.1, 2006.

[62] V. S. Somayazulu, S. K. Mitra and J. J. Shynk, "Adaptive Line Enhancement Using Multirate Techniques," *Acoustics, Speech, and Signal Processing*, vol. 2, pp. 928 – 931, 1989.

[63] Y. Mendelson, "Pulse Oximetry," *Wiley Encyclopedia of Biomedical Engineering*, John Wiley and Sons, Inc., 2006.

[64] W. S. Johnston and Y. Mendelson, "Extracting Heart Rate Variability from a Wearable Reflectance Pulse Oximeter," presented at 31st IEEE Annual Northeast Bioengineering Conference, 2005.

[65] W. S. Johnston and Y. Mendelson, "Extracting Breathing Rate Information from a Wearable Reflectance Pulse Oximeter Sensor," presented at 26th Annual International Conference of the IEEE EMBS, 2004.